

THESIS

THE IMPACT OF SHEAR RATE AND REVERSE FLOW ON CARDIAC MORPHOGENESIS AND GENE
EXPRESSION IN THE EMBRYONIC ZEBRAFISH HEART

Submitted by

Molly J Zeller

Graduate Degree Program in Cell and Molecular Biology

In partial fulfillment of the requirements

For the Degree of Master of Science

Colorado State University

Fort Collins, Colorado

Fall 2015

Master's Committee:

Advisor: Deborah Garrity

Donald Mykles
Patricia Bedinger
Lakshmi Prasad Dasi

Copyright by Molly Jeanne Zeller 2015

All Rights Reserved

ABSTRACT

THE IMPACT OF SHEAR RATE AND REVERSE FLOW ON CARDIAC MORPHOGENESIS AND GENE EXPRESSION IN THE EMBRYONIC ZEBRAFISH HEART

Missteps in formation of the embryonic heart can have drastic consequences, making cardiac malformations a common human birth defect. During development, biomechanical factors including shear stress and reverse flow impact cardiogenesis. Shear stress is an epigenetic biomechanical force acting upon endothelial cells. Normally, a short period of reverse flow occurs prior to atrioventricular valve formation during ventricle systole and atrial diastole. The goal of our research is to investigate how altered biomechanical forces acting on endocardial cells lead to genetic responses by the heart. The mammalian zinc finger transcription factor Krüppel-like factor 2 (KLF2) responds to shear stress signals. Here, we explore the zebrafish KLF genes: *klf2a*, *klf2b*, and *klf4*. Whole embryo RT-PCR indicates that the three genes are expressed throughout early development, with cardiac expression in all genes present by 48 hours post fertilization. To evaluate how changes in biomechanical environments trigger altered gene expression in endocardial cells, we used comparative qPCR to quantify *klf2a*, *klf2b*, and *klf4* expression levels in embryonic hearts with altered shear stress or reverse flow. Knockdown of the hematopoiesis gene *gata2* was found to decrease blood viscosity, thereby decreasing both shear stress and reverse flow. Knockdown of contractility gene *filaminCb* was found to decrease shear stress but significantly increase reverse flow. Using high-speed imaging we quantified these forces and correlated changes in *klf2a*, *klf2b*, and *klf4*

expression. *klf2a* expression levels decreased in response to changes in both blood viscosity and cardiac contractility. *klf2b* and *klf4* expression levels did not significantly change with these changes in biomechanical stresses. Our investigations considered the impact of blood viscosity versus cardiac contractility on KLF expression and determined that *klf2a* is a flow response gene. This data confirms previous studies that *klf2a* is in fact a flow response gene and shows that *klf2b* and *klf4* are not responsive to changes in blood viscosity or cardiac contractility. Future studies will use transcriptomic approaches to identify genes regulated by the KLF family in response to shear stress and reverse flow cues.

ACKNOWLEDGEMENTS

Thank you to Dr. Garrity and my committee members for providing me with guidance to complete this project. My parents were wonderful support throughout my schooling and they deserve all the thanks in the world. Special thanks goes to my grad school cohorts for helping me mentally and emotionally.

TABLE OF CONTENTS

Abstract.....	ii
Acknowledgements.....	iv
Chapter 1: Literature Review.....	1
Chapter 2: Introduction.....	27
Chapter 3: Results.....	30
Chapter 4: Discussion.....	60
Chapter 5: Materials and Methods.....	78
References.....	84
Appendix.....	90

CHAPTER 1: LITERATURE REVIEW

Zebrafish are a tropical freshwater fish used as a model organism for developmental genetics since the 1980s (Figure 1.1a) (Ackermann and Paw, 2003; Howe et al., 2013).

Researchers are interested in zebrafish because of the significant homology between fish genes and human genes (Howe et al., 2013). Howe and colleagues identified that 71.4% of human genes are orthologous to at least one zebrafish gene (Howe et al., 2013). These researchers also noted that zebrafish have approximately two genes to each human gene, thought to be in part due to teleost-specific genome duplication (Meyer and Schartl, 1999; Howe et al., 2013). This genome duplication occurred after the evolution of vertebrates from early deuterostomes (Meyer and Schartl, 1999). Some of these duplications turn into pseudogenes or DNA that is not transcribed for usage, but many become genes that are responsible for a variety of new functions. Zebrafish are advantageous when it comes to studying developmental biology because of their small size, quick generation, and their ability to produce numerous offspring. The adult zebrafish is often no larger than two inches in length and when fed properly, can breed weekly. Hundreds of embryos can be collected from one mating, which allows researchers to have many replicates for experiments.

The transparency of the zebrafish embryo at critical developmental stages, as well as its development external to the mother, makes the zebrafish useful to study organogenesis (Figure 1.1b). Zebrafish are used to study heart, vessel, blood, kidney, and muscle development as well as other aspects of developmental biology (Ackermann and Paw, 2003; Lin, 2012). In our work, we use zebrafish to study heart development. Development of the heart can be studied in

zebrafish because of the similarity of early morphological events between human and zebrafish heart development. Zebrafish embryos obtain oxygen through diffusion for the first five to seven days post fertilization (Kopp et al., 2010; Hoage et al., 2012). This characteristic allows for the study of mutant genes that affect the heart structure and function. Our study involves using these embryos before they are dependent on the heart for oxygen. Since young embryos will not die due to lack of oxygen carried via the blood stream, blood flow can be altered to observe the effects of biomechanical forces upon development of the embryonic heart.

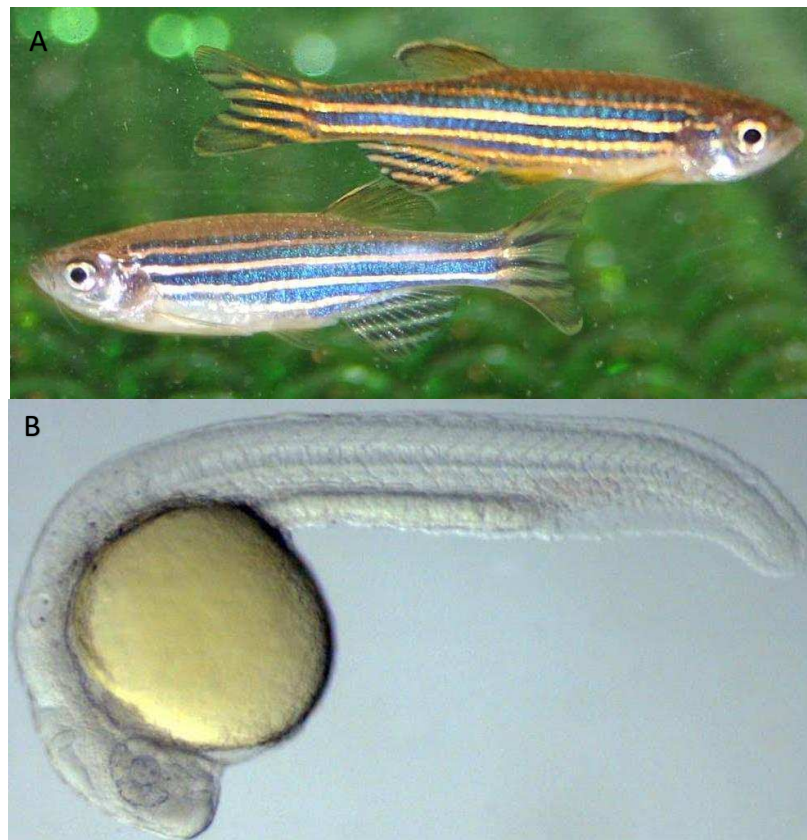


Figure 1.1 – **Zebrafish are used as a model organism.** A – Wildtype adult zebrafish. Male zebrafish is pictured on top while female zebrafish is picture on bottom. <http://www.livescience.com/25180-zebrafish-change-color-for-sex.html>. B – Zebrafish larva at approximately 24 hours post fertilization. <http://ugaresearch.uga.edu/gallery/one-more/>.

Morphogenesis of the heart is an essential process for life in complex animals. Many pathways and genes are involved in this process which can allow for mishaps to occur. These mishaps can cause congenital heart defects (CHD), which are estimated to be present in 4 to 10 per 1000 live births in humans (Figure 1.2) (Pierpont et al., 2007; Fahed et al., 2013). Researchers are identifying genes that are responsible for these defects as well as the epigenetics or environmental conditions that affect the function or expression of those genes. Animal models such as chick, mouse, and zebrafish are used in order to identify some of these factors.

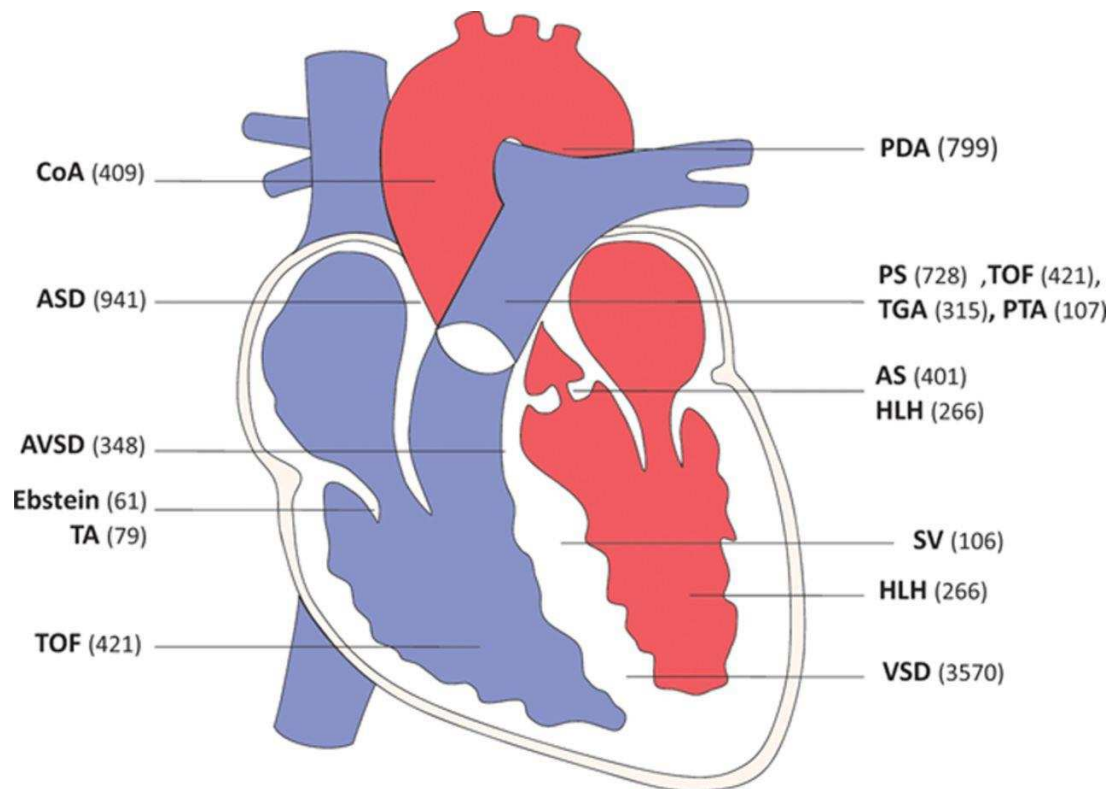


Figure 1.2- Locations of heart malformations that are usually identified in infancy, and estimated prevalence based on the CONCOR database. Numbers indicate the birth prevalence per million live births. CONCOR database is a national registry and DNA-bank of patients with congenital heart disease in the Netherlands (Van der Velde et al., 2005). AS – aortic stenosis; ASD – atrial septal defect; AVSD – atrioventricular septal defect; CoA – coarctation of the aorta; Ebstein – Ebstein anomaly; HLH – hypoplastic left heart; MA – mitral atresia; PDA – patent ductus arteriosus; PS – pulmonary stenosis; PTA – persistent truncus arteriosus; TA – tricuspid atresia; TGA – transposition of the great arteries; SV – single ventricle; TOF – tetralogy of Fallot; VSD – ventricular septal defect (Fahed et al., 2013).

Heart development starts very early in zebrafish development (Figure 1.3) (Bakkers, 2011). At just 5 hours post fertilization (hpf), cardiac progenitors (identified by fate-mapping experiments) are present in the lateral marginal zones of the cleavage stage embryo (Tu and Chi, 2012). Following gastrulation, cells from the anterior lateral plate mesoderm migrate towards the midline and differentiate into ventricular and atrial cardiomyocytes (Tu and Chi, 2012). Heart tube formation occurs around 24 hours post fertilization, at which point the embryo is still translucent and visualization of ongoing development is possible (Yelon, 2001). At 24 hours post fertilization the heart tube starts to elongate, and turn so that the ventricle becomes anterior and the atrium becomes posterior (Tu and Chi, 2012). This movement precedes the looping of the heart, ballooning of the chambers, and formation of the atrioventricular canal; looping ends around 48 hours post fertilization (Tu and Chi, 2012). After 48 hpf, the heart consists of a sinus venosus (the inflow tract that collects blood from cardinal veins and delivers it to the atrium), one atrium (a muscled cavity that receives deoxygenated blood and delivers it to the ventricle), one ventricle (receives blood from the atrium and delivers it to the body via the aorta). During this time, the bulbus arteriosus (a pear shaped “chamber” through which blood leaves the heart) develops (Grimes et al., 2006). While the heart is forming, cells are rearranging and beginning to communicate in a way that enables them to begin to pump blood through the heart via contraction.

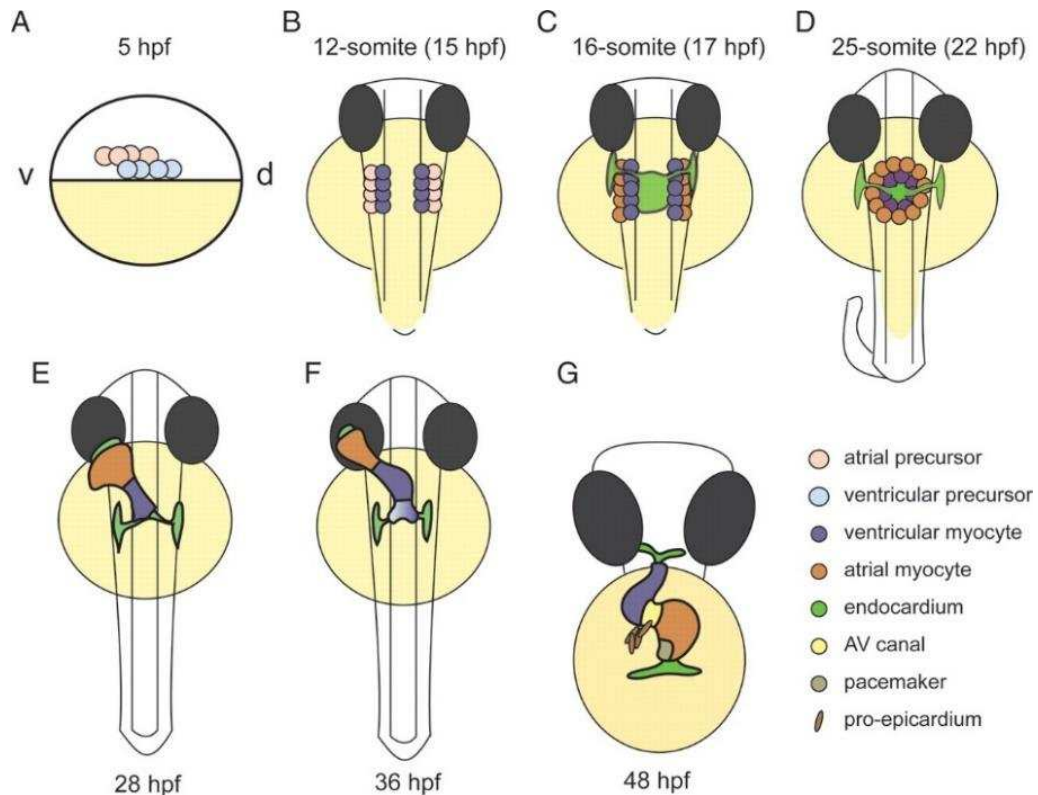


Figure 1.3 - Stages of cardiac development. At 5 h post fertilization, cardiac progenitor cells are located bilaterally in the lateral marginal zone. Atrial progenitor cells (pink) are located more ventrally than the ventricle progenitor cells (light blue). During mid- and late-somite stages, the myocardial tissue expands by continuous cardiogenic differentiation into more lateral regions of the anterior lateral plate mesoderm (ALPM) by the cardiogenic differentiation of future atrial myocytes (orange; venous differentiation). Cardiac morphogenesis transforms the cardiac disc into a cardiac tube. The endocardium forms the inner lining of the myocardial tube. At 28 hpf, the linear heart tube has formed, with the venous pole located at the anterior left and the arterial pole fixed at the mid-line. Cardiogenic differentiation continues at the arterial pole, and as a result new cardiomyocytes are added to this region (purple gradient). At 36 hpf, cardiac looping has started, with a displacement of the ventricle towards the mid-line, and the constriction at the position of the AV canal is first visible. The heart tube continues to loop and forms an S-shaped loop. Ellipsoid extra-cardiac pro-epicardial cells (brown) are located near the AV canal (yellow), from where they start to cover the myocardium with an epicardial layer. The pacemaker is present in the inner curvature of the atrium near the venous pole (dark green) (Bakkers, 2011).

Cardiac conduction is the process responsible for providing a coordinated beat in the heart, while contraction is defined as muscle constriction in response to the conduction signals. These processes underlie the mechanics of a heartbeat, which provides the force that propels blood flow. Since zebrafish are small, embryos obtain sufficient oxygenation by diffusion to survive without a beating heart for the first 5 days of life (Hoage et al., 2012). However, normal development of the heart itself nevertheless requires a heartbeat and intracardiac flow (Banjo

et al., 2013). When flow is perturbed, morphological defects such as an abnormal chamber shape and size, a reduction in looping, and defective valve formation occur (Hove et al., 2003). Heart beat and contraction influence the formation of the trabeculae (myocardial sheets), the atrioventricular valve, as well as other cardiac structures (Staudt and Stainier, 2012). The heartbeat relies on a coordinated conduction system that is maintained by a specialized network of cardiomyocytes and is seen in both larval and adult zebrafish (Staudt and Stainier, 2012). This conduction pattern allows contraction to move the blood cells efficiently through the heart, resulting in sustained blood flow (Staudt and Stainier, 2012). Although laminar flow begins as early as 20 hpf, conduction patterns begin to arise around 24-26 hpf, which indicates the presence of pacemaker tissue (Glickman and Yelon, 2002; Staudt and Stainier, 2012; Lee et al., 2013; Parker et al., 2014). Contractile patterns rely on the correct morphology of the heart as well as the correct formation of contractile sarcomeres (Staudt and Stainier, 2012). Along with flow, heart beat and contraction are necessary for the early development of the heart (Staudt and Stainier, 2012). Biomechanical factors related to contraction, stretch, or blood flow can affect both cell size and myofibril content (Lin et al., 2012).

Biomechanical factors are considered epigenetic factors because they modify gene expression without altering the genetic code. To determine whether these epigenetic factors could impact chamber morphology, *weak atrium (wea)* mutants were investigated (Lin et al., 2012). *wea* mutants have a loss of function mutation in the *atrial myosin heavy chain (amhc)* gene, which is expressed in the atrium but not the ventricle (Berdougo et al., 2003). Cell boundaries and Z-bands were labeled to observe cell size and myofibril content (Lin et al., 2012). At 28 hpf, cell size and myofibril content in *wea* mutants was similar to wild type

embryos, but at 38-50 hpf, cell size and myofibril content differed (Lin et al., 2012). Z-bands were not only fewer per cell in *wea* mutants, but also shorter (Lin et al., 2012). The changes observed in this experiment suggest that hemodynamic forces influence cell size and myofibril content in the developing ventricle. This data led the researchers to assess the hypertrophic behavior of individual cardiomyocytes to see if diminished blood flow impacted them (Lin et al., 2012). To do this, an *atrial myosin heavy chain* knockdown was used to recreate the *wea* mutant phenotype in embryos that had Z-bands labeled via *α -actinin3b:egfp* (Lin et al., 2012). Even though *amhc* is only expressed in the atrium and the ventricles do contract normally with normal sarcomeres, the ventricular chamber in *wea* mutants is smaller than wildtype (Auman et al., 2007). In wildtype embryos, cardiomyocyte hypertrophy (excessive development of a tissue) as part of the mechanism of chamber emergence (Lin et al., 2012). Few cardiomyocytes showed hypertrophic growth in the *wea* depleted embryos and the growth that did occur was less marked than that of wild type embryos (Lin et al., 2012). These results suggest that blood flow through the ventricle influences cardiomyocyte hypertrophy and myofibril content (Lin et al., 2012).

To demonstrate that the detection of flow is important for cardiac development, ventricular cells in mutant and wildtype fish were observed. In *wea* mutants, elongation and surface area growth is reduced in ventricular cells (Auman et al., 2007). Ventricular cell growth is a cell nonautonomous trait based on the observation that the *wea* ventricular cells grow normally when transplanted into wild-type hearts (Auman et al., 2007). This experiment supports the idea that detecting flow is a necessary feature of ventricular cells and is important for cardiac development.

In a study investigating endocardial cushion development, Bartman and colleagues showed that myocardial contractility, a biomechanical force, alone may be responsible for inconsistencies in cardiac morphology in wildtype embryos (Bartman et al., 2004). Endocardial cushions (ECs) are tissue swellings made of endocardial cells that develop along the anterior-posterior axis of the heart tube and are formed during late cardiac organogenesis (Bartman et al., 2004). ECs help in valve formation and in the case of four-chambered hearts, septae (Bartman et al., 2004). Epithelial-mesenchymal transformation (EMT), a process that allows for an epithelial cell to assume mesenchymal cell phenotypes, is a required sub-step for EC development and the events preceding and following EMT are being investigated (Kalluri and Weinberg, 2009). To determine if blood flow or myocardial function impacted EC development, various concentrations of 2,3-butanedione monoxime (2,3-BDM), a dose-dependent myofibrillar ATPase blocker, were applied along with tricaine (a fish anesthetic) to inhibit myocardial function (Bartman et al., 2004). At high concentrations of 2,3-BDM when blood flow is abolished, 58% of embryos formed an endocardial ring. Embryos that exhibited blood flow (at low concentrations of 2,3-BDM) still formed ECs, and conversely, when myocardial function was decreased (observed in embryos that lack a heartbeat), the number of embryos with functioning ECs decreased (Bartman et al., 2004). This result shows that poor myocardial function, not blood flow, is primarily responsible for the loss of endocardial cushion formation in mutant embryos. While blood flow is not shown to be important here, this is only a limited experiment looking at one type of morphology. This result also shows that myocardial function is an important factor in cardiac morphology, which will also be discussed here in this study.

An area of current interest within the field of embryonic heart development concerns how blood flow factors like shear stress and reverse flow impact gene expression and development of the heart. These factors involve analyzing different mechanisms of mechanotransduction which is a cellular process that converts mechanical stimuli into electrical, biochemical, and genetic responses (Sidi and Rosa, 2004; Miyasaka et al., 2011). Physical micro-environmental parameters that must be taken into consideration when discussing mechanotransduction include stresses and strains (Bukoreshtliev et al., 2013). Stresses are defined as the ratios of an applied force to the area upon which it is acting, which can then cause relative elongations or displacements of a material, or strains (Bukoreshtliev et al., 2013).

In zebrafish, mechanical strains diffuse throughout the tissue and are largely caused by physical forces (Banjo et al., 2013). By observing the function of *microRNA-21* (*miR-21*), which senses blood flow and uses these diffuse forces to regulate valve formation, Banjo and colleagues found that these forces act as a physical “morphogen” since they can be distributed throughout the area, causing anisotropic distribution of strains (Banjo et al., 2013). Expression of *miR-21* is dependent on hemodynamics as was shown in *silent heart* (*sih*) morphants (Banjo et al., 2013). When the heart beat is stopped in these morphants, expression of *miR-21* is not present at its normal expression locations in the constricted parts of the endocardium (Banjo et al., 2013). These results present the idea that blood flow stimulates *miR-21* expression, showing through correlation that *miR-21* is a component of a mechanotransduction pathway (Banjo et al., 2013).

One blood flow factor being investigated in this study is reverse flow fraction (RFF). RFF is defined as the flow of fluid opposite to the normal direction or path of blood circulation, or specifically the flow from the ventricle back to the atrium after contraction. Our group and others have developed high speed video methodology to record the blood cells as they move through the atrioventricular junction, which permits extraction of RFF and other parameters. Valves in the heart prevent reverse flow, but before valves are formed there is substantial regurgitation. Reverse flow may serve as a critical signal to endothelial cells based on the observation that malformed valves develop if flow is severely perturbed (Vermot et al., 2009). Reverse flow in zebrafish is highest in the AV canal during the second and third days of development, which are the times that precede valve formation (Vermot et al., 2009). A low percentage reverse flow fraction (RFF) indicates that little reverse flow is present, which may cause developmental defects like malformed heart valves (Vermot et al., 2009).

Along with reverse flow, shear stress is another flow defining factor. Shear stress is an epigenetic force that is classified as the frictional force caused by the pressure exerted upon the endocardium by blood cells (Gijssen et al., 2013). The total mechanical load that is detected by the endocardium is represented partially by shear stress (Gijssen et al., 2013). When shear stress is greatly increased or changed in some manner, the embryonic heart experiences detrimental effects. The endothelium is particularly sensitive to shear stress and appears to be a primary sensor of shear stress (Gijssen et al., 2013). In addition to RFF, the presence or magnitude of fluid shear stress appears to prompt biochemical pathways within endothelial cells during development that are required for chamber and valve morphogenesis (Santhanakrishnan and Miller, 2011). In developing chicks, left atrial ligation shapes how myofibers in the embryonic

heart form during cardiac morphogenesis and therefore impacts chamber dimensions specifically in the ventricle (Tobita et al., 2005). In chicks with venous obstruction, malformations in the ventricular septum and the pharyngeal arch artery also occur (Hogers et al., 1999). These changes are outcomes of a change in shear stress in the chick (Hove et al., 2003).

Shear stress is also important in the development of bone (Piekarski and Munro, 1977). A recent study in rats has shown that osteocytes are subject to a maximum shear stress stimulus but can also sense low-fluid shear stress (Verbruggen et al., 2014). Rosa and colleagues suggest that shear stress is the stimuli most recognized by osteocytes in comparison with mechanical strain (Rosa et al., 2015). This shows that shear stress is an important factor not only in cardiac morphogenesis, but also bone morphogenesis.

In zebrafish, the bead obstruction experiments by Hove et al (2003) suggest that hearts developing in conditions of impaired cardiac flow demonstrate three major phenotypes: an absent or malformed bulbus, abnormal cardiac looping, and abnormal development of the inflow and outflow tracts (Hove et al., 2003). Blood flow is also critical in the developing valves themselves for cell shape changes and leaflet invagination in zebrafish (Vermot et al., 2009). Stopping blood flow in zebrafish embryos by bead implantation results in erythrocyte accumulation within the heart chambers, leading to defects to the embryonic heart (Hove et al., 2003). These defects result in a dramatic reduction of shear forces against the heart and phenotypes mentioned above (Hove et al., 2003).

Genetic studies indicate that epidermal growth factor receptor tyrosine kinase (EGFR) has cardiovascular function in zebrafish (Goishi et al., 2003). Inhibiting EGFR in zebrafish by

EGFR kinase inhibitors and EGFR morpholinos results in impeded outflow into the aorta, impeded circulation in the axial and intersegmental vessels, and dilated pericardial sacs and heart chambers (Goishi et al., 2003). These phenotypes suggest that EGFR has a function in cardiovascular development, so manipulating EGFR can help determine whether shear forces have an impact on the formulation of the heart (Goishi et al., 2003).

Hove and colleagues performed studies to determine if shear stress has an impact on the development of the embryonic heart and by what mechanism, which involved looking at the levels of gene expression in cardiac endothelial cells (Hove et al., 2003; Auman et al., 2007). Flow-induced forces direct changes in cardiac endothelial cell gene expression (Davies, 1995). *In vivo* shear stress calculations predict wall shear stresses range from 2.5 dyn cm⁻² to 76 dyn cm⁻² in 36 hpf to 4.5 days post fertilization (dpf) embryos respectively (Hove et al., 2003). The stresses increase as the embryo grows and forms more blood cells. Shear stresses that are less than 1 dyn cm⁻² result in up- or down-regulation of gene expression in cardiac endothelial cells *in vitro* (Hove et al., 2003). Both the 36 hpf and the 4.5 dpf embryos demonstrate shear forces that are above the low threshold of detection by cardiac endothelial cells (Hove et al., 2003). This data suggests that shear forces play an important role in the regulation of cardiac morphogenesis during embryogenesis (Hove et al., 2003).

In chick, the changes of shear stress and aortic arch (AA) diameter are closely correlated (Kowalski et al., 2013). Throughout different stages of AA development, specifically stages 18-24, variable levels of shear stress were observed (Kowalski et al., 2013). At stages 18 and 24, shear stress levels were at 1-3 Pascals (Pa), while at stage 21 shear stress levels were in the 3-7 Pa range (Kowalski et al., 2013). The increased shear stress at the intermediate stages lead

researchers to speculate that increases in shear stress triggered changes in genetic signaling pathways that correlated with significant changes in AA growth (Kowalski et al., 2013). The decrease at stage 24 back to the original level (3-7 Pa) suggests mechanical restoration, which according to the author is a “theory introduced for biomechanically-regulated growth” (Kowalski et al., 2013). Taber’s chick embryonic studies describe how tissues respond to homeostatic or optimal loading conditions (Taber and Eggers, 1996; Taber et al., 2001). Kowalski’s computational fluid dynamics simulations determined that the diameters of AAs statistically correlate with shear stress and vessel diameter (Kowalski et al., 2013). Combining these thoughts provides a hypothesis to investigate the relationship between hemodynamics with development of cardiac vasculature to lead to insight into forms of CHD.

As the heart develops, communication needs to occur among cells, proteins, and extracellular components to relay the effects of mechanotransduction. These communications are called mechanotransduction. Mechanotransduction research is often focused on sensory cells that are near areas of dynamic change (Jaalouk and Lammerding, 2009). These cells range from hair cells in the inner ear, endothelial cells in the heart and vasculature, and cells lining the gut. Tissues must be able to respond to changes in their environment and these sensory cells can initiate the communication. The sensory cells may contain cilia which will be responsible for relaying messages to the intercellular network. In the developing heart, sensory cells have not yet been identified and mechanotransduction is not yet fully understood (Boselli et al., 2015). Current interest lies in figuring out what pathways are involved in relaying information from the sensory cells to downstream targets.

One way to observe mechanotransduction and the messages sent from one cell to another is to learn how the cells are sensing flow via molecular mechanisms. The zinc finger transcription factor Krüppel-like factor 2 (Klf2) is important in mechanisms linking shear stress signals to changes in gene expression in mammals (Dekker et al., 2005). This zinc-finger transcription factor also regulates many vasoactive endothelial genes (Lee et al., 2006). Studies in mammals have shown KLFs to be important in the control of hematopoietic and other types of cell differentiation (Oates et al., 2001). Mammalian KLFs share the same ancestral gene, Krüppel as in *Drosophila* (Nagai et al., 2009). In *Drosophila*, *Krüppel* is involved in early development and segmentation of the thorax and abdomen (Nagai et al.). Mammalian KLFs are involved in embryogenesis and fetal development (Nagai et al.). In zebrafish, *klf2a* is orthologous to the *KLF2* that is expressed in mouse and chick (Oates et al., 2001). Mouse embryos with a deficiency of *KLF2* die after E11.5 (when the atria are separating from the ventricles) from heart failure that is caused by a loss of peripheral vascular resistance resulting in defective endothelial cell function (Lee et al., 2006). Mouse *KLF2* is expressed in embryonic endocardial cells and is up-regulated by a loss of endocardial signaling in the cerebral cavernous malformation (CCM) pathway (Zhou et al., 2015). The CCM pathway is responsible for preventing postnatal vascular malformations and is required in endocardial cells (Zhou et al., 2015). CCM pathway genes were deleted in mice which resulted in embryonic heart failure and reduced myocardial growth (Zhou et al., 2015). Zhou and colleagues demonstrated that *KLF2* and *KLF4* are regulated by MEKK3 (a mitogen-activated protein kinase that binds CCM2 in endothelial cells) in response to fluid flow (Zhou et al., 2015).

In chick, a venous clip leads to a disruption in blood flow which results in an increase in *KLF2* mRNA levels in endothelial/endocardial cells (Groenendijk et al., 2005). The change in expression levels of *KLF2* is caused by an increase in cardiac shear stress (Groenendijk et al., 2005). A study by Groenendijk and colleagues shows that the most pronounced changes in shear stress occurred in the upstream slope of the outflow tract (Groenendijk et al., 2005). This location is susceptible to a multitude of cardiac malformations such as ventricular septal defects, semilunar valve abnormalities, and outflow tract malformations (Groenendijk et al., 2005). Since *KLF2* expression is related to shear stress changes, Groenendijk and colleagues proposed that *KLF2* mis-regulation might contribute to development of some or all of these malformations. Moreover, *KLF2* regulates the expression of other shear stress-related genes, *endothelin-1 (ET-1)* and *endothelial nitric oxide synthase (NOS-3)* (Groenendijk et al., 2005). These two genes are downstream of *KLF2* and are responsible for pathways that are involved in cardiac processes (Figure 1.4) (Groenendijk et al., 2005).

Studies in zebrafish have also supported a critical role for *klf2a* as a flow-responsive gene. As previously mentioned, *klf2a* is a transcription factor that is responsive to shear stress and is expressed in endothelial cells (Groenendijk et al., 2005; Lee et al., 2006; Wang et al., 2011). Zebrafish *klf2a* is a flow-response gene and its expression is highest in the atrioventricular junction (AVJ) in the developing heart (Vermot et al., 2009). Genetic knockdown studies indicate that *klf2a* is essential for endocardial morphogenesis including both valve formation and endocardial cell surface area which contribute to normal heart function (Vermot et al., 2009; Dietrich et al., 2014).

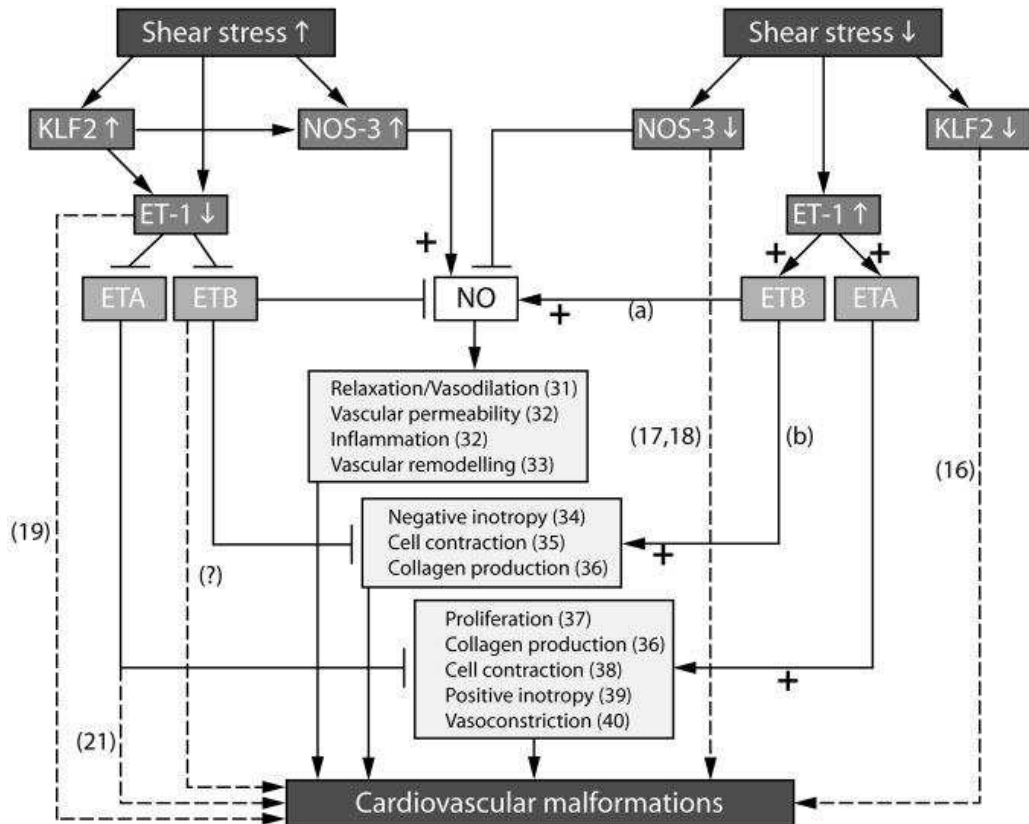


Figure 1.4 - Scheme, showing the presumed influences of altered gene expression by changes in shear stress on biological processes leading to congenital heart malformations. a, described in endothelial cells. b, described in smooth muscle cells and fibroblasts. '?' indicates unclear whether ETB deficiency results in cardiovascular malformations; +, increase in NO or the processes; interrupted arrow, knockout studies showing cardiovascular malformations. (Groenendijk et al., 2005)

In the zebrafish *sih* mutant, embryos do not have a contractile heart (Parmar et al., 2006). In *sih* homozygous embryos and other mutants with reduced, increased reversed, or absent blood flow, *klf2a* expression is down-regulated or absent and hearts exhibit increased valve dysgenesis. These data are consistent with the hypothesis that *klf2a* acts downstream of biomechanical factors related to blood flow, and is transcriptionally responsive to these forces (Parmar et al., 2006; Vermot et al., 2009). When *klf2a* is knocked down via morpholino, embryos showed the expected normal cardiac contractility and normal blood flow at 48 hpf (Dietrich et al., 2014), but the atrioventricular valves function was reduced by 96 hpf in 52% of

embryos (Vermot et al., 2009). These morphants, however, still showed similar heart rate and blood flow patterns compared to control embryos (Vermot et al., 2009).

Dietrich and colleagues found that embryos with overexpression of *klf2a* via endothelial promoter constructs showed a significant decrease in endocardial cell sizes, suggesting that *klf2a* mediates endocardial cell size in response to blood flow (Dietrich et al., 2014).

Collectively, these data suggest that *klf2a* serves as a critical molecular link mediating valve formation as a response to normal biomechanical input derived from blood flow.

There are a total of 22 Krüppel-like factors in zebrafish (ZFIN.org). Other zebrafish Krüppel-like factor genes that are paralogous to *klf2a* include *klf2b* and *klf4* (Oates et al., 2001). Klf2a is the smallest protein of the three with 347 amino acids while Klf2b and Klf4 have 363 and 409 amino acids respectively. The Klf2b and Klf4 proteins are similar to mammalian KLF2 mostly in the C-terminal region where the zinc finger domains are located (Figure 1.6A) (Oates et al., 2001). The C-terminus consists of three tandem zinc finger domains which are highly conserved throughout the KLF family members (Figure 1.5A) (Oates et al., 2001). In contrast, regions outside of the finger domains are strongly diverged throughout the KLF family (Oates et al., 2001). Zebrafish Klf2a, Klf2b, Klf4 and mouse KLF2 and KLF4 share 5 blocks of conserved sequence within the N-termini (Figure 1.5C) (Oates et al., 2001). These blocks are separated by divergent regions and contain potentially functional domains (Oates et al., 2001). Thus, these zebrafish KLF genes encode proteins with significant similarity to the mammalian protein.

Although transcriptional profiling studies do indicate cardiac expression for *klf2b*, little is known about the function of this gene other than its role as a transcription factor (Bastian et al., 2008). One study showed, by *in situ* hybridization, that at 48 hpf *klf2b* expression is present

in the central mesenchyme of the pectoral fin bud and in the adjacent cleithrum of the shoulder girdle (Yokoi et al., 2009). Based on *in situ* hybridization, no expression has been reported later than 48 hpf, although expression has been shown in ectoderm, neural crest, and periderm in early embryonic stages from 50% epiboly to 20-25 somites (Thisse, 2001).

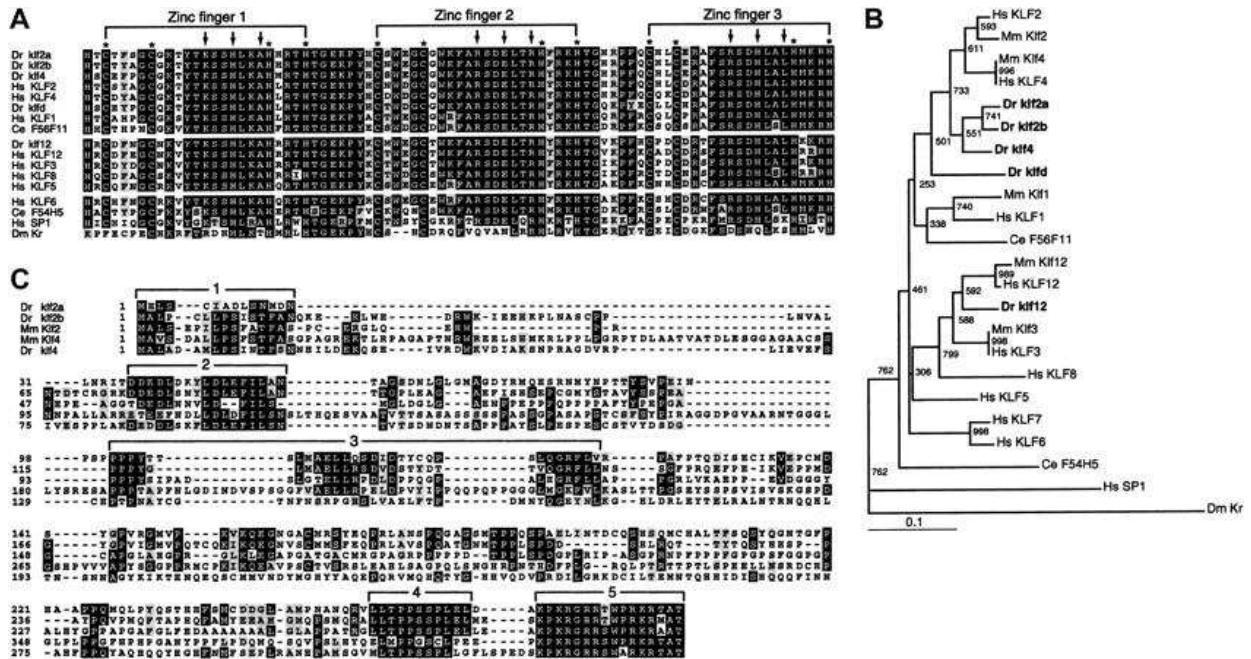


Figure 1.5 - **Evolutionary relationships among Krüppel-like factor (KLF) genes.** (A) Amino acid alignment of the C-terminal zinc finger domains of zebrafish KLF proteins with selected vertebrate KLF proteins and *Drosophila* KRUPPEL. Amino acid identity is marked with black and similarity with gray highlighting. Asterisks mark the invariant zinc-chelating residues, and the arrows indicate those residues that contact the DNA. (B) Phylogenetic tree of the evolutionary relation of zebrafish KLF genes to their close vertebrate relatives and *Drosophila* Krüppel, based on the sequences of the zinc finger domains of the respective proteins. Numbers give the bootstrap support for given nodes in the phylogram. (C) Amino acid alignment, excluding the zinc finger domain, of the N-termini of zebrafish Klf2a, Klf2b, and Klf4 proteins with their closest vertebrate relatives Klf2 (Lklf) and Klf4 (Gklf). Regions of high similarity are numbered and indicated with brackets; see text for details (Oates et al., 2001).

Expression of *klf4* was detected in the hatching gland, lateral line ganglia, neuromasts, and blood (Thisse, 2004). Depletion of *klf4* in zebrafish via morpholino led to anemia, pericardial edema, hatching defects, and a defect in hemoglobinisation of the red blood cells (Gardiner et al., 2007; Bastian et al., 2008). In mice and human endothelial cells, *klf4* regulates

endothelial inflammation (Hamik et al., 2007). *klf4* also plays a role in dedifferentiation and reprogramming of somatic cells, and is under intense study as a mediator of induced pluripotency in the generation of iPS cells (Christen et al., 2010). In *bungee* mutant zebrafish, a missense mutation in the zebrafish *protein kinase D2* (*pkd2*) gene caused valve formation to be perturbed by depleting endocardial Notch signaling in cardiac cushions (Just et al., 2011). In these mutant hearts, *klf2a* and *klf4* RNA levels are severely reduced at the AV boundary and the cardiac outflow tract (Just et al., 2011). The *bng* mutants do not form AV valves (Just et al., 2011). *klf2a* regulates Notch expression and is necessary for valve formation (Parker et al., 2014). The role of *klf4* in regulating valve formation has not yet been determined, but its cardiac expression and altered phenotype in *bng* mutants suggest a potential contribution to valve formation.

Since *klf2a* is a known flow response gene, to understand its mechanism, Vermot and colleagues' blood flow was altered by altering blood viscosity and modulating pacemaker activity in zebrafish (Vermot et al., 2009). These researchers manipulated a gene that encodes hematopoietic transcription factor *gata2*. Along with *gata1*, *gata2* is a hematopoietic transcription factor that is expressed during early embryogenesis (Stainier et al., 1995). Zebrafish embryos that are homozygous for a loss-of-function mutation in *gata2* show a significant loss in hematopoietic stem cells, but have no malformations in vasculature (Stainier et al., 1995). This result makes knocking down *gata2* ideal for identifying phenotypes associated with change in shear stress and reverse flow since no other consequences in the vascular system or overall body plan are observed. The data shown in Figure 1.8 represents the phenotypes obtained when *gata1* or *gata2* were knocked down via morpholino (Vermot et al.,

2009). Two main outcomes associated with this gene knockdown include lowered blood viscosity and altered hematocrit levels (Figure 1.8) (Vermot et al., 2009). Normally, wild type embryos exhibit a reverse flow fraction of 35% (Vermot et al., 2009). When morpholinos were injected (separately), *gata1* morphant embryos demonstrated increased RFF (45% of the cardiac cycle), hematocrit levels were reduced 90%, but embryos still developed normal valves at 96 hpf. In contrast, *gata2* morphant embryos demonstrated decreased RFF (17%), hematocrit levels were reduced by 70%, and embryos exhibited severe valve defects (Vermot et al., 2009). This great reduction in reverse flow leads to 36% of embryos with normal valve development compared to 100% in the control and 78% in the *gata1* knockdown (Vermot et al., 2009). These data indicate that surprisingly, RFF rather than hematocrit levels per se, was the phenotype associated with valve dysgenesis. To further determine whether valve dysgenesis was related to a decrease in RFF, the effects of double *gata* knockdown were explored. When *gata1* and *gata2* were injected simultaneously, RFF was close to wildtype levels at 50%, hematocrit was severely reduced, and valve formation was normal (Vermot et al., 2009). Collectively, these data pinpoint appropriate amounts of RFF as a necessary factor for normal valve development (Vermot et al., 2009).

Reverse blood flow has been examined in other species as well. In response to hypoxia at 5% and 10% oxygen levels, quail embryos show an increase in reverse flow in about half of the tested specimens (Gu et al., 2012). Gu and colleagues did not report whether chick embryos developed any developmental defects associated with acute hypoxia. However, heart rate was noticeably slower, with some embryos skipping beats, eventually leading to death (Gu et al., 2012). This study was done in quail embryos before valve development, around the stage of

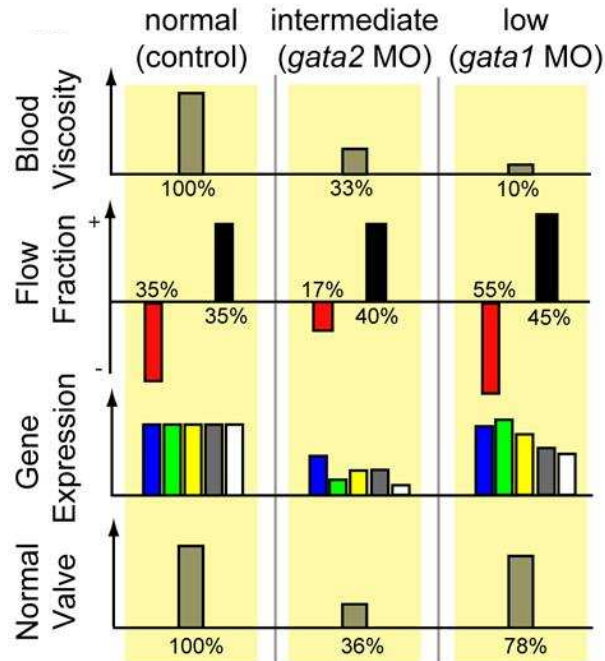


Figure 1.8 – **Overview of outcomes by manipulating oscillatory flow by decreasing circulating blood cells.** Outline showing results of morpholino injections versus control. Gene expression color code (in order): *bmp4*, *notch1b*, *edn1*, *nrg1*, *klf2a* (Vermot et al., 2009).

A second method for manipulating flow dynamics in the embryonic heart arose from our study of filamin C (*flnc*), a sarcomeric protein expressed exclusively in skeletal and cardiac muscle (Valdes-Mas et al., 2014). Human filamin C mutations result in a filamin-related myofibrillar myopathy (Ruparelia et al., 2012). Myofibrillar myopathies (MFM) are a result of muscle dissolutions or muscle break down, starting at the Z-disc. In skeletal muscle of MFM patients, aggregation of sarcomeric proteins and fibril fibrosis (tissue thickening) is exhibited (Ruparelia et al., 2012; Valdes-Mas et al., 2014). Clinical studies show that patients with *flnc* mutations have a higher frequency of cardiac death (Valdes-Mas et al., 2014). Although its precise role is not known, *flnc* is implicated in familial human hypertrophic cardiomyopathy (Valdes-Mas et al., 2014).

Ruparelia and colleagues described a *filamin Cb (flncb)* zebrafish mutant called *stretched out (sot)* (Ruparelia et al., 2012). *sot* mutants demonstrated defects in muscle and motor neuron development, specifically in the integrity of slow muscle fibers (Figure 1.9a) (Birely et al., 2005). The zebrafish genome also encodes a *filamin Cb* paralog, *filamin Ca*. When both genes are knocked down via morpholino, the somites show failure to develop or maintain almost all slow muscle fibers (Figure 1.9a) (Ruparelia et al., 2012). Unlike *sot (flncb)* mutants, the double *flnc* knockout also affects fast muscle fibers (Ruparelia et al., 2012). Although the *flnc* depletion phenotypes for skeletal muscle were reported, (Ruparelia et al., 2012), cardiac phenotypes are not yet described. Skeletal muscle and cardiac muscle are similar in that both are striated, exhibit strong contractions, and contain sarcomeres – the contractile unit of muscle. In skeletal muscle, filamin C is a key component of muscle integrity and is localized at the junction of the Z-disc and the sarcolemma, known as the costamere (Ruparelia et al., 2012). Filamin C plays an important role in the maintenance of muscle structure especially during the onset of contraction (Thompson et al., 2000; Ruparelia et al., 2012). The main role of cardiac muscle is contraction which is responsible for moving blood throughout the body. Failure to maintain muscle structure in the heart could lead to devastating effects for the organism. A study examining hypertrophic cardiomyopathy (HCM) identified *filamin C* has a potential gene implicated in this human disease (Valdes-Mas et al., 2014). Valdes-Mas and colleagues describe multiple *flnc* variants within families who have a history of HCM and show that these variants affect cardiac muscle structure (Valdes-Mas et al., 2014).

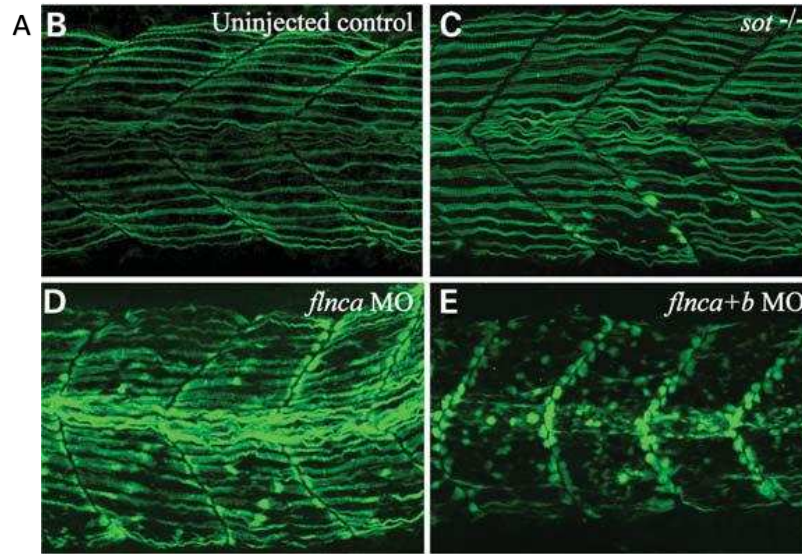


Figure 1.9a – *sot*, *filamin Cb* MO, *filamin Ca* MO, and *filamin Ca+Cb* MO phenotypes (B) Slow myosin heavy chain antibody labeling of uninjected control embryos at the 26-somite stage showing normal striated muscle fibers. (C) Sporadic failure of slow muscle fibers and the aggregation of myosin at the somatic boundaries is evident in *sot* mutants and *flnca* morphants (*flnca* MO). (E) Loss of both filamin C proteins results in failure of all slow muscle fibers (Ruparelia et al., 2012).

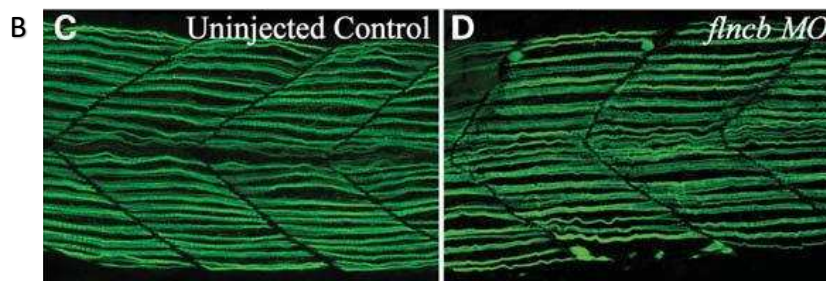


Figure 1.9b – *sot*, *filamin Cb* MO, *filamin Ca* MO, and *filamin Ca+Cb* MO phenotypes (C and D) F59 antibody labeling of slow muscle in uninjected (C) and *flncb* morpholino-injected embryos (D) showing reproduction of the *sot* phenotype (Ruparelia et al., 2012).

This study will examine how biomechanical factors such as flow and cardiac contraction impact gene expression of flow response genes or the formation of chambers and valves. Using tools such as morpholinos, high speed imaging, and qPCR, we investigated hypotheses of how shear stress and reverse flow impact the developing heart. The anticipated outcome of the study is to identify biomechanical factors that may play a role in atherosclerosis, cardiomyopathies, and other heart malformations.

In Aim 1, we observed the expression levels of *klf2a*, *klf2b*, and *klf4* via RT-PCR in both whole embryos and embryonic hearts, and *in situ* hybridization. In Aim 2, we examined the influence that shear stress and reverse flow exerts on the expression of *klfs* in the developing zebrafish heart. We manipulated the expression of two genes to alter shear stress and reverse flow.

First, to extend the study of Vermot and colleagues on the role of reverse flow on *klf2a* expression, we knocked down *gata2* and examine the expression levels of *klf2a*, *klf2b*, and *klf4* (using *klf2a* as an expected positive control) in zebrafish hearts at 56 hpf. At 48 hpf, high speed imaging will accurately measure reverse blood flow fractions as well as shear rate (frictional force within the heart caused by blood flow) in response to the lowered blood viscosity. This data will then be analyzed together to see how changes in blood viscosity affect the expression of *klf2b* and *klf4*, compared with *klf2a*.

Second, using the recent findings from our lab regarding *flncb*, we will use morpholinos to knock down this gene to investigate whether there are changes in shear stress and reverse flow in response to a change in muscle structure and perhaps contractility. Videos of these morphants were observed in our lab and a visible increase in reverse flow was noted, hinting that flow patterns in the embryonic heart are abnormal. After videos are analyzed to provide quantitative information on the hemodynamics in the 48 hpf heart, we will then dissect embryonic hearts at 56 hpf to collect RNA. We will then explore expression levels of *klf2a*, *klf2b*, and *klf4* in response to the knockdown of *flncb*.

Together, this data will provide insight into the hemodynamics of the wildtype embryonic heart compared to hemodynamics in response to a change in blood viscosity or

heart contractility. This project will provide data that will show that hemodynamics is an important contributor to the morphology of the developing heart, which will provide insights into congenital heart diseases.

CHAPTER 2: INTRODUCTION

Congenital heart defects are birth defects estimated to arise every 50 per 1000 births (Pierpont et al., 2007). To investigate mechanisms that may cause congenital heart defects, model organisms such as the mouse, chick, and zebrafish are very useful. The mouse is a model organism for developmental biology because it is a mammal. However, offspring develop inside of the mother so they are not ideal for observing early development. The chick is a tool for developmental biology because chickens generate large eggs that develop outside of the mother while a downside is that offspring are generated in lower yields. Zebrafish are ideal because they are vertebrates, their heart develops similarly to human hearts, they have transparent embryos that develop outside of the mother, and they give clutches of embryos in the hundreds.

Hemodynamics is the study of blood flow. Reverse flow, blood pressure, and shear stress are examples of important variables in hemodynamics. In the present study, we focus on analyzing reverse flow and shear rate through the heart. Previously, Vermot and colleagues found that reverse flow and shear stress are important for valve development in zebrafish (Vermot et al., 2009). We can improve on this study by more accurately measuring reverse flow through the heart by using blood volume fractions rather than time fractions. Here, shear rate will be analyzed as a factor instead of shear stress because we argue that viscosity should not be presumed to act as a set integer given that hemodynamics conditions in the heart are not constant.

In this study, we have analyzed reverse flow and shear rate in embryos depleted for *gata2* and *flnbc* using morpholino antisense oligonucleotides. The *gata2* transcription factor is responsible for blood cell differentiation and when knocked down will result in lowered blood hematocrit, and therefore, lowered blood viscosity (Galloway et al., 2005). The *flnbc* sarcomeric protein contributes to cardiac and skeletal muscle structure and when knocked down is predicted to result in a change in cardiac contractility (Ruparelia et al., 2012). Knocking down these two genes down by morpholino is an approach to manipulate reverse flow and shear rate in two different ways. In embryos knocked down for either gene, we observed survival, day four phenotypes, heart rate, cardiac output, reverse flow, shear rate, velocity of the blood, and gene expression.

In wildtype or knockdown embryo hearts, we analyzed *klf2a*, *klf2b*, and *klf4* via qPCR for changes in expression levels that occur in response to lowered blood viscosity and changes in contractility. As described in Chapter 1, *klf2a* is a known flow response gene (Dekker et al., 2002). We hypothesize that *klf2b* and *klf4* are functionally similar to *klf2a* and are also flow response genes.

In addition to analyzing potential flow response genes, we want to observe specific changes in cardiac function of the heart in response to lowered blood viscosity and changes in contractility. We hypothesize that lowered blood viscosity will result in reduced reverse flow and reduced shear rate through the AVJ. In hearts with altered contractility, we hypothesize that these embryos will exhibit increased reverse flow with increased shear rate.

Utilizing the data gained from this study, we will be able to understand how our target genes *klf2a*, *klf2b*, and *klf4* change in expression level in response to changes in hemodynamics,

and how contractility and changes in blood viscosity alter expression levels and hemodynamics.

This information will allow future researchers to connect what genes are important in identifying mechanisms of congenital heart defects.

CHAPTER 3: RESULTS

klf2a, *klf2b*, and *klf4* are expressed at time points crucial to heart development in the embryo

To determine that our target genes are expressed in the embryo at times that are relevant to heart development, we performed RT-PCR using whole embryo RNA at a number of development stages. Heart progenitors are present as early as five hours post fertilization (hpf) (Bakkers, 2011). We started our developmental RT-PCR at two hpf in order to see if the genes were expressed before the cardiac progenitors are present. Figure 3.1 shows the results of the developmental RT-PCR using whole embryos. *klf2a*, *klf2b*, and *klf4* are all expressed from two hpf to 72 hpf in whole embryos. Therefore, they are expressed at times crucial to heart development in the embryonic zebrafish.

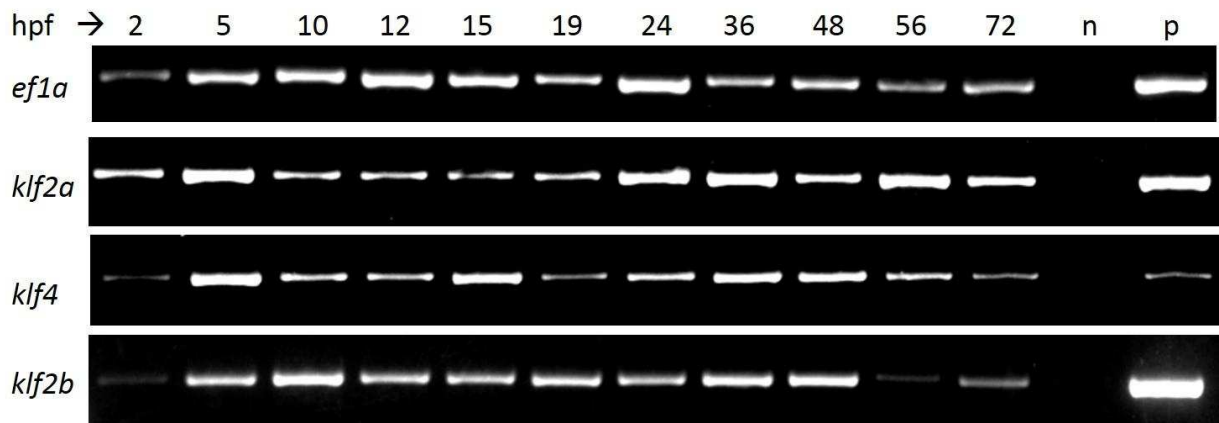


Figure 3.1 – *klf2a*, *klf2b*, and *klf4* are expressed in early development. Whole embryo RT-PCR using gene-specific primers. *klf2a*, *klf2b*, and *klf4*, are expressed from two hpf to 72 hpf. *Elongation factor 1 α* (*ef1 α*) is used as a positive control.

klf2a, *klf2b*, and *klf4* are expressed specifically in the heart

To determine whether *klf2a*, *klf2b*, and *klf4* are expressed specifically in the heart, we next tested for expression at stages including the heart tube (around 24 hpf) to the beginnings of valve formation (96 hpf) (Figure 3.2a). *klf2a* and *klf4* are expressed in all stages examined, but *klf2b* does not have detectable expression until 48 hpf in the heart.

Since *klf4* is an early marker of blood in the zebrafish, and expressed highly in the hematopoietic system (Oates et al., 2001; Gardiner et al., 2007), we needed to make sure that the expression in the heart samples was not solely due to blood still present in the heart at the time of dissection. To explore this idea, we utilized the *gata2* morpholino. By knocking down *gata2*, we were able to obtain zebrafish embryos with no blood in their circulatory system and therefore dissect hearts free of blood. The PCR experiment with *gata2* morpholino-injected embryos and non-injected wildtype embryos used cDNA that was extracted from embryos at 72 hpf and 96 hpf, times in which blood is robustly circulating through the heart. We hypothesized that *klf4* expression was not solely due to blood that was present in the heart, but due to actually being expressed in heart tissue. In the PCR results, *klf4* is still detected in extracted hearts that contain no blood (Figure 3.2b).

To determine the location of *klf2a*, *klf2b*, and *klf4* expression in the heart, we performed *in situ* hybridization in wildtype embryos. *cmhc2* (a cardiac myofibril assembly protein expressed throughout the heart) provided a positive control to show where the heart tissue was located at each stage (Figure 3.3). Hearts were outlined and placed on to their respective stages to show cardiac expression. *klf2a* was expressed in the heart at 36, 48, 56, 72, and 96 hpf (Figure 3.3). Expression of *klf2a* was observed in the AVJ. *klf2b* expression was found at 36, 48, 56, 72,

and 96 hpf (Figure 3.3). *klf2b* expression was located in the ventricle and AVJ from 48 to 96 hpf. *klf4* expression was detected at 36 and 48 hpf in the hatching gland (Figure 3.3). No detectable expression of each gene was found at 24 hpf (Figure 3.3). Cardiac expression for *klf2a* and *klf2b* is restricted to the AVJ and ventricle. This seems to be consistent throughout heart development up to 96 hpf.

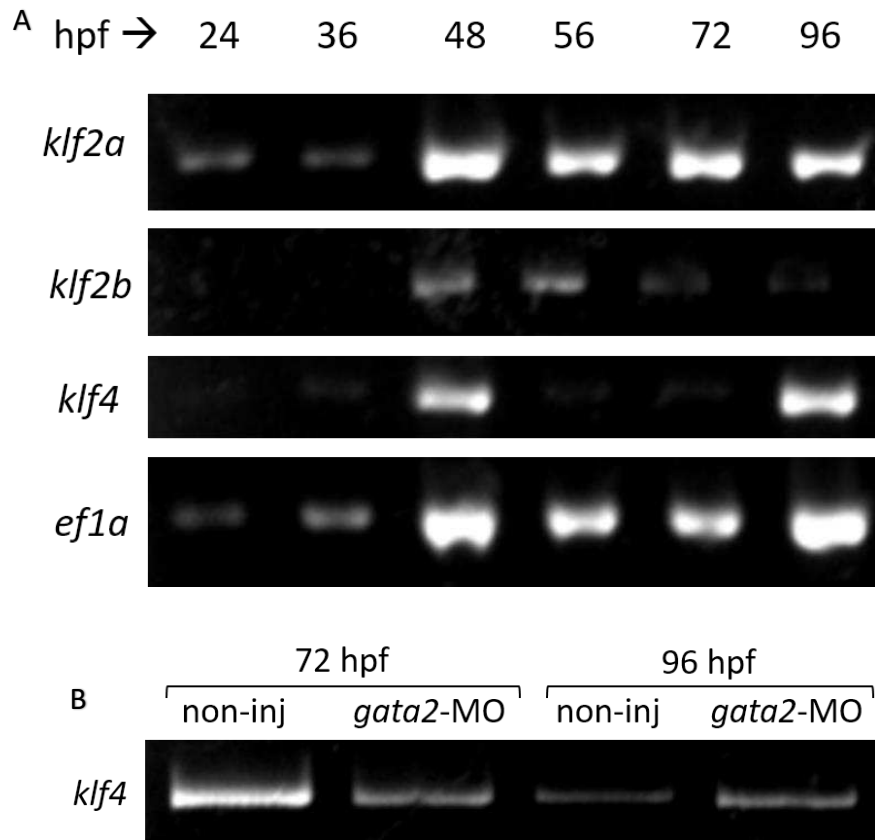


Figure 3.2 – *klf2a*, *klf2b*, and *klf4* are expressed in the embryonic zebrafish heart. RT-PCR of isolated heart cDNA at stages encompassing early heart development. cDNA was transcribed using 2 micrograms of RNA. A – Expression patterns of *klf2a*, *klf2b*, and *klf4* in embryonic stages during heart development. B – Comparing *klf4* expression patterns in embryos with no blood (*gata2* –MO) versus non-injected control embryos at both 72 hpf and 96 hpf shows that *klf4* is expressed in the heart when no blood is present.

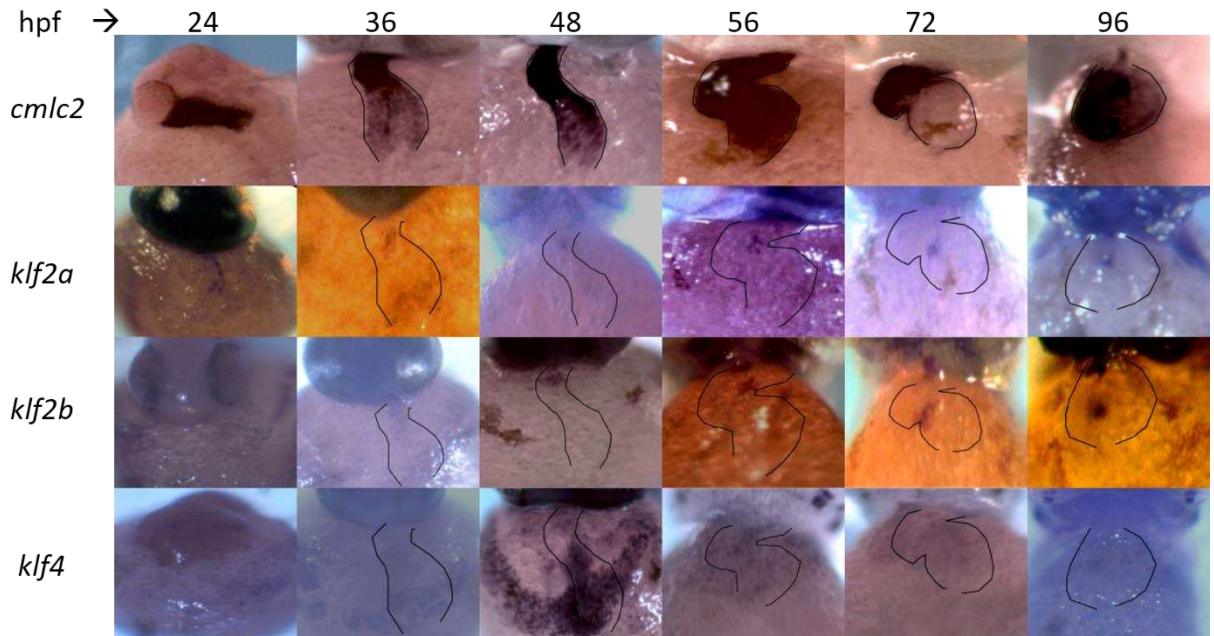


Figure 3.3 – Cardiac expression locations of *cm1c2*, *klf4*, *klf2a*, and *klf2b*. *In situ* hybridization showing expression locations of *klf2a*, *klf2b*, and *klf4*. Gene expression for *klf2a*, *klf2b*, and *klf4* is found in the heart at stages corresponding to heart development. *cm1c2* is used as a positive control to show location and shape of heart at each stage. Hearts are outlined and transposed on respective stages.

Decreased blood viscosity results in severe cardiac phenotypes and embryonic lethality

Once we determined expression patterns of *klf2a*, *klf2b*, and *klf4*, we investigated the effect of hemodynamics on heart development. Using depletion of *gata2*, we lowered blood viscosity in embryos. To observe how embryos with decreased blood viscosity are affected over a period of time, embryos were kept for ten days after injections and scored for survival (Figure 3.4a). The *gata2* morpholino results in lowered blood viscosity in the embryo. In addition, observations were made on the fourth day to investigate late-stage heart phenotypes compared to control embryos (Figure 3.4b). Embryos were scored for the following phenotypes: death, cardiac edema (edema around pericardial sac), stringy heart (heart that does not form ballooned chambers), low or no blood flow, reduced blood flow (visually reduced from wildtype blood flow, but flowing blood still present), wild-type blood flow, non-compact

heart (heart does not compact), no ventricle contraction (silent ventricle), weak or arrhythmic contractions, small chambers (chambers are visibly smaller than wildtype), other body edema (edema not related to pericardial sac, e.g. over the yolk sac), body axis defects (defects that affect patterning of body axis). Overall, embryos with lowered blood viscosity survived well, but the morphology of these embryos was altered, affecting the structure of the heart and impacting flow through the heart (Figure 3.4). These results show that a decrease in blood viscosity results in morphological cardiac defects with a modest effect on survival.

Changes in contractility results in severe cardiac phenotypes and embryonic lethality

Our next approach to determining the effect of hemodynamics on cardiac morphogenesis is to deplete *fn1cb*. The knockdown of *fn1cb* results in a change in muscle structure due to *fn1cb* encoding a sarcomeric protein found in skeletal and cardiac muscle (Ruparelia et al., 2012). With this change in a sarcomeric protein comes a change in contractility which results in disrupted flow through the embryonic heart. The embryos with a change in contractility were tracked for survival rates and observed on day four of development for cardiac phenotypes (Figure 3.5). Non-injected wildtype embryos and 25N control morpholino-injected embryos showed overtly normal development (with the exception of one embryo in 25N control morpholino-injected group dying), but the *fn1cb* morpholino-injected embryos exhibited phenotypes such as: wildtype, death, cardiac edema, stringy heart, low or no blood flow, left/right asymmetry (where the heart loops with the ventricle on the left and atrium on the right), and silent ventricle (Figure 3.5b). 25N control morpholinos consist of 25 random base pairs in order to control for the morpholino injection. Compared to embryos with lowered

blood viscosity, the embryos with a change in cardiac contractility exhibited less effect on visible morphology and flow in the embryonic heart. These results show that a change in contractility and muscle structure of the heart overtly affected flow in at least 25% of embryos and produced modest morphological cardiac defects and death in about 20% of embryos.

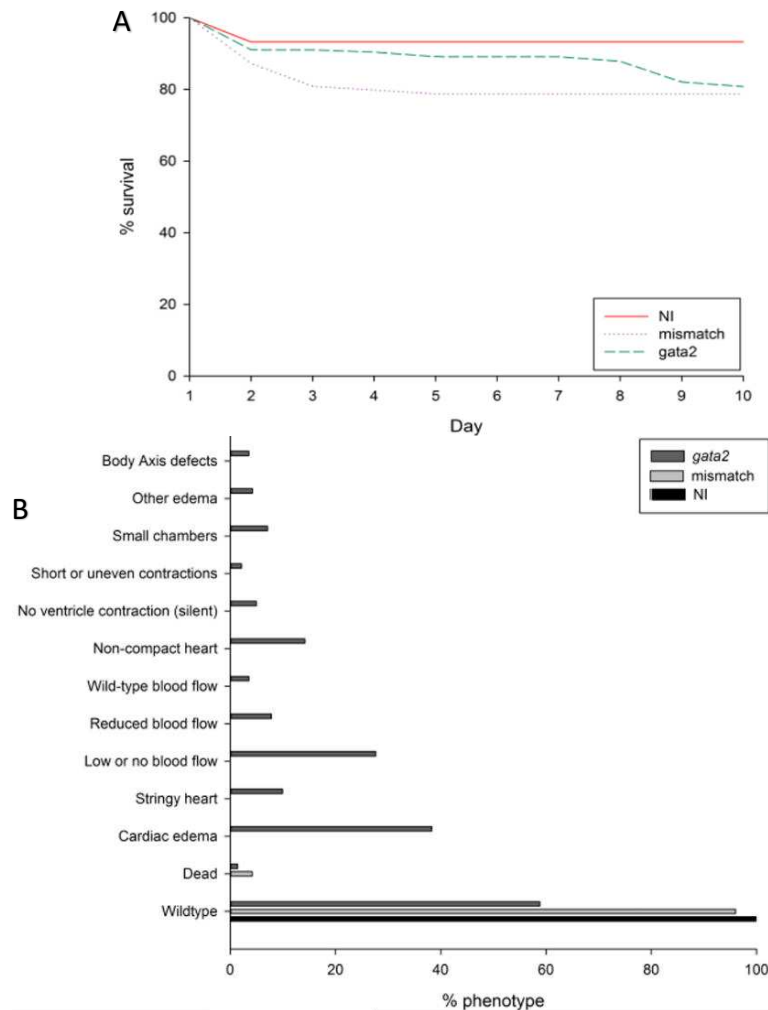


Figure 3.4 – **Survival rate and four day phenotypes for *gata2* morpholino-injected embryos.** A – Survival rates of *gata2* morpholino-injected embryos (n=156), *gata2* mismatch morpholino-injected embryos (n=94), and non-injected wildtype embryos (n=59). On day 10, 80.8% of *gata2* morpholino-injected embryos were still alive. 78.7% of *gata2* mismatch morpholino-injected embryos were still alive and 93.2% of non-injected wildtype embryos were alive. B – Phenotypes on day four are shown. All non-injected wildtype embryos exhibited normal development (n=37). 96.0% of the *gata2* mismatch morpholino-injected embryos were wildtype with 4.2% dead (n=25). *gata2* morpholino-injected embryos exhibited a multitude of phenotypes: 58.9% were wildtype, 1.4% were dead, 38.3% had cardiac edema, 10.0% had a stringy heart, 27.7% had little to no blood flow, 7.8% had reduced blood flow, 3.6% had wildtype blood flow (not counting wildtype), 14.1% had non-compact heart, 5.0% had a silent ventricle, 2.1% had short or uneven contractions, 7.1% had small chambers, 4.3% had edema unrelated to the pericardial sac, and 3.6% had body axis defects (n=140).

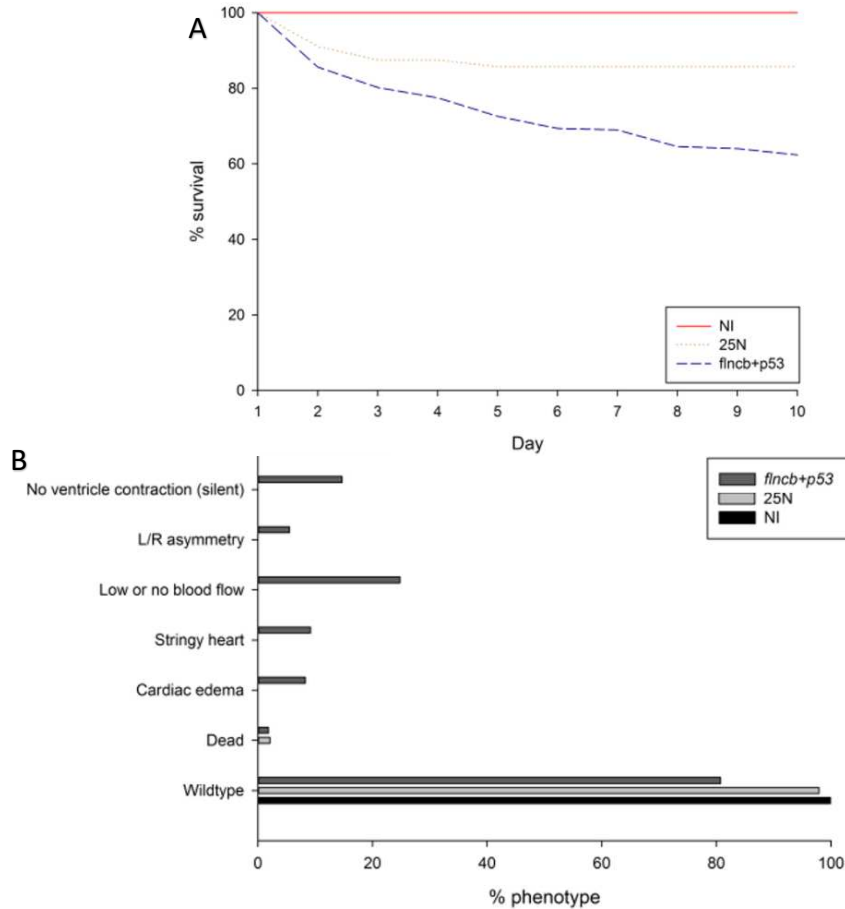


Figure 3.5 – **Survival rate and four day phenotypes for *flncb* morpholino-injected embryos.** A – Survival rates of *flncb* morpholino-injected embryos (n=111), 25N control morpholino-injected embryos (n=56), and non-injected wildtype embryos (n=17). On day 10, 62.3% of *flncb* morpholino-injected embryos were still alive, while 85.7% of 25N control morpholino-injected embryos were still alive. 100% of non-injected wildtype embryos survived. B – Phenotypes of day four embryos. 100% of the non-injected wildtype embryos were wildtype (n=9). 97.9% of 25N control morpholino-injected embryos were wildtype while 2.1% were dead on day four (n=48). *flncb* morpholino-injected embryos exhibited many phenotypes: 80.7% were wildtype, 1.8% were dead, 8.3% had cardiac edema, 9.2% had a stringy heart, 24.8% had low or no blood flow, 5.5% had left/right asymmetry, and 14.7% had a silent ventricle (n=109).

Changes in hemodynamic patterns occur in the atrioventricular junction in embryos with decreased blood viscosity

Reverse flow in the AVJ is defined as the portion of blood that is moving through in the reverse direction. Previously, Vermot and colleagues used the same *gata2* morpholino to assess reverse flow (Vermot et al., 2009). They found that reverse flow is decreased in response to lowered blood viscosity (Vermot et al., 2009). In their study, they measured reverse flow

fraction by taking the total number of frames that exhibited reverse flow in their high speed videos and dividing that number by the total number of frames per cycle. Thus RFF^{Vermot} represents the fraction of time in one cardiac cycle during which reverse flow occurs. (Vermot et al., 2009). Note that this approach does not measure blood volume directly. Vermot and colleagues found that in non-injected wildtype embryos, 35% of the cardiac cycle contained reverse flow (Vermot et al., 2009). Therefore, reverse flow is a normal feature in early developmental stages, prior to valve development at the AVJ. By measuring the time dependent fraction (RFF^{Vermot}) we find that there is a significant decrease of reverse flow in response to lowered blood cell count (Figure 3.6a). However, we detected a reverse flow time fraction of 0.9% in the *gata2* morpholino-injected embryos. Although this result is small it does result in a statistically significant result ($p < 0.05$ relative to wildtype controls). In contrast, Vermot found, in *gata2* morphants, 17% of the cardiac cycle exhibited reverse flow. The difference in the magnitude of the detected RFF was a surprise, given that the same morpholino and embryos of the same age were used.

The potential limitation of measuring RFF according to time fractions is that it does not account for the size of the embryo, nor does it directly measure the amount of blood that is currently in the embryo. Johnson took advantage of the data inherent in the high speed videos to create a more accurate method for assessing RFF (Johnson et al., 2013a). Johnson measured reverse flow with reference to volume rather than time. He defined RFF as the amount of blood moving in the reverse direction in one cardiac cycle divided by the total accumulated volume in one cardiac cycle (Johnson et al., 2013b; Johnson et al., 2013a). We therefore measured $RFF^{Johnson}$ (Figure 3.6b). *gata2* morpholino-injected controls exhibited a $RFF^{Johnson}$ of 0.005

(Figure 3.6b). The *gata2* mismatch morpholino-injected control embryos and the non-injected wildtype control embryos however exhibited RFFs^{Johnson} of 0.008 and 0.017 respectively (Figure 3.6b). This method still shows a decrease in reverse flow however, no statistical significance was found between *gata2* morpholino-injected embryos and the controls via ANOVA (p=0.158).

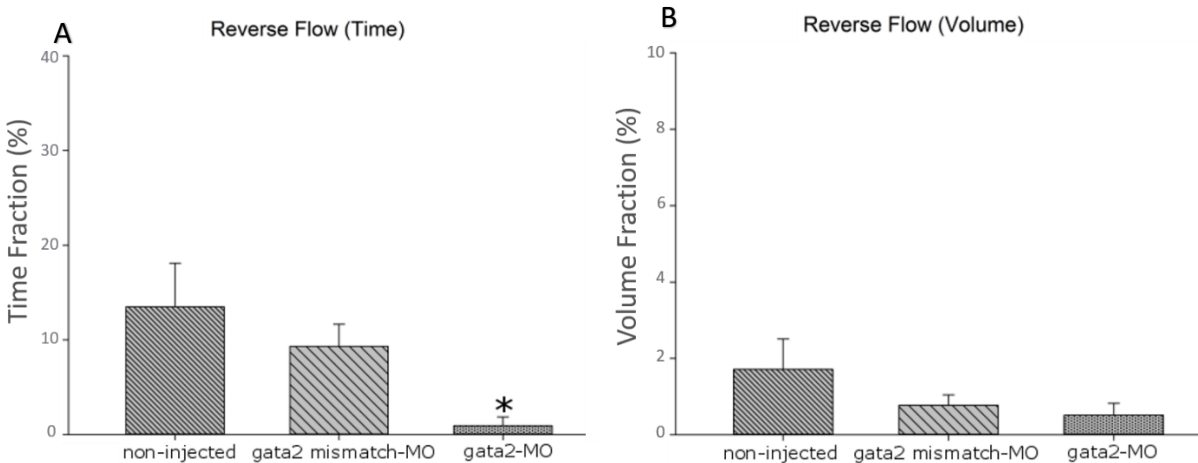


Figure 3.6 – **Average reverse flow fractions at the AVJ in *gata2* morpholino-injected embryos.** Data was collected from high speed video analyses. Error bars represent standard error of the mean. Values are unit-less ratios. A – Reverse flow fractions measured dependently on time of blood flow in one cardiac cycle. *gata2* morpholino-injected embryos (n=16) with a reverse flow time fraction of 0.009 show a significant decrease in reverse flow compared to the controls. *gata2* mismatch morpholino-injected embryos (n=30) had a reverse flow time fraction of 0.093 and non-injected wildtype embryos (n=17), 0.135. *p<0.05, Dunn’s method. ANOVA p=0.008. B – Reverse flow fraction measured with volumes of blood through the AVJ. No significant difference was found in *gata2* morpholino-injected embryos with a reverse flow volume fraction of 0.005 compared to *gata2* mismatch morpholino-injected embryos’ reverse flow volume fraction of 0.008 and non-injected wildtype embryos’ reverse flow volume fraction of 0.017. ANOVA p=0.158.

Reduced blood flow changes heart rate but does not affect the overall function of the embryonic heart

To understand how decreased blood viscosity affects heart rate and cardiac output, we analyzed high speed videos of the embryonic heart. Videos were taken ventrally at 48 hpf in *gata2* morpholino-injected embryos, *gata2* mismatch morpholino-injected embryos, and non-injected wildtype embryos. Heart rate was measured by kymographs analyzed in a MATLAB program developed by Brennan Johnson, a previous lab member, as described (Johnson et al.,

2013a). In embryos with reduced blood viscosity, heart rate was significantly decreased in comparison to the non-injected wildtype embryos (Figure 3.7a). Surprisingly, heart rate was also significantly decreased in the *gata2* mismatch morpholino-injected embryos, designed to serve as a gene-specific morpholino control.

Using the high speed imaging analyses, the accumulated volume (volume of blood that has passed through the atrioventricular junction (AVJ) over one cardiac cycle) can also be measured to estimate the stroke volume, which is defined as the net volume of blood pumped to the body per stroke (Johnson et al., 2013a). Stroke volume is an estimate based on the velocity (speed) of the blood moving through the AVJ and the diameter at the AVJ (Johnson et al., 2013a).

We hypothesized that lowering blood viscosity would alter stroke volume and therefore overall cardiac function of the heart. However, stroke volume in the *gata2* morpholino-injected embryos was not significantly different from the stroke volume in the non-injected wildtype embryos or mismatch control embryos, based on ANOVA ($p=0.553$) (Figure 3.7b).

Cardiac output is measured by multiplying stroke volume by heart rate. Cardiac output was not statistically different among the three treatments, based on ANOVA ($p=0.766$) (Figure 3.7c). The similarity between the cardiac outputs of the three groups shows that a reduction in blood viscosity did not influence on these measures of cardiac function by 48 hpf.

Decreasing the blood viscosity does not affect the velocity of blood through the atrioventricular junction

Average normalized velocity represents a way to show the pattern of velocity at the AVJ varies across the cardiac cycle. In the graphs below, negative values indicate flow moving in the reverse direction. Overall, the velocity patterns in *gata2* knockdown and *fincb* knockdown embryos appear to be highly similar to wildtype except for the portion of the cycle during which reverse flow is occurring.

Changes in blood viscosity have no effect on average velocity through the AVJ (Figure 3.8c). Average velocity is a calculation of the velocity over the entire cardiac cycle and is shown as a pattern through the cardiac cycle in Figure 3.8a. There is a slight increase in the *gata2* morpholino-injected embryos compared to the non-injected embryos and the *gata2* mismatch morpholino-injected embryos, but this increase is not a statistically significant difference. Therefore, the decrease in blood viscosity had no effect on average velocity of the blood through the AVJ.

To determine whether a specific part of the cycle shows differences between treatments, average velocity during 15-40% of the cardiac cycle was calculated (Figure 3.8d). A significant difference was found between *gata2* morpholino injected embryos and non-injected wildtype control embryos (Tukey test, $p < 0.01$).

The blood velocity, measured at the center of the atrioventricular junction, is an additional indicator of functional efficacy in the embryonic heart. Maximum velocity represents the highest speed the blood cells are moving through the AVJ (Figure 3.8b or the peak of the graph in Figure 3.8a). Analysis of peak values by ANOVA showed that between groups, there is

no change in maximum velocity. Therefore, the decrease in blood viscosity had no effect on maximum velocity.

Contractility changes result in an increase in reverse flow through the atrioventricular junction

To determine how a change in contractility affects reverse flow fraction at the AVJ, we measured reverse flow by both time and volume in *flncb* morpholino-injected embryos. We hypothesized that there would be an increase in reverse flow through the AVJ if the heart muscle contraction patterns were altered. The hypothesis was supported since *flncb*-depleted embryos exhibited a significant increase in reverse flow through the AVJ (Figure 3.9).

Using RFF^{Vermot} , a significant increase of reverse flow is found compared to controls (Figure 3.9a). Embryos with a change in contractility exhibited a RFF^{Vermot} of 0.283. The 25N morpholino-injected control embryos and the non-injected wildtype control embryo $RFFs^{\text{Vermot}}$ were measured at 0.125 and 0.135 respectively.

When RFF was assessed by volume (RFF^{Johnson}), the 25N morpholino-injected control embryos and the non-injected wildtype control embryo exhibited approximately 1.2 and 1.7% of the volume of blood moving in the reverse direction per cardiac cycle while *flncb* morpholino-injected embryos exhibit approximately 6% of the volume of blood moving in the reverse direction (Figure 3.9b). This difference is statistically significant ($p < 0.05$).

A change in contractility reduces heart rate but does not change the overall cardiac output of the heart

In the next set of experiments, to understand how a change in contractility affects heart rate and cardiac output, we used the *flnc* morpholino, as described earlier, to measure heart rate and stroke volume. In *flncb*-depleted embryos, in response to a change in contractility, the heart rate decreased significantly (Figure 3.10a). The decrease in heart rate of *flncb* morpholino-injected embryos is statistically significant in comparison to both the non-injected wildtype embryos ($p < 0.001$) and the 25N control morpholino-injected embryos ($p = 0.004$).

Since *flncb* morpholino injections affect cardiac muscle structure, we hypothesized that cardiac function would be disrupted. However, our hypothesis was not supported as no statistically significant difference in stroke volume was found between groups (Figure 3.10b) ($p = 0.482$).

Multiplying the heart rate and stroke volume together provides the cardiac output. Changing the heart rate by *flncb* knockdown did not show a difference in overall cardiac output of the heart (Figure 3.10c). The cardiac output for *flncb* morpholino-injected embryos were not statistically significant from the control groups (ANOVA $p = 0.241$). Therefore, decreasing the heart rate by decreasing contractility by *flncb* depletion was not sufficient to affect the cardiac output of the embryonic heart.

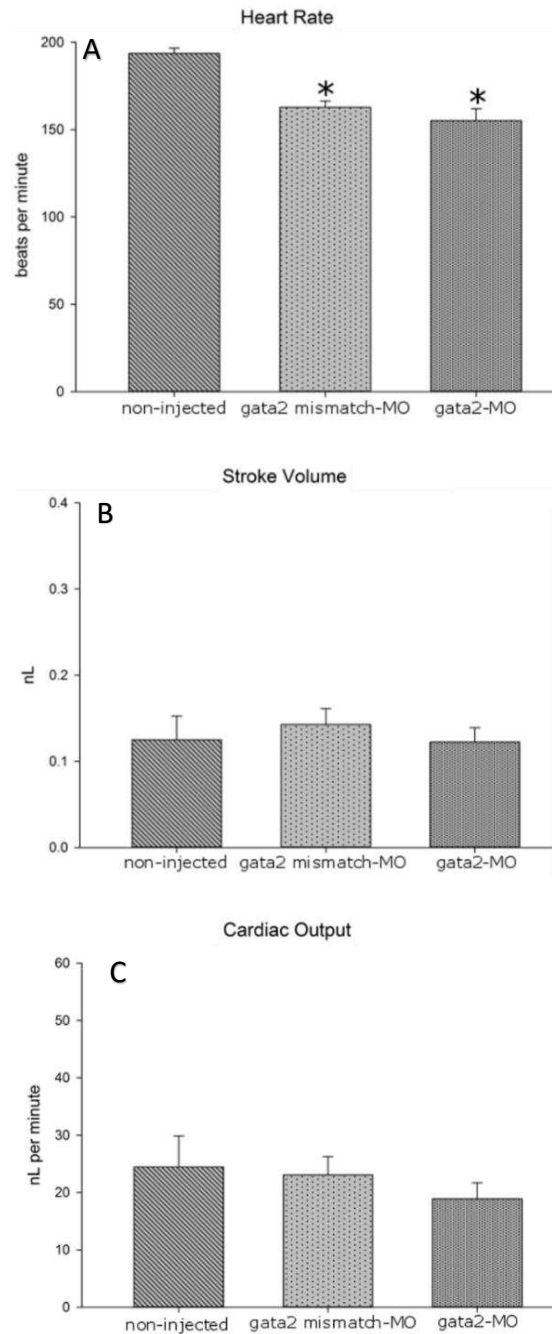


Figure 3.7 – Average means for heart rate, stroke volume, and cardiac output for *gata2* knockdowns. Data was collected from high speed video analyses. Error bars represent standard error of the mean. A – In *gata2* morpholino-injected embryos, heart rate is decreased (155.2 bpm, n=16). *gata2* mismatch morpholino-injected embryos also show a decrease in heart rate (162.7 bpm, n=30). Wildtype non-injected embryos displayed a heart rate of 193.5 bpm (n=17). * $p < 0.05$, Tukey test. ANOVA $p < 0.001$. B – *gata2* morpholino-injected embryos had a stroke volume of 0.123 nL, *gata2* mismatch morpholino-injected embryos had a stroke volume of 0.143 nL, and non-injected wildtype embryos had a stroke volume of 0.125 nL. No statistically significant difference was detected via ANOVA ($p = 0.553$). C – Cardiac output measurements between *gata2* morpholino-injected embryos, *gata2* mismatch morpholino-injected embryos, and non-injected wildtype embryos are similar. ANOVA $p = 0.766$. *gata2* morpholino-injected embryos exhibited cardiac output at a rate of 18.9 nL/min. *gata2* mismatch morpholino-injected embryos had a cardiac output rate of 23.0 nL/min and non-injected wildtype embryos saw cardiac output at 24.4 nL/min.

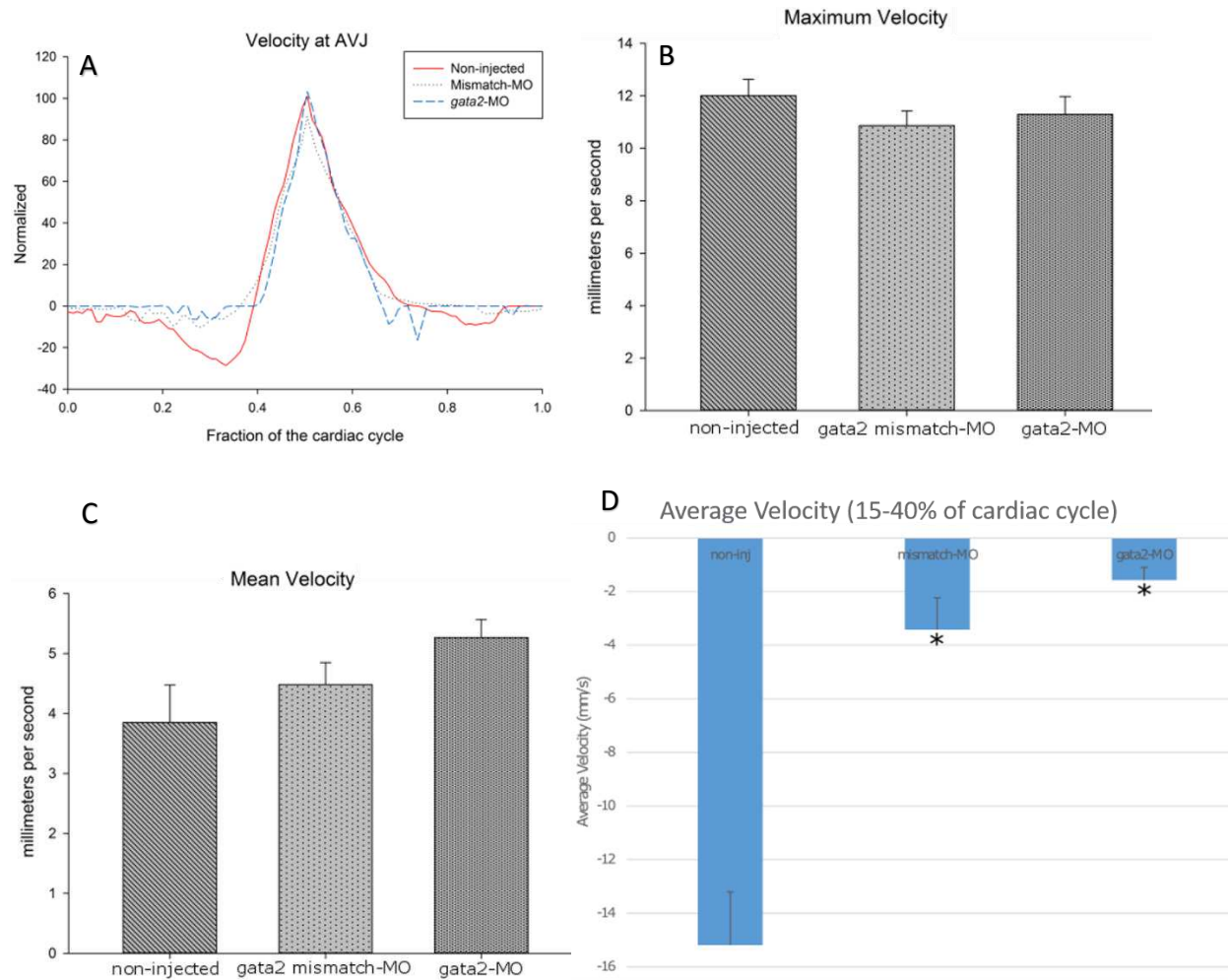


Figure 3.8 – Average means for maximum velocity and average velocity through the AVJ in *gata2* morpholino-injected embryos. Data was collected from high speed video analyses. Error bars represent standard error of the mean. A – Average normalized velocity at the AVJ across the cardiac cycle. Patterns across groups remain the same except for times where reverse flow occurs. B – No difference was found in the maximum velocity through the AVJ in hearts from each group. Maximum velocity for *gata2* morpholino-injected embryos was 11.3 mm/s (n=16). *gata2* mismatch morpholino-injected embryos had a velocity of 10.9 mm/s (n=30) and non-injected wildtype embryos, 12.0 mm/s (n=17). ANOVA p=0.299. C – A slight increase was noted in the velocity of *gata2* morpholino-injected embryos however no significant difference was present. Average velocity for *gata2* morpholino-injected embryos was 5.3 mm/s. *gata2* mismatch morpholino-injected embryos and non-injected wildtype embryos had average velocities of 4.5 mm/s and 3.9 mm/s respectively. ANOVA p=0.139. D – The average velocity 15%-40% through the cardiac cycle. *gata2* morpholino-injected embryos and 25N morpholino-injected embryos exhibited negative velocity during this early portion of the cardiac cycle, but not as negative as non-injected wildtype embryos. *gata2* morpholino-injected embryos and 25N morpholino-injected embryos are statistically significantly different than non-injected wildtype embryos. ANOVA p<0.001. Average velocity of *gata2* morpholino-injected embryos during this time point was -1.58 mm/s. Non-injected wildtype controls and 25N morpholino-injected embryos had velocities of -15.12 and -3.42 mm/s respectively. *p<0.01, Tukey test.

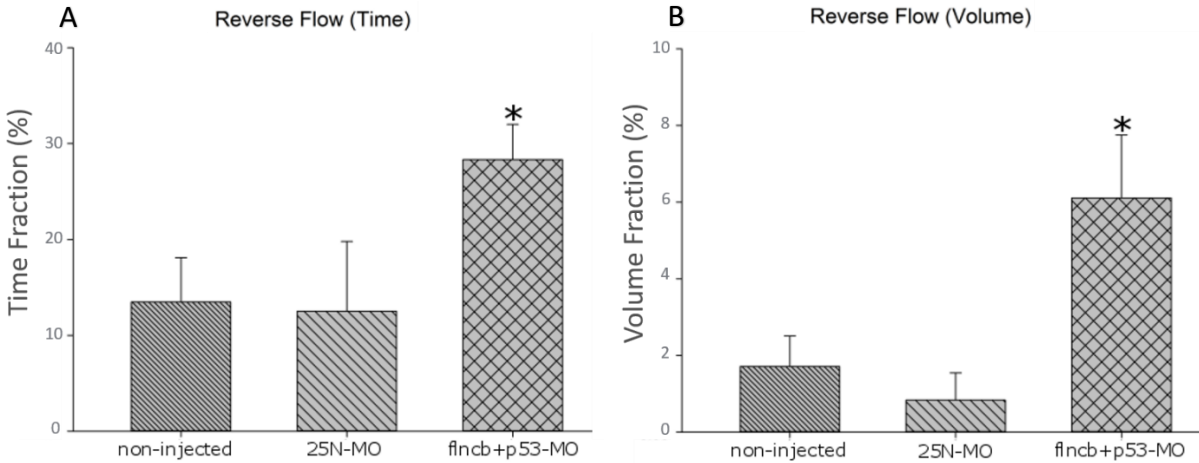


Figure 3.9 – **Average reverse flow fractions at the AVJ in *flncb* morpholino-injected embryos.** Data was collected from high speed video analyses. Error bars represent standard error of the mean. A – *flncb* morpholino-injected embryos exhibit a significant increase in reverse flow compared to controls. *flncb* morpholino-injected embryos had a reverse flow time fraction of 0.283 (n=19). 25N control morpholino-injected embryos saw a reverse flow time fraction of 0.125 (n=12) and non-injected wildtype embryos, 0.135 (n=17). *p<0.05, Dunn’s method. ANOVA p=0.011 B – The volume of blood moving in the reverse direction is much higher in *flncb* embryos than in control embryos. The *flncb* morpholino-injected embryos saw a reverse flow volume fraction of 0.06, 25N control morpholino-injected embryos – 0.012, non-injected wildtype embryos – 0.017. *p<0.05, Dunn’s method. ANOVA p<0.001.

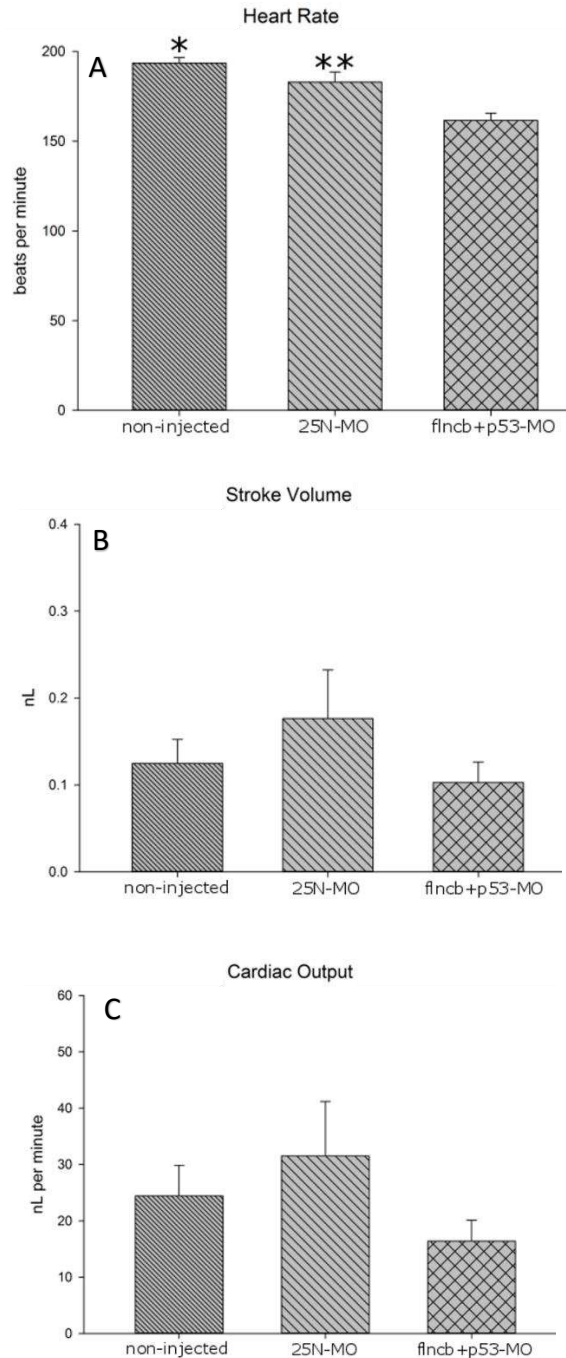


Figure 3.10 – Average means for heart rate, stroke volume, and cardiac output for *flncb* knockdowns. Data was collected from high speed video analyses. Error bars represent standard error of the mean. A – Heart rate in *flncb* morpholino-injected embryos is significantly different from both non-injected embryos and 25N control morpholino-injected embryos. *flncb* morpholino-injected embryos had a heart rate of 162.0 bpm (n=19). 25N control morpholino-injected embryos saw a heart rate of 180.9 bpm (n=12) and non-injected wildtype embryos, 193.5 bpm (n=17). *p<0.001, Tukey test. **p=0.004, Tukey test. ANOVA p<0.001. B – Stroke volumes between groups is not significantly different. *flncb* morpholino-injected embryos exhibited a stroke volume of 0.100 nl while 25N control morpholino-injected embryos had a stroke volume of 0.185 nl and non-injected wildtype embryos, 0.125 nl. ANOVA p=0.482. C – Measurements did not result in a significant difference in cardiac output. *flncb* morpholino-injected embryos saw a cardiac output rate of 16.0 nl/min, 25N control morpholino-injected embryos – 32.6 nl/min, and non-injected wildtype embryos – 24.4 nl/min. ANOVA p=0.241.

Changing contractility of the embryonic heart changes the average velocity of blood through the atrioventricular junction

To observe whether or not a change in contractility affects the velocity of blood moving through the AVJ, we measured maximum velocity and average velocity. These measurements provide information as to how fast blood is moving through the embryonic heart (Figure 3.11b). We next plotted average velocity at the AVJ across the cardiac cycle. Overall patterns were similar except for the time in the cycle where reverse flow occurs (Figure 3.11a). An ANOVA test p value of 0.090 shows that there is no statistically significant difference between maximum velocity values.

Consistent with the increased reverse flow fraction, the average velocity (over the entire cardiac cycle) of the blood in *fncb* morpholino-injected embryos was significantly lower than the control embryos (Figure 3.11c). To zoom in on the time in the cycle where reverse flow is occurring, average velocity from 15-40% of the cardiac cycle was calculated (Figure 3.11d). A Tukey test shows that *fncb* morpholino injected embryos and 25N morpholino-injected embryos are both significantly different from non-injected wildtype embryos ($p < 0.01$).

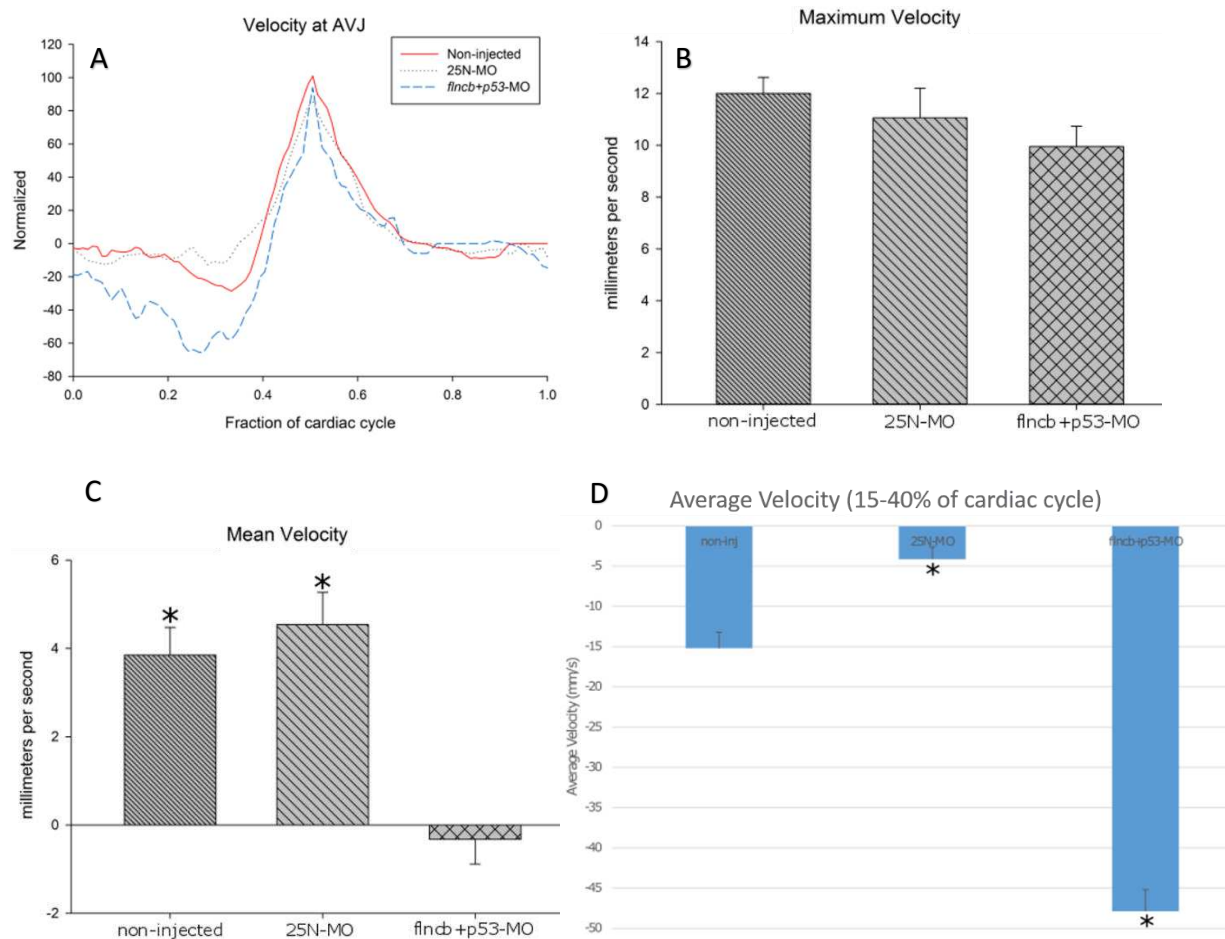


Figure 3.11 – Average means for maximum velocity and average velocity through the AVJ in *flncb* morpholino-injected embryos. Data was collected from high speed video analyses. Error bars represent standard error of the mean. A – The average normalized velocity at the AVJ across the cardiac cycle. Patterns across groups remain the same except for times where reverse flow occurs. B – The means of maximum velocities are not significantly different across groups. *flncb* morpholino-injected embryos had a maximum velocity of 10.0 mm/s (n=19) while 25N control morpholino-injected embryos were at their maximum velocity at 11.3 mm/s (n=12). Non-injected wildtype embryos had the highest maximum velocity with 12.0 mm/s (n=17). ANOVA p=0.090. C – The average velocity across the AVJ in *flncb* morpholino-injected embryos differs from control embryos. *flncb* morpholino-injected embryos had an average velocity of -0.3 mm/s, 25N control morpholino-injected embryos - 4.6 mm/s, non-injected wildtype embryos - 3.9 mm/s. *p<0.05, Tukey test. ANOVA p<0.001. D – The average velocity 15%-40% through the cardiac cycle. *flncb* morpholino-injected embryos exhibited negative velocity during this early portion of the cardiac cycle. *flncb* morpholino-injected embryos and 25N morpholino-injected embryos are statistically significantly different than non-injected wildtype embryos. ANOVA p<0.001. Average velocity of *flncb* morpholino-injected embryos during this time point was -47.87 mm/s. Non-injected wildtype controls and 25N morpholino-injected embryos had velocities of -15.19 and -4.12 mm/s respectively. *p<0.01, Tukey test.

Diameter of the atrioventricular junction does not change in response to alterations in hemodynamics, but diameter of atrium changes in response to lowered blood viscosity

To determine if morphological changes occurred as early as 48 hpf, we calculated diameter of the AVJ at 48 hpf. Our hypothesis for the *gata2* morpholino-injected embryos was that the diameter would change because knocking down *gata2* changes blood viscosity which may result in morphological defects. However, our results did not support this hypothesis because no change in diameter sizes throughout the groups was observed (Figure 3.12a).

Our hypothesis for the *flncb* morpholino-injected embryos was that AVJ diameter will change since we are knocking down the gene encoding a protein involved in muscle structure. No data yet shows that *flncb* is expressed in the AVJ, however by changing muscle structure of the whole heart, diameter could be affected. Our hypothesis was not supported since there was no change in diameter across the AVJ in *flncb* morpholino-injected embryos (Figure 3.12b).

To determine if diameter in the heart changes elsewhere in response to hemodynamics, the average atrial diameter was measured (Figure 3.13). *flncb* morpholino-injected embryos showed no change in atrial diameter while *gata2* morpholino-injected embryos showed a significant decrease in atrial diameter ($p < 0.001$).

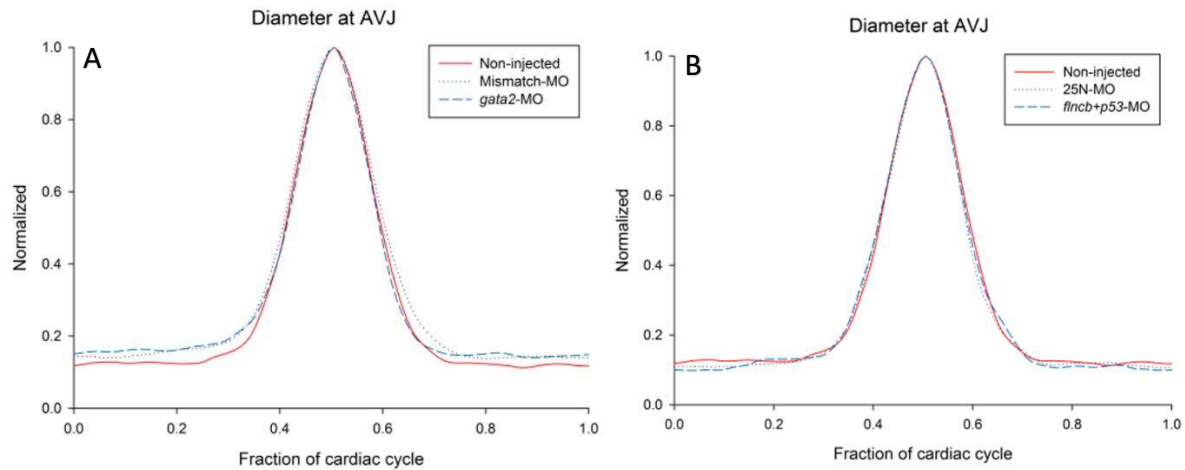


Figure 3.12 – **Average diameter across AVJ.** Data was collected from high speed video analyses. A – Diameter across AVJ in *gata2* morpholino-injected embryos and respective controls. Patterns across groups are very similar. B – Diameter across AVJ in *flncb* morpholino-injected embryos and respective controls. No changes in average diameters were observed.

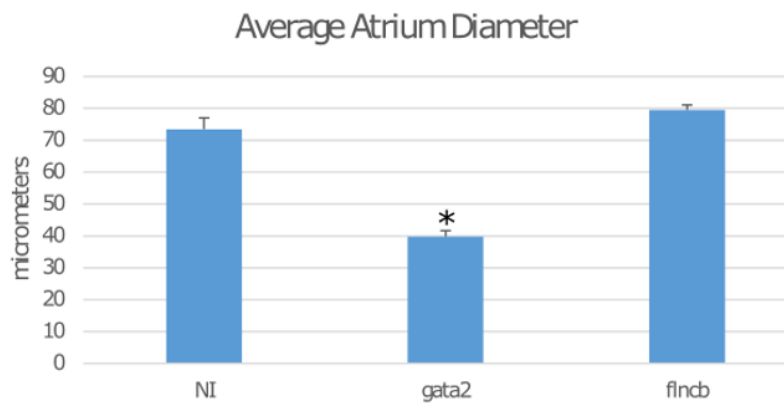


Figure 3.13 – **Average atrium diameter.** The average diameter across the atrium during the cardiac cycle. *flncb* morpholino-injected embryos show no significant difference in atrium diameter compared to non-injected wildtype controls. *gata2* morpholino-injected embryos show a statistically significant difference compared to non-injected wildtype controls. Average atrium diameter of *flncb* morpholino-injected embryos, 79.52 μm . Average atrium diameter of *gata2* morpholino-injected embryos, 39.76 μm . Average atrium diameter of non-injected wildtype embryos, 73.47 μm . * $p < 0.001$, Tukey test. ANOVA $p < 0.001$.

Flow rate through atrioventricular junction does not change in response to hemodynamic differences at 48 hours post fertilization, although shear rate experiences significant changes

To identify how flow patterns are affected by changes in hemodynamic forces, we estimated flow rate by multiplying blood velocity by the area of the AVJ. Flow rate is the speed at which flow is moving through a measured orifice, in this case the AVJ. This flow rate data is presented in nanoliters per minute or Q; the observed variation is shown across a cardiac cycle for both treatments (Figure 3.14). In *gata2* morpholino-injected embryos (Figure 3.14a), flow rate was very similar to respective controls, and no significant differences were found when comparing the maximum Q. In *flnca* morpholino-injected embryos (Figure 3.14b), flow rate is also similar across the cycle, and no significant differences were found when comparing maximum Q values.

Shear rate is the biomechanical force applied to the walls of the orifice being measured. The flow rate (Q) represents a required coefficient for calculating shear rate. Shear rate ($\tau - \tau$) is calculated by multiplying Q by 4 and then dividing by the radius cubed and multiplied by pi (π) (Figure 3.15). Here, shear rate is used instead of shear stress because it eliminates the need for measuring viscosity. We argue that viscosity (μ) cannot be assumed in the embryonic heart because of the varying blood flow that may occur at the AVJ due to the flow alteration treatments.

We find that shear rate varies even in non-injected wildtype embryos as flow moves through the heart (Figure 3.16). To facilitate comparisons among the treatments, we chose to look at shear rate when the AVJ is open (Figure 3.17). The peaks observed relate to measurements when the AVJ diameter is small (i.e. AVJ is closing) and results in a large number

due to the radius being cubed. Both changes in hemodynamics respond to shear rate in the same manner. In *gata2* morpholino-injected embryos, shear rate was significantly decreased compared to non-injected wildtype embryos when the AVJ was open. Similarly, *flncb* morpholino-injected embryos showed a significant decrease. These results represent a form of cardiac function different from our previous stroke volume and cardiac output results that were not significantly different.

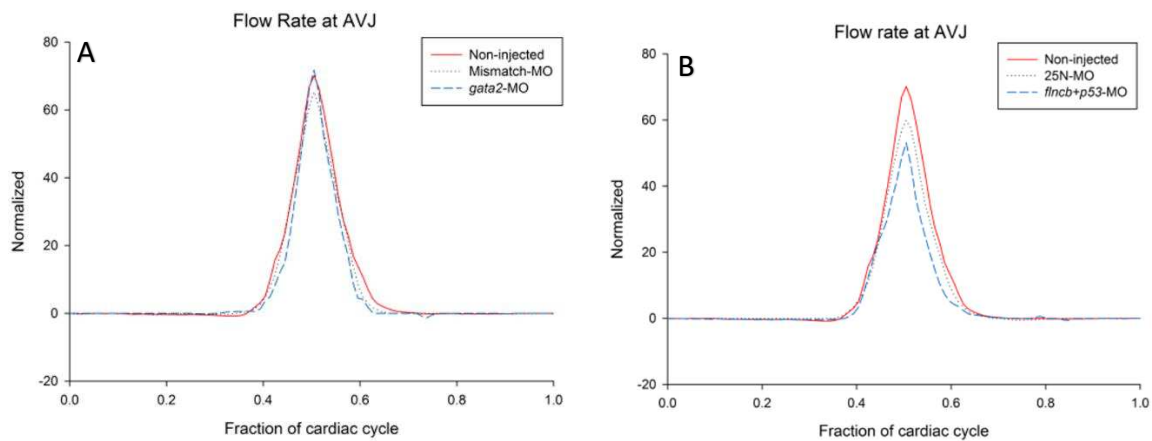


Figure 3.14 – **Averaged flow rate patterns at AVJ across a cardiac cycle.** Data was collected from high speed video analyses. A – Average flow rates for *gata2* morpholino-injected embryos (n=16), *gata2* mismatch morpholino-injected embryos (n=30), and non-injected wildtype embryos (n=17). No significant difference was found at max Q between groups. ANOVA p=0.480. B – Average flow rates for *flncb* morpholino-injected embryos (n=19), 25N control morpholino-injected embryos (n=12), and non-injected wildtype embryos (n=17). No significant difference was found at max Q between groups. ANOVA p=0.149.

$$\tau = \frac{4Q}{\pi r^3}$$

Figure 3.15 – **Shear rate equation.** Shear rate as calculated by knowing the flow rate (Q) and diameter of the AVJ.

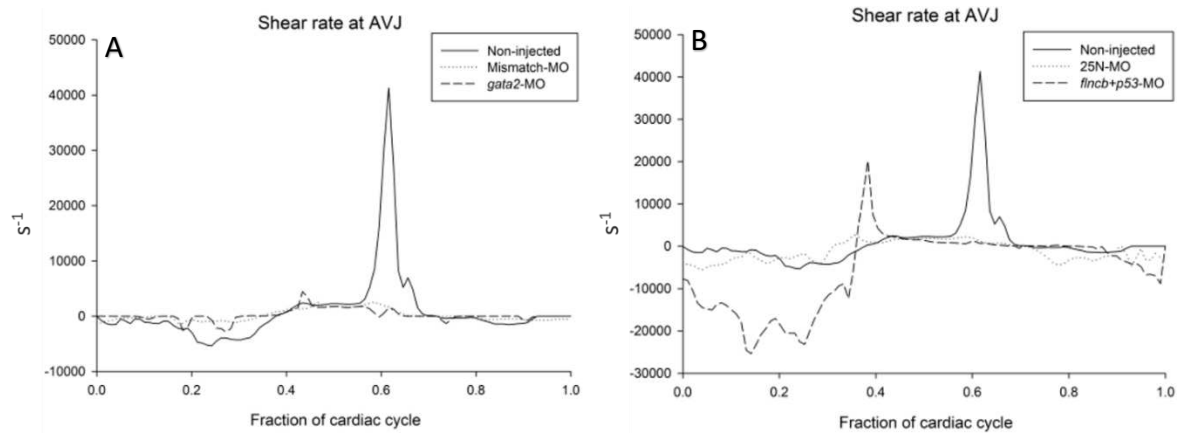


Figure 3.16 – **Shear rate patterns at the atrioventricular junction.** Data was collected from high speed video analyses. A – Shear rate pattern of *gata2* morpholino-injected embryos across an entire cardiac cycle. *gata2* knockdown shear rate is significantly lower than non-injected wildtype embryos ($p < 0.05$, Tukey test). ANOVA $p = 0.009$. B – This figure is a portion of Figure 3.16a from 0.4545 to 0.5555 of the cardiac cycle. Shear rate pattern of *flncb* morpholino-injected embryos across an entire cardiac cycle. *flncb* morpholino-injected embryos exhibit a much lower shear rate over the entire cardiac cycle than non-injected wildtype embryos ($p < 0.05$, Tukey test). ANOVA $p < 0.001$.

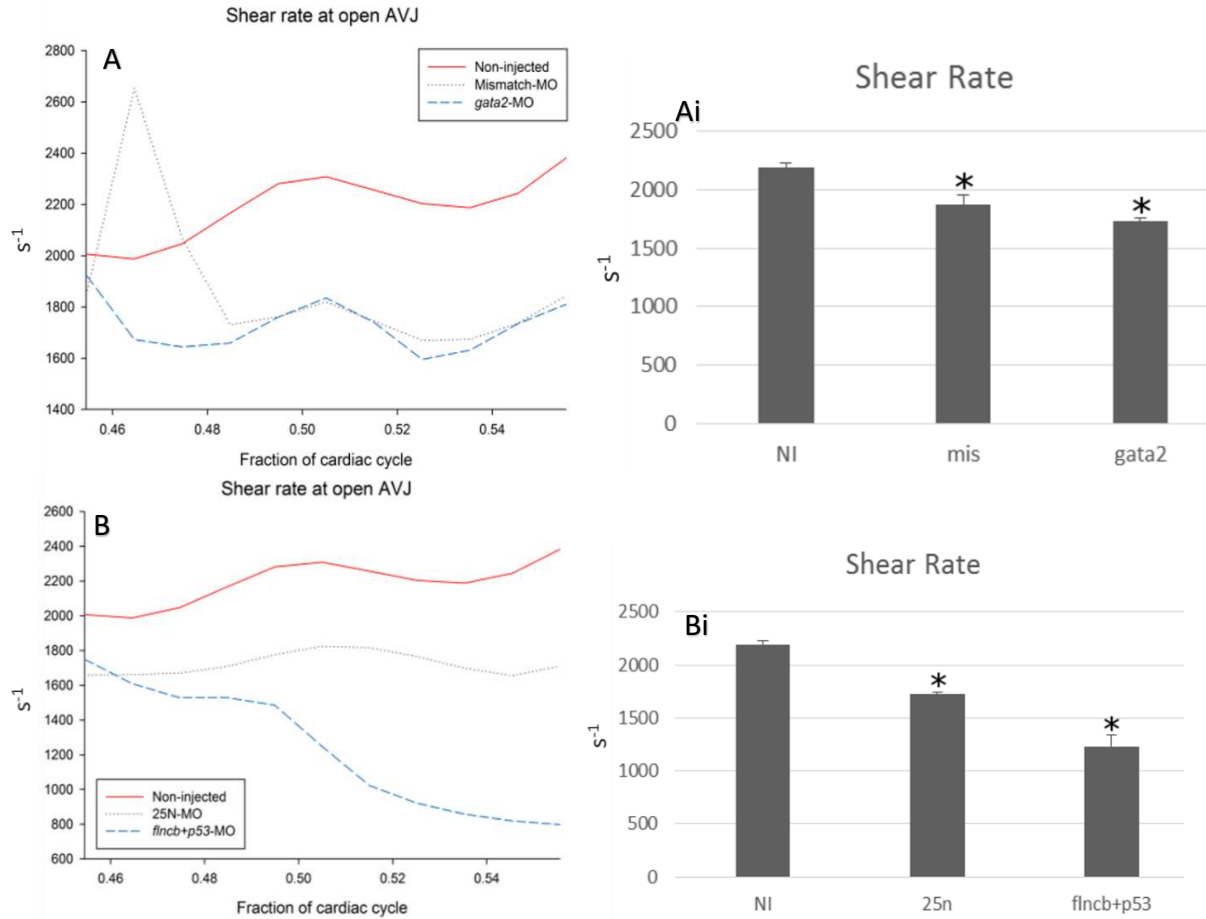


Figure 3.17 – **Shear rate when the atrioventricular junction is open.** Data was collected from high speed video analyses. A – Shear rate pattern through the AVJ when the AVJ is open in *gata2* morpholino-injected embryos. *gata2* morpholino-injected embryos (and *gata2* mismatch morpholino-injected embryos) exhibit a shear rate significantly lower than non-injected wildtype embryos ($p < 0.05$, Tukey test). ANOVA $p < 0.001$. Ai – Average values from A. B – Shear rate pattern through the AVJ when the AVJ is open in *flncb* morpholino-injected embryos. *flncb* morpholino-injected embryos exhibit a different pattern and an overall lower shear rate than non-injected wildtype embryos ($p < 0.05$, Tukey test). ANOVA $p < 0.001$. Bi – Average values from B.

*Lowered blood viscosity impacts *cmlc2* and *klf2a* expression levels*

In order to investigate the response of potential flow response genes to lowered blood viscosity, we utilized qPCR. The graph in Figure 3.18a indicates transcript copy numbers per microgram of RNA present for each gene in the *gata2* morpholino-injected embryos (red bars) versus the control, non-injected wildtype embryos (light grey bars). Using a standard curve and absolute quantification, we detected a significant difference in copy numbers of *klf4* and *klf2a* in *gata2* morpholino-injected embryos versus non-injected wildtype embryos ($p < 0.05$ – *klf2a*, $p < 0.001$ – *klf4*) (Figure 3.18a). Values are represented in Table 3.1.

In order to compare how lowered blood viscosity affected expression levels of these genes, we utilized relative quantification (Figure 3.18b). Relative quantification was used to take into account the non-injected control gene expression levels directly compared to the experimental expression levels. This graph shows expression ratios of each gene in comparison to the non-injected control. Values are represented in Table 3.2. Lowered blood viscosity results in a decrease in expression of both *cmlc2* and *klf2a* ($p = 0.03$, both) (Figure 3.18a). No significant difference was found in *klf4* and *klf2b*.

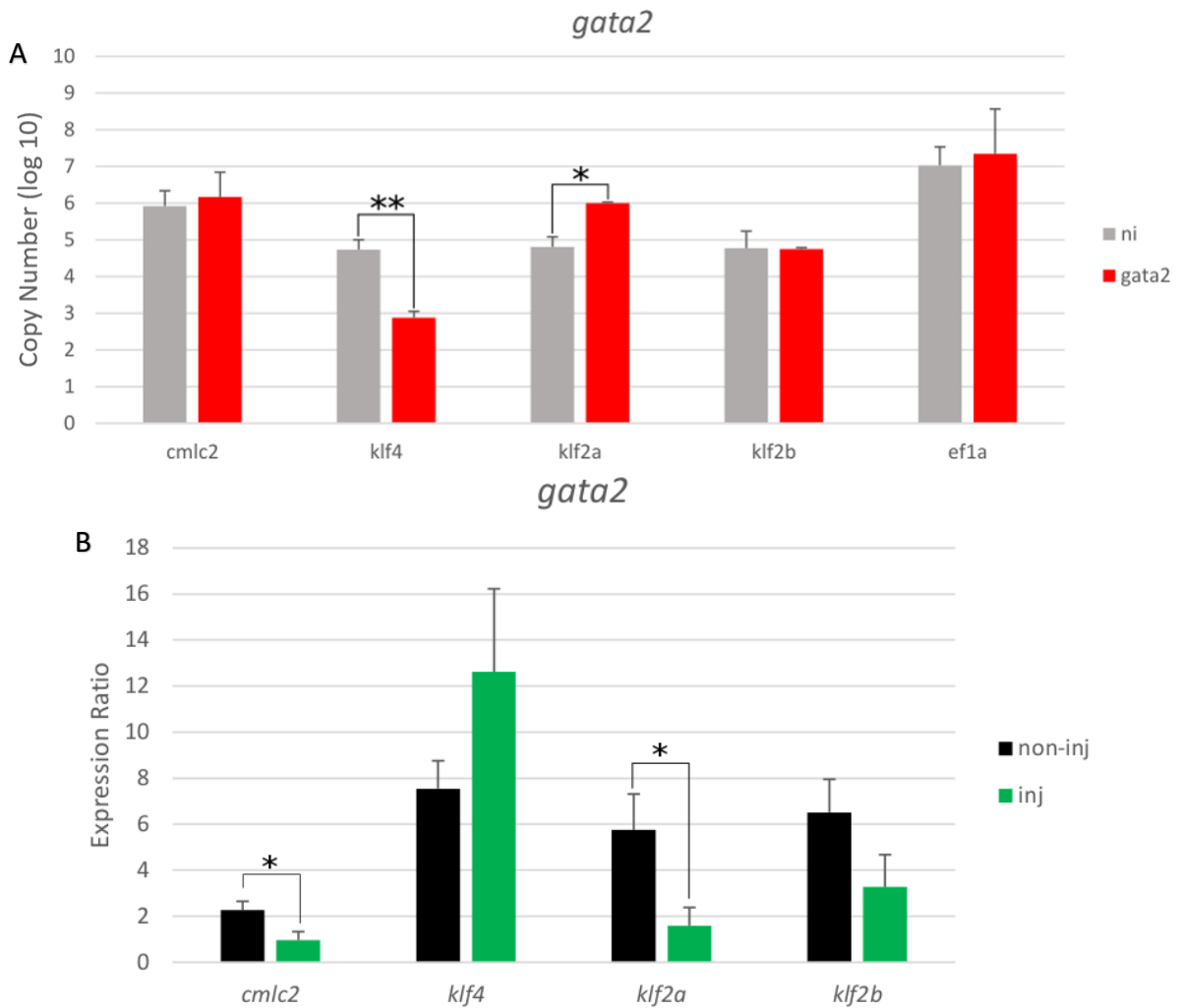


Figure 3.18 – Absolute and relative quantification on embryonic hearts with lowered blood viscosity at 56 hpf. Error bars represent standard error of the mean. Non-injected embryos n=10. Injected embryos n=11. A – Absolute quantification of *gata2* morpholino-injected embryos and non-injected wildtype embryos. Copies of cDNA per microgram of RNA per each gene and respective control. Copy numbers of *klf4* and *klf2a* are significantly different in *gata2* morpholino-injected embryos than in non-injected wildtype control embryos. *p<0.05, **p<0.001, Welch’s t-test. B – Relative quantification of *gata2* morpholino-injected embryos and non-injected wildtype embryos. Expression ratio of genes and respective controls. Expression ratios of *cmlc2* and *klf2a* are significantly decreased in *gata2* morpholino-injected controls than in non-injected wildtype control embryos. *p=0.03, Welch’s t-test.

Changes in cardiac contractility impact expression levels of klf2a

Next, we investigated expression levels of our target genes in response to a change in cardiac contractility. Using absolute quantification, we found no significant difference in *flncb* morpholino-injected embryos versus non-injected wildtype embryos (Figure 3.19a). Values for copy numbers are represented in Table 3.1.

Using relative quantification, we identified that changes in cardiac contractility result in a decrease in expression of *klf2a* ($p=0.04$) (Figure 3.19b). Values for expression ratios are represented in Table 3.2.

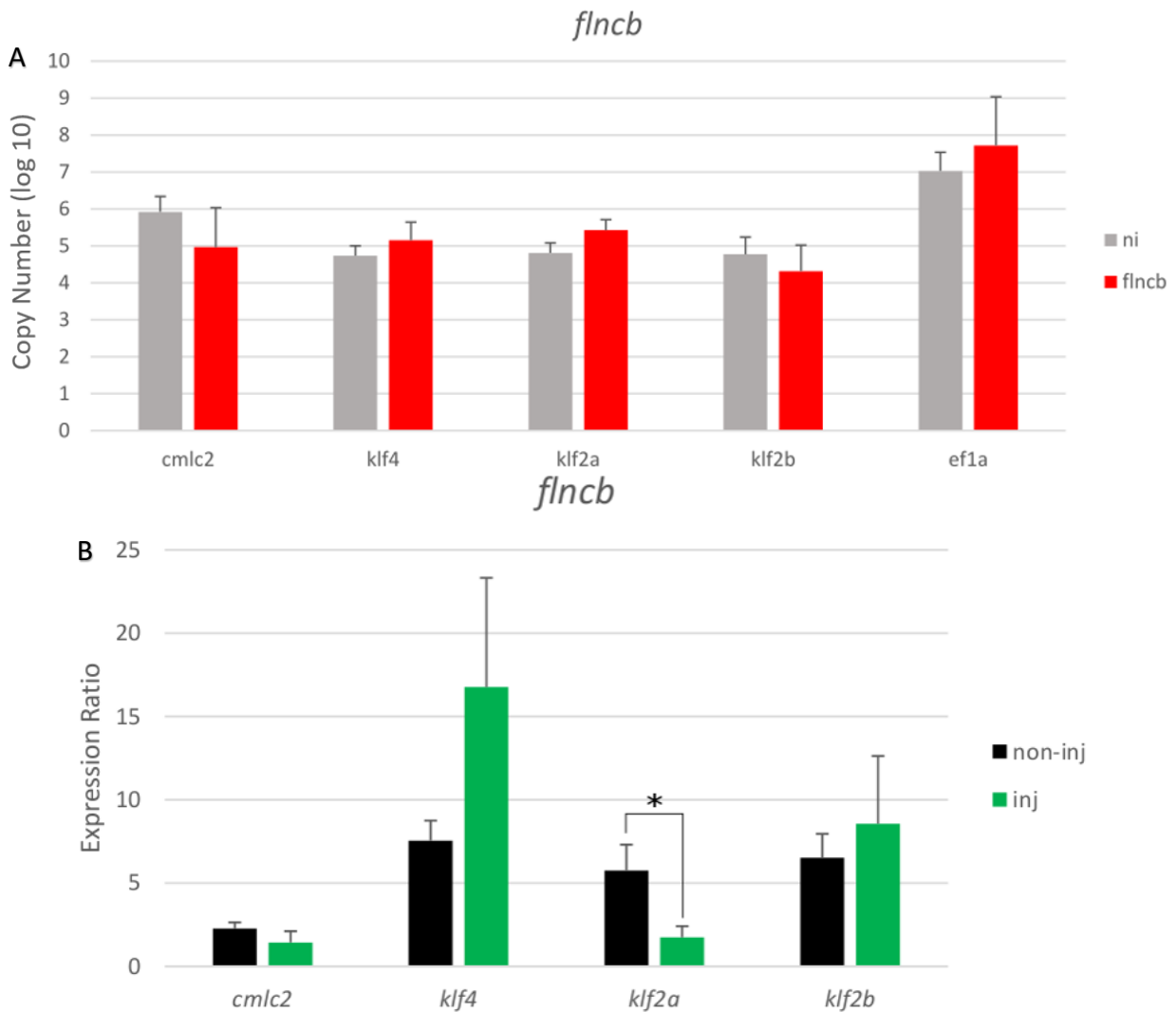


Figure 3.19 – **Absolute and relative quantification of embryonic hearts with defective contractility at 56 hpf.** Error bars represent standard error of the mean. Non-injected embryos n=10. Injected embryos n=11. A – Absolute quantification of *flncb* morpholino-injected embryos and non-injected wildtype embryos. Copies of cDNA per microgram of RNA per each gene and respective control. No significant difference was noted by Welch’s t-test. B – Relative quantification of *flncb* morpholino-injected embryos and non-injected wildtype embryos. Expression ratio of genes and respective controls. *klf2a* expression is significantly decreased in *flncb* morpholino-injected embryos than in non-injected wildtype control embryos. *p=0.04, Welch’s t-test.

Table 3.1 – Mean copy numbers for absolute quantification.

	<i>cmlc2</i>	<i>klf4</i>	<i>klf2a</i>	<i>klf2b</i>	<i>ef1a</i>
Mean copy number (non-injected)	836179.8	54289.2	64251.0	59269.2	10632931.1
Mean copy number (<i>gata2</i>)	1475948.9	752.0	991941.5	56027.9	22364784.8
Mean copy number (<i>flncb</i>)	91908.5	141817.7	266503.0	20778.8	52137701.6

Table 3.2 – Mean expression ratios for relative quantification.

	<i>cmlc2</i>	<i>klf4</i>	<i>klf2a</i>	<i>klf2b</i>
Mean expression ratio (non-injected)	2.272062	7.551815	5.753338	6.517471
Mean expression ratio (<i>gata2</i>)	0.961174	12.62508	1.586341	3.273325
Mean expression ratio (<i>flncb</i>)	1.438658	16.76632	1.742081	8.567849

CHAPTER 4: DISCUSSION

Expression patterns of klf2a, klf2b, and klf4

One of the main goals of this study was to identify cardiac expression of *klf2a*, *klf2b*, and *klf4*. First, to verify that these genes were expressed at time points in the embryo that were relevant to heart development, expression in whole embryos from time points from two hours post fertilization to 72 hours post fertilization was investigated (Figure 3.1). All genes were expressed at two hours post fertilization (around the time of the zebrafish mid-blastula transition) which leads us to believe that these genes are transcribed at the start of development. This is important to know because cardiac progenitors start moving towards the midline to their final destination in the anterior lateral plate mesoderm (ALPM) at about five hours post fertilization (Bakkers, 2011). The endocardium and hematopoietic cells of the primitive myeloid lineage are also formed from the ALPM (Bakkers, 2011). Therefore, it is possible that these genes are involved in early heart development starting with the cardiac progenitors. An interesting future study would be to see if the target genes *klf2a*, *klf2b*, and *klf4* are expressed in the ALPM at early stages to see if they are involved in early heart development stages as well as the later stages that we investigate here.

Our next goal was to identify the specific times and locations in the heart that *klf2a*, *klf2b*, and *klf4* were expressed. We looked at embryonic cardiac expression at 24, 36, 48, 56, 72, and 96 hours post fertilization via RT-PCR and *in situ* hybridization. We found that at almost all stages investigated, cardiac expression was found in all genes (Figure 3.2a). Specifically, expression in the AVJ was noted for *klf2a* and *klf2b*. *cmhc2*, which encodes a protein involved in

cardiac myofibril assembly, was chosen as a control in the *in situ* hybridizations because it is robustly expressed throughout the heart at all stages (Yelon et al., 2000). The expression of *cmhc2* allows for identification of the shape of the heart at respective stages which can be used to determine location of the AVJ at each stage.

klf2a is broadly expressed during cardiac development, which is consistent with previous work (Dekker et al., 2002) (Figure 3.3). Expression of *klf2a* does not constrict to the AVJ until 36 hours post fertilization. From then on, *klf2a* expression is detectable only in the AVJ. *klf2a* is known to be expressed in the heart and is also known to be expressed in the AVJ (Vermot et al., 2009). Our work confirms that *klf2a* is expressed in the AVJ and is important because previous studies correlate misexpression of *klf2a* with cardiac morphologies (Wang et al., 2011; Dietrich et al., 2014; Heckel et al., 2015; Renz et al., 2015).

klf2b was not expressed in the heart at 24 and 36 hours post fertilization, as detected by RT-PCR. This expression pattern mimicked what we found in the *in situ* hybridizations and indicates that *klf2b* is not involved in early heart development, but is involved in the later heart development stages. Because of the potential functional redundancy with *klf2a*, we investigated the location of *klf2b* expression in the heart. We found cardiac expression for *klf2b* located mainly in the ventricle and AVJ. This expression pattern is a novel finding because currently all that is known about *klf2b* is its involvement in embryonic patterning (Kotkamp et al., 2014).

To investigate whether or not cardiac expression of *klf4* is actually from heart and not blood, we depleted blood in embryos. These *gata2* depleted embryos have no blood circulating at 72 and 96 hours post fertilization. At these times *klf4* is expressed in the heart (Figure 3.2b)

which verifies that the RT-PCR expression in Figure 3.2a is partially due to true cardiac expression. We found no cardiac expression of *klf4* in the heart at 24 hours post fertilization via *in situ* hybridization. However cardiac expression does occur at 24 hours post fertilization via RT-PCR. This discrepancy most likely reflects the lower sensitivity of *in situ* hybridization relative to RT-PCR. Cardiac expression is evident at 48 and 56 hours post fertilization, however, and may represent both cardiac expression and blood expression. Although only diffuse cardiac expression of *klf4* is observed, we hypothesize that it is not detectable by *in situ* hybridization and is still a potential flow response gene.

After verifying expression patterns of the *klf*-family genes, the next set of experiments tested whether these genes were flow response genes. To investigate, we changed the hemodynamics in the embryonic heart. We lowered blood viscosity by depleting *gata2*, and we reduced contractility of the heart by depleting *flnca*. By knocking down *gata2*, the number of blood cells that are circulating throughout the embryonic vasculature is reduced. Knocking down *flnca* results in a change in cardiac muscle structure. These knockdowns provide an avenue to investigate altered hemodynamics in the embryonic heart via high speed imaging and the changes in gene expression of three key *klf* candidate flow response genes.

To identify the effect of lowered blood viscosity on embryonic survival, we observed the embryos for ten days. Only 19.2 % of *gata2* morpholino-injected embryos died by day ten (Figure 3.4a). This percentage was similar to the *gata2* mismatch morpholino-injected embryos, where 21.3% died by day ten. This similarity suggests a possible contribution from off target effects of the mismatch morpholino. In the literature, approximately 15-20% of morpholinos have some degree of toxic effects, leading to death (Ekker and Larson, 2001). If death rate is

too high, a *p53* morpholino can be added to ameliorate off target and apoptotic effects (Gerety and Wilkinson, 2011). In contrast, 6.8% of non-injected wildtype embryos died, which indicates that some embryos do not survive due to factors not related to morpholino injection. Based on the results here, we conclude that lowered blood viscosity does not severely affect survival before day ten. This result coincides with the fact that embryos can survive with a non-functioning cardiovascular system until about day five through seven (Kopp et al., 2010; Hoage et al., 2012). The developing embryos obtain oxygen through diffusion so the embryos have an oxygen source if no blood is circulating. Since these embryos survive for a relatively long time it allows researchers to investigate the impact of lowered blood viscosity during major steps in cardiac development without the complications of hypoxia.

In comparison, *flncb* morpholino-injected embryos saw 37.7% death at day ten (Figure 3.5a). The 25N control morpholino-injected embryos had 14.3% death and the non-injected wildtype embryos had 0% death. The importance here is the fact that the control injected embryos here survived better and shows that a randomly assigned base pair morpholino (25N-MO) has less off target effects when compared to mismatch morpholinos that are only five base pairs different than their target gene. 37.7% death is higher than what was observed in the *gata2* morpholino-injected embryos. This death rate indicates that the *flncb* depletion is more detrimental to the embryo, than simple injection which could mean that *flncb* promotes the overall survival of the heart.

In order to see what effects decreased blood viscosity and changes in contractility have on heart development through valve morphogenesis stages, we observed hearts at four days post fertilization. Multiple phenotypes were seen at day four in *gata2* morpholino-injected

embryos and 39.7% of these embryos exhibited a cardiac phenotype (Figure 3.4b). Some embryos exhibited more than one phenotype, and where the most common phenotypes were cardiac edema (38.3%) and a change in blood flow either no blood flow (27.7%) or reduced blood flow (7.8%). These two are common phenotypes in *gata2* knockdowns have been seen in previous work (Vermot et al., 2009). Some morphological phenotypes included stringy heart (10.0%), non-compact heart (14.1%), and silent ventricles (5.0%). Stringy heart is the term to describe a chamber (usually the atrium) that is stretched out and visibly looks like a string. Sometimes waves of contractions move through the stringy chambers, but often they are silent (non-contracting). This phenotype usually will result in death as early as day five, once the embryo starts relying on blood to transport oxygen. Silent hearts will not be able to pump blood sufficiently to the rest of the body. We defined the non-compact heart as a heart that was not fully looped and resemble a younger stage of development. The embryos with this phenotype would probably survive, as the heart is still able to pump blood through albeit less efficiently. 5.0% of embryos had a silent ventricle and while these ventricles may look normal structurally, they are not pumping blood to the rest of the body. These embryos will also perish around day five. In summary, lowered blood viscosity results in cardiac morphologies that alter the way blood is circulated to the rest of the body.

In the *flncb* morpholino-injected embryos, the most common cardiac phenotypes observed were a change in blood flow (24.8% - no blood flow) and a silent ventricle (14.7%). Previous reports of *flncb* knockdowns focused on skeletal muscle describing the failure of both slow and fast twitch muscle fibers (Ruparella et al., 2012). We expected to see a change in contraction, including the possibility of silent ventricles. As mentioned with the *gata2*

morpholino-injected embryos, a silent ventricle will result in early death around day five. A surprising phenotype was the decrease in blood flow which was expected in the *gata2* morpholino-injected embryos, but not necessarily predictable for *fln1b* depletion. A change in blood flow most likely comes from pooling in the body because the heart is not contracting well enough to pump blood efficiently through the entire circulatory system. These phenotypes are useful for observing the overall comparative effects are of lowered blood viscosity and changes in contractility.

Hemodynamics and the embryonic zebrafish heart

In order to quantify the effects of altered hemodynamic factors on heart function, videos of 48 hours post fertilization embryos were analyzed. These videos provide reverse flow and shear rate data and also data such as heart rate, stroke volume, and velocity of the blood, all of which will be correlated with gene expression changes.

Heart rate in a non-injected wildtype embryo starts at around 25 beats per minute at 24 hours post fertilization and peaks at 230-250 beats per minute at five days post fertilization (Schwerte, 2009). We observed the embryos at 48 hours post fertilization and recorded an average heart rate of 193.5 beats per minute. Our findings are higher than previously published heart rates. In 1999, Barrionuevo and Burggren recorded embryonic heart rate (prior to hatching) at approximately 150 beats per minute (Barrionuevo and Burggren, 1999). In 2013, however, using more modern high speed imaging, Dalman and colleagues recorded heart rate in 48 hours post fertilization embryos at approximately 130 beats per minute (Dalman et al., 2013). While neither method describes the frame rate of their high speed imaging, our images

are captured in 1500 frames per second videos and calculated with sophisticated MATLAB software. Using our very accurate heart rate calculations we saw a decrease in heart rate in embryos with lowered blood viscosity and in embryos with altered cardiac contractility. Embryos with lowered blood viscosity exhibited an average heart rate of 155.2 beats per minute and embryos with altered cardiac contractility exhibited an average heart rate of 162.0 beats per minute. This approximate 17% decrease in heart rate is statistically significant and demonstrates that both blood viscosity and muscle structure are important in maintaining a functioning heart.

While thinking about function, the next question to ask is how does the lower heart rate affect the overall output of the heart? Stroke volume is the amount of blood that is pumped through the heart to the body in one cycle of cardiac contraction. Cardiac output is the product obtained from multiplying stroke volume by heart rate. Cardiac output may be considered a rubric for overall cardiac function of the heart. Average cardiac output for *gata2* morpholino-injected embryos was 18.9 nl/min, which shows that these hearts are able to pump 18.9 nanoliters of blood through the heart to the body in one minute. Non-injected wildtype embryos exhibited an average cardiac output of 24.4 nl/min. This is higher than the value observed in embryos with lowered blood viscosity, but this difference was not statistically significant. Embryos with altered cardiac contractility also saw a decrease in cardiac output, but nothing significantly different. These findings show that even though heart rate was changed because of the effects of altered viscosity and contractility, the heart was still functioning as a normal pump. Findings like this are important to show that hearts can still function with changes in hemodynamics. These findings could also explain why the morphants have a survival

rate that is not severely reduced. The hearts are functioning with the ability to maintain circulation and compensate for the lowered heart rates, lowered blood viscosity, and a change in muscle structure.

Since the change in blood viscosity and change in muscle structure did not affect overall cardiac output of the heart, yet a range of cardiac phenotypes was observed in many of the embryos, we hypothesized that other factors, like reverse flow, were changing. Vermot and colleagues have shown that in *gata2* morpholino-injected embryos, the fraction of the cardiac cycle exhibiting reverse flow is decreased (Vermot et al., 2009). Based our video data, we redefined reverse flow as the volume of blood that is moving in the reverse direction divided by the total volume of blood, making this measurement a unit-less fraction. In contrast, Vermot measured reverse flow as a fraction of time, the length of time the blood is moving in the reverse direction divided by the total length of the cardiac cycle (Vermot et al., 2009).

We measured reverse flow with time dependent fractions and volume dependent fractions. In embryos with lowered blood viscosity, we saw a decrease in reverse flow in both measurements (Figure 3.6). With our way of defining reverse flow using the volume fraction, we did not find a statistically significant change. However, there was still a difference of 1.2%, stating that the embryos with lowered blood viscosity have 1.2% less volume of blood moving in the reverse direction compared to the non-injected wildtype embryos. This result is consistent with the data generated by Vermot in that the same trend is found (a decrease in RFF), although the magnitude of RFF in both the wildtype and knockdown embryos was much less. Nevertheless, we did see a statistically significant difference in the time fractions between the two control groups and the *gata2* morpholino-injected embryos. Embryos with lowered

blood viscosity had 1.0% of the time in the cardiac cycle containing reverse flow. In the non-injected wildtype embryos average the reverse flow fraction (time) was 13.5% of the cycle containing reverse flow.

Embryos with altered cardiac contractility had an increase in reverse flow (Figure 3.9). This increase was found in both the time fraction and the volume fraction. Using the volume fraction measurements, *fIncb* morpholino-injected embryos produced a reverse flow fraction of 6% while non-injected wildtype embryos saw a reverse flow fraction of 1.7%. This difference is statistically significant and reassures us that *fIncb* knockdown does result in an increase in reverse flow. Measuring by the time fraction also shows the same trend. Non-injected wildtype embryos have a reverse flow fraction of 13.5% while *fIncb* morpholino-injected embryos have a reverse flow fraction of 28.3%, which is also a statistically significant difference.

By comparing the two types of fractions (volume and time), we can see that they both show the same trends. However, measuring reverse flow using volume is advantageous. An advantage to this approach is that it measures a characteristic (volume of blood within the heart, moving retrogradely) that is more relatable to the phenotypes being observed. Viscosity of the blood is affected by *gata2* morpholino knockdown (which correlates with a lower volume), and *fIncb* morpholino knockdown embryos exhibit decreases in blood flow (also correlating with lower blood volume). Another advantage is that measuring with volume will account for the size of the embryo. By taking the size of the heart into account, the data can be more accurately portrayed. Measuring reverse flow as a fraction of time could be advantageous in morphants that are affected by timing of the contraction (i.e. arrhythmia). A limitation to measuring with time is that it does not account for the size of the embryo or the amount of

blood actually moving through the heart. Therefore, future studies should be focused on the volume fraction rather than the time fraction, which will allow for a better portrayal of reverse flow in the embryonic heart.

After discussing the pros and cons of the fractions, we need to think about how reverse flow is affected by lowered blood viscosity. *gata2* is a hematopoietic transcription factor that is responsible for controlling early hematopoiesis (Galloway et al., 2005). In *gata2* morpholino-injected embryos, without a high number of blood cells moving through the heart, cells at the AVJ are freer to move through and there is less pressure to push cells backwards when the ventricle contracts. A decrease in viscosity affects heart development, and does not allow for the correct formation of valves in the AVJ (Vermot et al., 2009). When flow is perturbed, signaling of the correct pathways does not occur and therefore development of the valves is affected. An ongoing important question in the field is to identify the genes that are misregulated with a disruption of flow.

flnbc is a gene encoding a sarcomeric protein that when knocked down, results in decreased skeletal and cardiac muscle integrity (Ruparelia et al., 2012). When a sarcomeric protein is disrupted, contraction of the respective muscle is affected. Without regular contractions in the heart, blood flow is predicted to change. Consistent with this prediction, the hearts of *flnbc* morpholino-injected embryos exhibited an increase in reverse flow. In these embryos, hearts had a decreased heart rate and altered cardiac contractility, which resulted in allowing more blood to flow back through the AVJ during ventricle contraction. This same trend was also seen in work involving anesthetizing the embryo (Johnson et al., 2013a). Johnson anesthetized embryos with tricaine and recorded a RFF of 80% (Johnson et al., 2013a). While

tricaine does not have the same effect as depletion of a sarcomeric protein, it does relax muscles, which accounts for an alteration in contraction. The alteration in contraction results in lowered heart rate in both cases (anesthetized and *fIncb* knockdown), however *fIncb* knockdown does not result in a change in cardiac output while tricaine results in a significant decrease in cardiac output (28.4 nl/min in wildtype to 3.1 nl/min in anesthetized) (Johnson et al., 2013a). This comparison helps us understand that *fIncb* does not influence the overall cardiac output of the heart instead only alters muscle contraction which slightly alters blood flow in the developing heart. Future studies can use this information to focus on the exact mechanism.

With our video analyses, we are also able to determine diameter of the AVJ and the velocity of the blood through the AVJ. In embryos with lowered blood viscosity, we hypothesized that the diameter of the AVJ would not change. Later in development when flow knockdown is affecting valve development would be a time when one could suggest a change in AVJ diameter. Our hypothesis was supported as we saw no change in AVJ diameter at 48 hours post fertilization in embryos with lowered blood viscosity and altered cardiac contractility (Figure 3.12a).

Surprisingly, diameter of the AVJ in embryos with altered cardiac contractility was not affected. We hypothesized that since muscle structure was being perturbed, that the size or shape of the heart would change. However, the diameters of the AVJs in each group were very similar (Figure 3.12b). This does not mean that the size of other orifices in the heart (atrial inlet, outflow tract) have not changed, but our only objective in this study is measuring the AVJ. Our

high speed videos and analyses could be used to determine the impact on atrial inlet and outflow tract.

The non-significant findings of diameter differences between treatments should not go unremarked because they show us that lowering blood viscosity and altering cardiac contractility do not drastically affect the shape or size of the AVJ through 48 hpf, and does not ultimately lead to lethality in more than 20% of knockdown embryos. More work should be done to make this observation conclusive, but these findings can provide the framework for future studies.

We hypothesized that diameter may change elsewhere in the heart other than the AVJ. To observe this, the average diameter of the atrium was measured throughout the cardiac cycle (Figure 3.13). *flnclb* morpholino-injected embryos showed no significant difference when compared to controls, however *gata2* morpholino-injected embryos showed a statistically significant difference compared to non-injected wildtype embryos. These results show that blood viscosity must play a role in the ballooning of the atrial chamber, while contractility does not affect the overall shape and morphology of the AVJ or atrium.

Velocity of the blood is measured using Johnson's novel calculations (Johnson et al., 2013a). In embryos with altered cardiac contractility, average velocity is significantly different than in control embryos. The average velocity for embryos with altered cardiac contractility is negative (-0.3 mm/s) while non-injected and control embryos have larger positive values for velocity (3.9 mm/s and 4.6 mm/s respectively). The negative velocity shown represents flow moving in the reverse direction. The current data do not pinpoint any one part of the cycle that is responsible for this since this value is averaged from the whole cardiac cycle. Nevertheless, it

corresponds with the results from the reverse flow fraction measurements. Embryos with altered contractility had a greater reverse flow fraction and a negative number for the average velocity, suggesting overall that the amount of time that blood is spent moving in the reverse direction in the AVJ is notable.

In order to pinpoint the part of the cycle that is responsible for blood moving in the reverse direction, the average velocity from 15-45% of the cardiac cycle was calculated. Times were chosen based on the velocities shown during the whole cardiac cycle. Average velocity for *fincb* morpholino-injected embryos was -36.90 mm/s while non-injected wildtype embryos exhibited an average velocity of -5.88 mm/s. Tukey tests show that this is a significant difference. These values were calculated to show that the early part of the cycle where blood is moving from the atrium to the ventricle is where the direction of blood is mostly in reverse.

Embryos with lowered blood viscosity exhibited no statistically significant change in maximum or average velocity. With a change in blood viscosity one could hypothesize that velocity of the remaining blood cells would increase. While there was no statistically significant difference, the trend in Figure 3.8b did show a slight increase from non-injected wildtype embryos (4.5 mm/s) to *gata2* morpholino-injected embryos (5.3 mm/s). This finding is still interesting because it shows a trend in the direction that was expected, just not a significant trend.

Along with reverse flow, forward flow and shear stress through the AVJ are important factors in this study. Embryos with lowered blood viscosity and those with altered cardiac contraction show similar flow patterns and no significant difference was found at maximum flow (Figure 3.14). Since flow is the amount of blood that is moving through the heart in one

minute, we can use this information to calculate shear rate. Shear rate is used instead of shear stress because we cannot reliably account for viscosity in each of the treatments. *gata2* knockdown effectively alters the viscosity of the blood, therefore changing the velocity of the fluid that is being measured through the AVJ; for this reason, we cannot assume a constant viscosity across measurements. However, using the calculation in Figure 3.15 to calculate shear rate, shear rate patterns were decreased (Figure 3.16). The peaks that are visible result from when the radius of the AVJ gets too small (i.e. when AVJ is closing). Embryos with lowered blood viscosity did exhibit a significantly lower overall shear rate ($p < 0.05$) (Figure 3.16a).

Looking at the whole cardiac cycle makes it hard to see significant differences by eye. When we look at shear rate only when the AVJ is open, embryos with lowered blood viscosity have a lower shear rate than non-injected wildtype embryos (Figure 3.17a). One thing to keep in mind is that the *gata2* mismatch morpholino-injected embryos are also significantly different from non-injected wildtype embryos when the AVJ is open. This result could be another artifact of using the mismatch morpholino as a control. We did hypothesize that lowered blood viscosity would result in lowered shear rate because lowering blood viscosity reduces the amount of shear that is passing through the orifice.

We hypothesized that embryos with altered cardiac contractility would exhibit an increase in shear rate. Our results did not support that hypothesis, as *flncb* morpholino-injected embryos exhibited a statistically significantly lower shear rate than non-injected wildtype embryos (Figure 3.16b). When the AVJ is open, the controls demonstrated similar trends of increasing in shear as the AVJ closes. Embryos with altered cardiac contractility decrease in

shear rate as the AVJ closes. We can conclude from this data that as reverse flow increases, shear rate decreases.

The shear rate in both sets of treated embryos is significantly lower. Previous work reports that shear rate decreases as the embryo ages from three days post fertilization to six days post fertilization (Jamison et al., 2013). The embryos in this study are analyzed at two days post fertilization and already have significantly lower shear rate than non-injected wildtype control embryos. By starting at a lower shear rate, morphological consequences may occur. It is possible that genes that are altered by shear rate are turned on or off too soon because of the early decrease in shear rate. Future work can identify timing of the gene expression changes and the downstream targets of these genes.

klf2a, klf2b, and klf4 expression levels in response to changes in hemodynamics

To determine how the target genes *klf2a*, *klf2b*, and *klf4* respond to changes in hemodynamics, we investigated the gene expression levels via absolute and relative quantification. Our findings show significant changes in expression levels of *klf2a* and *cmlc2* in embryos with lowered blood viscosity and altered cardiac contractility. *klf2a* is known to be down regulated in response to *gata2* knockdown (Vermot et al., 2009). We hypothesized since *klf2b* and *klf4* are similar in sequence and expression to *klf2a*, *klf2b* and *klf4* will be down regulated in embryos with lowered blood viscosity. In embryos with altered cardiac contractility, we hypothesized *klf2a*, *klf2b*, and *klf4* would show an increase in expression levels.

First, we determined the transcript copy numbers for each gene via absolute quantification (Figure 3.18a, 3.19a). This type of quantification compares the number of copies

of cDNA obtained from one microgram of mRNA. *klf4* and *klf2a* exhibited statistically significant changes in transcript copy number in embryonic hearts with lowered blood viscosity than control embryos. *klf4* exhibited a decrease in transcript copy numbers while *klf2a* exhibited a slight increase in transcript copy numbers. All other genes had no significant differences in comparisons of transcript copy numbers.

Utilizing these numbers, relative quantification was explored to examine the effects of lowered blood viscosity on the expression levels of our target genes (Figure 3.18b). In embryos with lowered blood viscosity, no significant differences were found in *klf4* and *klf2b*.

In contrast, *klf2a* and *cmlc2* both showed significant decreases in expression levels with lowered blood viscosity. *klf2a* is an internal positive control to verify that we are seeing results reported in previous work. The expression level of *klf2a* decreased as was previously shown (Vermot et al., 2009) and not only verifies that *klf2a* is in fact a flow response gene, but it reassures us that our analyses are correct.

We decided to investigate *cmlc2* along with our target genes because *cmlc2* is expressed robustly throughout heart development and is involved in cardiac myofibril assembly (ZFIN.org), although *cmlc2* was not predicted to be a flow response gene. However, looking at its expression levels can tell us if the heart is experiencing structural changes. In response to lowered blood viscosity, we observed a significant decrease in *cmlc2* expression. Putting this information together suggests that decreasing the blood viscosity in the heart does impact cardiac muscle cells, and might affect sarcomere structure or integrity. This result is novel, linking the hemodynamics to changes in the structure and development of the embryonic

heart. To further investigate, one could use immunohistochemistry or electron microscopy to identify changes in cardiac structure in more detail.

No significant differences were found via absolute quantification of the target genes in embryos with altered cardiac contractility compared to control embryos (Figure 3.19a). These findings once again reflect the copy numbers of cDNA for every microgram of RNA. In order to compare expression levels between control embryos and embryos with altered contractility, we must use relative quantification. *cmlc2*, *klf2b*, and *klf4* expression did not exhibit statistically significant results using relative quantification, but *klf2a* expression was significantly decreased.

klf2a was previously described as a flow response gene, but our study is the first to investigate the transcriptional response to knockdown of a sarcomeric protein, *fn1cb*. In embryos with altered cardiac contractility, we find *klf2a* expression to be significantly decreased (Figure 3.19b). This finding is important because it suggests that *klf2a* may respond to shear rate and not reverse flow as previously thought (Vermot et al., 2009). As a reminder, reverse flow increased in embryos with altered cardiac contractility. Previously it was thought that *klf2a* responded more to reverse flow than shear rate (Vermot et al., 2009). The current results show a decrease in *klf2a* expression each time shear rate is significantly decreased (but not reverse flow). These results support Vermot's data that *klf2a* expression decreases in response to lowered blood viscosity. However, Vermot concluded that response to be due to changes in reverse flow alone. Our *gata2* knockdown results along with our *fn1cb* knockdown results show that shear stress is the determining factor in the changes in *klf2a* expression levels. This conclusion can be made by observing the reverse flow fractions and shear rates in the *fn1cb* morpholino injected embryos. To further clarify that shear rate is the determining

factor in changes in *klf2a* expression levels, a future study could increase shear rate and measure *klf2a* expression. These results also reiterate that *klf2a* is a flow response gene and in particular, suggests that *klf2a* may function specifically as a shear rate response gene.

Table 4.1 – Review of results. (Underline means not statistically significant relative quantification results.)

Lowered blood viscosity	↓ heart rate	↓ reverse flow	↓ shear rate	↓ <i>klf2a</i>	<u>↓ <i>klf2b</i></u>	<u>↑ <i>klf4</i></u>	↓ <i>cmlc2</i>
Change in contractility	↓ heart rate	↑ reverse flow	↓ shear rate	↓ <i>klf2a</i>	<u>↑ <i>klf2b</i></u>	<u>↑ <i>klf4</i></u>	<u>↓ <i>cmlc2</i></u>

To conclude, hemodynamic properties of the embryonic heart are affected by depletion of two very different factors, a hematopoietic transcription factor and a sarcomeric cardiac muscle protein. The changes in hemodynamics result in morphological defects, decreased heart rate, and alterations to reverse flow and shear rate. As reviewed (also shown in Table 4.1), lowered blood viscosity results in lower heart rate, lower reverse flow and a decrease in shear rate compared to control embryos. Embryos with altered cardiac contraction exhibited lower heart rate, increased reverse flow and a lower shear rate than control embryos. To connect hemodynamics with changes in gene expression, we have demonstrated that *klf2a* transcription responds to shear rate rather than reverse flow. Our data also suggest that *cmlc2* responds to endocardial shear which in turn promotes restructuring of the heart. More work will be necessary to confirm this, but results could lead to insights on cardiac morphologies. A final important conclusion is that our three target genes *klf2a*, *klf2b*, and *klf4* are not functionally redundant. While *klf4* and *klf2b* may still have flow response qualities, they are not significantly altered by changes in blood viscosity or cardiac contractility.

CHAPTER 5: MATERIALS AND METHODS

Fish Care

All zebrafish were kept at 27-28°C. Adult zebrafish were fed brine and flakes daily and babies were fed Ziegler's liquid diet. Baby zebrafish were introduced into the system at five days post fertilization. They were introduced initially into no-flow water, then moved to slow flow at 14 days, and regular flow at three months. Babies were fed liquid diet until three months, but flakes were added to their diet at 14 days. Breeding began as early as three months post fertilization. Fish lines were replenished after fish stopped breeding or they were aged two years. Old fish were euthanized humanely according to the guidelines approved by the Animal Care and Use Committee. The wild type lines used were TL (Tupfel Long Fin) and WIK. Tg(cmlc2:GFP) homozygous fish were crossed with wild type lines for experimental use. All embryos were developmentally staged according to Kimmel et al (Kimmel et al., 1995).

Dechoriation and Fixation of Embryos

Zebrafish embryos were dechorionated using Pronase® a protease extracted from *Streptomyces griseus* (CALBIOCHEM). Pronase® degrades proteins in the chorion. Pronase® was used at a stock concentration of five mg/ml. Two milliliters of Pronase® was added to a petri dish of embryos in approximately 20 milliliters of E3 water. Embryos were swirled around intermittently for about five minutes until the chorions started to come off of the embryos. The embryos were then placed into a 1.5 ml tube and fixed. Fixation was performed with a solution of 4% paraformaldehyde. This solution was made from a stock solution of 32% paraformaldehyde (Electron Microscopy Sciences). Embryos were then incubated at 4°C

overnight or 2 hours at room temperature (25°C). Once the embryos were fixed, the paraformaldehyde was removed and 100% methanol was added for long term storage at -20°C. The embryos were then used for *in situ* hybridization.

In situ hybridization protocol

In situ hybridization was performed according to a protocol from Thisse and Thisse (Thisse and Thisse, 2008).

PCR and Gel Electrophoresis

PCR was done using GoTaq® (Promega). Gel electrophoresis was done according to a standard protocol. For most tests done, a 0.8% Gene Pure LE agarose (ISC BioExpress) gel was used. TAE buffer was used as a running buffer and solvent for gels. Gels were pre-cast with ethidium bromide and ethidium bromide was also added to the running buffer just before starting the gel. Gels were imaged using GelDoc (Bio-Rad) and Image Lab software (Bio-Rad). If needed, bands were extracted using a light box and a razor blade. The DNA was then extracted from the gel bands using QIAEX®II Gel Extraction Kit (Qiagen). For imaging and resolution uses, Metaphor™ (Lonza) agarose was used according to supplied protocol and prepared at 4%.

RNA extraction and cDNA synthesis

RNA was extracted at various embryo ages using Tri-Reagent. The Tri-Reagent-LS (Molecular Research Center, Inc.) supplied protocol was used for all RNA extractions. RNA was measured using a NanoDrop (Thermo Scientific). cDNA synthesis was done using AMV Reverse Transcriptase (Promega) with the supplied protocol.

Primers

All primers used were designed by author using Primer3Plus (Untergasser et al., 2007).

Primers are shown in Table 5.1. Primers were used in all reactions at a 1:5 dilution from 100 mM stock.

Table 5.1 – List of primers used in PCRs.

Target gene	Forward sequence	Reverse sequence	Product size (bp)
<i>ef1α</i>	CGGTGACAACATGCTGGAGG	ACCAGTCTCCACACGACCCA	220
<i>klf2a</i>	GCCAGAGCTATCAAGGCAAC	TGCCACATCCAGAAAAAGTG	245
<i>klf2b</i> (qPCR only)	GAGGGCACTGTATGCTTTAC	GGCTAGGTTTGAACAGTAGATG	219
<i>klf2b</i> (RT-PCR only)	GCCATGTATGAGGAGGCAAT	CCTCCCAGTTGCAGTGGTAT	246
<i>klf4</i>	CACGAAACCAACAACACCTG	ACTGCTGTTGATGCGAGATG	257
<i>cmlc2</i>	AGTTCAAGAGGCTGCTAATG	AAGCTGCTGATGTGAATGT	220

Microinjections

Setting up fish: Fish were set up in one or two pairs per tank the afternoon before the injection date. Dividers were pulled 20-30 minutes before injections were started.

Injection mixes: The injection mix contains morpholinos (Gene Tools, LLC), rhodamine dextran dye (Molecular Probes/Invitrogen #D-1824), Danieau's buffer, and if needed, water.

Final concentrations of morpholinos were as follows: 0.2mM *gata2* (3rd Exon/Intron

morpholino, seq: CATCTACTCACCAGTCTGCGCTTTG), 0.2mM *gata2* mismatch (seq:

CATCCACTCACTAGTCTACGCTGTG), 0.275mM *flcnb* (seq: GAGTTTTCTAATGGCCCTTACCTGC), and

0.2mM 25-N random control oligo (seq: NNNNNNNNNNNNNNNNNNNNNNNNNNNNN). The final

concentration of the rhodamine dextran dye is 0.025%. The final concentration of Danieau's

buffer was 0.3X. *p53* (seq: GCGCCATTGCTTTGCAAGAATTG) morpholino was added to *flcnb*

injections to account for toxicity (Robu et al., 2007).

Injection needles: Needles were made from 1 mm thin walled borosilicate capillaries (World Precision Instruments, Inc.) pulled using the Sutter-97 needle puller (Sutter Instrument Co.) [Settings: Pressure=50 Velocity=100 Delay=200 Temperature=736]. The needles were broken on the day of the injection experiment. They were broken while looking through the microscope, breaking them into a bevel shape at a diameter that provides enough strength not to bend when it hits the chorion, but is thin enough to not damage a large portion of the embryos. The needles were loaded using 2 μ l of injection mix.

Injections: Embryos were injected with 0.524 nl of injection mix at the 1-cell stage to the 8-cell stage. They were injected into the yolk in the opposite side from point of needle entry. Embryos were injected for 0.2 seconds and at 50 hPa with 15hPa as the backpressure. The embryos were then checked at 4-6 hpf to remove damaged, dead, unfertilized and poorly injected embryos. Well-injected embryos were classified as embryos that have all cells in the dome fluorescing the rhodamine dextran dye (red). The well-injected embryos were then counted and then moved forward for the remainder of the experiment. These embryos were stored in E3 at 28°C (with methylene blue to limit bacterial and fungal growth). Methylene blue was added from a 1:2000 stock (100 μ l/petri dish).

Microscopy and Still Images

All microscopy was done using an Olympus SZX12 microscope. Still images were taken using a Spot Insight camera and analyzed using Spot software.

High Speed Videos

Imaging Equipment: Videos were recorded with a high speed camera (Photron, FASTCAM SA3) mounted to a stereomicroscope (Olympus, SZX12 with SZX-AL20X lens attachment). Recordings were captured at 1500 frames/s (fps) in bright field lighting (Schott, Ace fiber optic light source 150W microscope illuminator). Photron FASTCAM Viewer software was used to control the camera and to save image files.

Image Processing: All image processing and data analysis was performed using an in-house MATLAB interface. Image processing was done using methods from a previous lab member, Brennan Johnson, as described (Johnson et al., 2013a).

Image Analyses: Raw images were first registered by removing any artifacts from shaking during image acquisition and normalizing by accounting for light intensity across frames using a spatiotemporal (ST) plot. Image sequences were then analyzed for heart rate, diameter, and velocity. All other data was inferred from those three data points. Please refer to Appendix 1 for detailed and program-specific steps on analyses. All data was provided via the MATLAB interface created by Johnson except for reverse flow time fractions (Johnson et al., 2013a). These fractions were calculated in ImageJ software (Schneider et al., 2012). Number of frames that contained blood moving in the reverse direction were divided by the total number of frames in one cycle.

qPCR

qPCR was done with LightCycler® 480 SYBR Green I Master mix (Roche Diagnostics). Reactions were done in 10 µl volumes and on a 384 well plate. qPCR was analyzed using both absolute quantification and relative quantification methods using a standard curve. Absolute

quantification was presented as the log of the copy numbers per microgram of RNA. Relative quantification was presented as an expression ratio. Zebrafish *ef1α* was used as the endogenous control (McCurley and Callard, 2008). Data was normalized to endogenous control, $\frac{[\text{target gene}]}{[ef1\alpha]}$. The normalized values were then divided by the lowest normalized value for select gene (or non-injected control) to obtain the expression ratio: $\frac{\text{normalized}_x}{\text{normalized}_{lowest}}$, where normalized_x is any normalized value for the select target gene (or non-injected control).

Statistics

Statistics via ANOVA were done using SigmaPlot (version 12.0) (Systat Software). Video data normality was checked via Shapiro-Wilk on all means. When normality of means passed, equal variance was tested with Levene's mean test which was then followed by a One Way ANOVA. In the event of a significant p value from the ANOVA, an all pairwise multiple comparison was done via Tukey test. When normality of means failed, Kruskal-Wallis One Way ANOVA on ranks was used. In the event of a significant p value from the ANOVA on ranks, an all pairwise multiple comparison was done via Dunn's method.

qPCR data was analyzed via Welch's t-test in Microsoft Excel.

REFERENCES

- Ackermann GE, Paw BH. 2003. Zebrafish: A genetic model for vertebrate organogenesis and human disorders. *Frontiers in Bioscience* 8:D1227-D1253.
- Auman HJ, Coleman H, Riley HE, Olale F, Tsai H-J, Yelon D. 2007. Functional modulation of cardiac form through regionally confined cell shape changes. *Plos Biology* 5:604-615.
- Bakkers J. 2011. Zebrafish as a model to study cardiac development and human cardiac disease. *Cardiovascular Research* 91:279-288.
- Banjo T, Grajcarek J, Yoshino D, Osada H, Miyasaka KY, Kida YS, Ueki Y, Nagayama K, Kawakami K, Matsumoto T, Sato M, Ogura T. 2013. Haemodynamically dependent valvulogenesis of zebrafish heart is mediated by flow-dependent expression of miR-21. *Nature Communications* 4.
- Barrionuevo WR, Burggren WW. 1999. O-2 consumption and heart rate in developing zebrafish (*Danio rerio*): influence of temperature and ambient O-2. *American Journal of Physiology-Regulatory Integrative and Comparative Physiology* 276:R505-R513.
- Bartman T, Walsh EC, Wen KK, McKane M, Ren JH, Alexander J, Rubenstein PA, Stainier DYR. 2004. Early myocardial function affects endocardial cushion development in zebrafish. *Plos Biology* 2:673-681.
- Bastian F, Parmentier G, Roux J, Moretti S, Laudet V, Robinson-Rechavi M. 2008. Bgee: Integrating and comparing heterogeneous transcriptome data among species. *Data Integration in the Life Sciences, Proceedings* 5109:124-131.
- Berdougo E, Coleman H, Lee DH, Stainier DYR, Yelon D. 2003. Mutation of weak atrium/atrial myosin heavy chain disrupts atrial function and influences ventricular morphogenesis in zebrafish. *Development* 130:6121-6129.
- Birely J, Schneider VA, Santana E, Dosch R, Wagner DS, Mullins MC, Granato M. 2005. Genetic screens for genes controlling motor nerve-muscle development and interactions. *Developmental Biology* 280:162-176.
- Boselli F, Freund JB, Vermot J. 2015. Blood flow mechanics in cardiovascular development. *Cellular and Molecular Life Sciences* 72:2545-2559.
- Bukoreshtliev NV, Haase K, Pelling AE. 2013. Mechanical cues in cellular signalling and communication. *Cell and Tissue Research* 352:77-94.
- Christen B, Robles V, Raya M, Paramonov I, Belmonte JCI. 2010. Regeneration and reprogramming compared. *Bmc Biology* 8.
- Dalman MR, Liu Q, King MD, Bagatto B, Londraville RL. 2013. Leptin expression affects metabolic rate in zebrafish embryos (*D-rerio*). *Frontiers in Physiology* 4.
- Davies PF. 1995. FLOW-MEDIATED ENDOTHELIAL MECHANOTRANSDUCTION. *Physiological Reviews* 75:519-560.
- Dekker RJ, van Soest S, Fontijn RD, Salamanca S, de Groot PG, VanBavel E, Pannekoek H, Horrevoets AJG. 2002. Prolonged fluid shear stress induces a distinct set of endothelial cell genes, most specifically lung Kruppel-like factor (KLF2). *Blood* 100:1689-1698.
- Dekker RJ, van Thienen JV, Rohlena J, de Jager SC, Elderkamp YW, Seppen J, de Vries CJM, Biessen EAL, van Berkel TJC, Pannekoek H, Horrevoets AJG. 2005. Endothelial KLF2 links

- local arterial shear stress levels to the expression of vascular tone-regulating genes. *American Journal of Pathology* 167:609-618.
- Dietrich AC, Lombardo VA, Abdelilah-Seyfried S. 2014. Blood Flow and Bmp Signaling Control Endocardial Chamber Morphogenesis. *Developmental Cell* 30:367-377.
- Ekker SC, Larson JD. 2001. Morphant technology in model developmental systems. *Genesis* 30:89-93.
- Fahed AC, Gelb BD, Seidman JG, Seidman CE. 2013. Genetics of congenital heart disease: the glass half empty (vol 112, pg 707, 2013). *Circulation Research* 112:E182-E182.
- Galloway JL, Wingert RA, Thisse C, Thisse B, Zon LI. 2005. Loss of Gata1 but not Gata2 converts erythropoiesis to myelopoiesis in zebrafish embryos. *Developmental Cell* 8:109-116.
- Gardiner MR, Gongora MM, Grimmond SM, Perkins AC. 2007. A global role for zebrafish klf4 in embryonic erythropoiesis. *Mechanisms of Development* 124:762-774.
- Gerety SS, Wilkinson DG. 2011. Morpholino artifacts provide pitfalls and reveal a novel role for pro-apoptotic genes in hindbrain boundary development. *Developmental Biology* 350:279-289.
- Gijzen F, van der Giessen A, van der Steen A, Wentzel J. 2013. Shear stress and advanced atherosclerosis in human coronary arteries. *Journal of Biomechanics* 46:240-247.
- Glickman NS, Yelon D. 2002. Cardiac development in zebrafish: coordination of form and function. *Seminars in Cell & Developmental Biology* 13:507-513.
- Goishi K, Lee P, Davidson AJ, Nishi E, Zon LI, Klagsbrun M. 2003. Inhibition of zebrafish epidermal growth factor receptor activity results in cardiovascular defects. *Mechanisms of Development* 120:811-822.
- Grimes AC, Stadt HA, Shepherd IT, Kirby ML. 2006. Solving an enigma: Arterial pole development in the zebrafish heart. *Developmental Biology* 290:265-276.
- Groenendijk BCW, Hierck BP, Vrolijk J, Baiker M, Pourquie M, Gittenberger-de Groot AC, Poelmann RE. 2005. Changes in shear stress-related gene expression after experimentally altered venous return in the chicken embryo. *Circulation Research* 96:1291-1298.
- Gu S, Jenkins MW, Peterson LM, Doughman Y-Q, Rollins AM, Watanabe M. 2012. Optical coherence tomography captures rapid hemodynamic responses to acute hypoxia in the cardiovascular system of early embryos. *Developmental Dynamics* 241:534-544.
- Hamik A, Lin Z, Kumar A, Balcells M, Sinha S, Katz J, Feinberg MW, Gerzsten RE, Edelman ER, Jain MK. 2007. Kruppel-like factor 4 regulates endothelial inflammation. *Journal of Biological Chemistry* 282:13769-13779.
- Heckel E, Boselli F, Roth S, Krudewig A, Belting HG, Charvin G, Vermot J. 2015. Oscillatory Flow Modulates Mechanosensitive klf2a Expression through trpv4 and trpp2 during Heart Valve Development. *Current Biology* 25:1354-1361.
- Hoage T, Ding Y, Xu X. 2012. Quantifying Cardiac Functions in Embryonic and Adult Zebrafish. *Methods In Molecular Biology* 843:11-20.
- Hogers B, DeRuiter MC, Gittenberger-de Groot AC, Poelmann RE. 1999. Extraembryonic venous obstructions lead to cardiovascular malformations and can be embryolethal. *Cardiovascular Research* 41:87-99.

- Hove JR, Koster RW, Forouhar AS, Acevedo-Bolton G, Fraser SE, Gharib M. 2003. Intracardiac fluid forces are an essential epigenetic factor for embryonic cardiogenesis. *Nature* 421:172-177.
- Howe K, Clark MD, Torroja CF, Torrance J, Berthelot C, Muffato M, Collins JE, Humphray S, McLaren K, Matthews L, McLaren S, Sealy I, Caccamo M, Churcher C, Scott C, Barrett JC, Koch R, Rauch G-J, White S, Chow W, Kilian B, Quintais LT, Guerra-Assuncao JA, Zhou Y, Gu Y, Yen J, Vogel J-H, Eyre T, Redmond S, Banerjee R, Chi J, Fu B, Langley E, Maguire SF, Laird GK, Lloyd D, Kenyon E, Donaldson S, Sehra H, Almeida-King J, Loveland J, Trevanion S, Jones M, Quail M, Willey D, Hunt A, Burton J, Sims S, McLay K, Plumb B, Davis J, Clee C, Oliver K, Clark R, Riddle C, Elliott D, Threadgold G, Harden G, Ware D, Mortimer B, Kerry G, Heath P, Phillimore B, Tracey A, Corby N, Dunn M, Johnson C, Wood J, Clark S, Pelan S, Griffiths G, Smith M, Glithero R, Howden P, Barker N, Stevens C, Harley J, Holt K, Panagiotidis G, Lovell J, Beasley H, Henderson C, Gordon D, Auger K, Wright D, Collins J, Raisen C, Dyer L, Leung K, Robertson L, Ambridge K, Leongamornlert D, McGuire S, Gilderthorp R, Griffiths C, Manthravadi D, Nichol S, Barker G, Whitehead S, Kay M, Brown J, Murnane C, Gray E, Humphries M, Sycamore N, Barker D, Saunders D, Wallis J, Babbage A, Hammond S, Mashreghi-Mohammadi M, Barr L, Martin S, Wray P, Ellington A, Matthews N, Ellwood M, Woodmansey R, Clark G, Cooper J, Tromans A, Grafham D, Skuce C, Pandian R, Andrews R, Harrison E, Kimberley A, Garnett J, Fosker N, Hall R, Garner P, Kelly D, Bird C, Palmer S, Gehring I, Berger A, Dooley CM, Ersan-Ueruen Z, Eser C, Geiger H, Geisler M, Karotki L, Kirn A, Konantz J, Konantz M, Oberlaender M, Rudolph-Geiger S, Teucke M, Osoegawa K, Zhu B, Rapp A, Widaa S, Langford C, Yang F, Carter NP, Harrow J, Ning Z, Herrero J, Searle SMJ, Enright A, Geisler R, Plasterk RHA, Lee C, Westerfield M, de Jong PJ, Zon LI, Postlethwait JH, Nusslein-Volhard C, Hubbard TJP, Crollius HR, Rogers J, Stemple DL. 2013. The zebrafish reference genome sequence and its relationship to the human genome. *Nature* 496:498-503.
- Jaalouk DE, Lammerding J. 2009. Mechanotransduction gone awry. *Nature Reviews Molecular Cell Biology* 10:63-73.
- Jamison RA, Samarage CR, Bryson-Richardson RJ, Fouras A. 2013. In Vivo Wall Shear Measurements within the Developing Zebrafish Heart. *Plos One* 8.
- Johnson BM, Garrity DM, Dasi LP. 2013a. Quantifying Function in the Early Embryonic Heart. *Journal of Biomechanical Engineering-Transactions of the Asme* 135.
- Johnson BM, Garrity DM, Dasi LP. 2013b. The Transitional Cardiac Pumping Mechanics in the Embryonic Heart Cardiovascular Engineering and Technology.
- Just S, Berger IM, Meder B, Backs J, Keller A, Marquart S, Frese K, Patzel E, Rauch G-J, Katus HA, Rottbauer W. 2011. Protein Kinase D2 Controls Cardiac Valve Formation in Zebrafish by Regulating Histone Deacetylase 5 Activity. *Circulation* 124:324-U157.
- Kalluri R, Weinberg RA. 2009. The basics of epithelial-mesenchymal transition. *Journal of Clinical Investigation* 119:1420-1428.
- Kimmel CB, Ballard WW, Kimmel SR, Ullmann B, Schilling TF. 1995. STAGES OF EMBRYONIC-DEVELOPMENT OF THE ZEBRAFISH. *Developmental Dynamics* 203:253-310.
- Kopp R, Schwerte T, Egg M, Sandbichler AM, Egger B, Pelster B. 2010. Chronic reduction in cardiac output induces hypoxic signaling in larval zebrafish even at a time when convective oxygen transport is not required. *Physiological Genomics* 42A:8-23.

- Kotkamp K, Moessner R, Allen A, Onichtchouk D, Drieyer W. 2014. A Pou5f1/Oct4 dependent Klf2a, Klf2b, and Klf17 regulatory sub-network contributes to EVL and ectoderm development during zebrafish embryogenesis. *Developmental Biology* 385:433-447.
- Kowalski WJ, Dur O, Wang Y, Patrick MJ, Tinney JP, Keller BB, Pekkan K. 2013. Critical Transitions in Early Embryonic Aortic Arch Patterning and Hemodynamics. *Plos One* 8.
- Lee J, Moghadam ME, Kung E, Cao H, Beebe T, Miller Y, Roman BL, Lien C-L, Chi NC, Marsden AL, Hsiai TK. 2013. Moving Domain Computational Fluid Dynamics to Interface with an Embryonic Model of Cardiac Morphogenesis. *Plos One* 8.
- Lee JS, Yu C, Shin JT, Sebzda E, Bertozzi C, Chen M, Mericko P, Stadtfeld M, Zhou D, Cheng L, Graf T, MacRae CA, Lepore JJ, Lo CW, Kahn ML. 2006. Klf2 is an essential regulator of vascular hemodynamic forces in vivo. *Developmental Cell* 11:845-857.
- Lin Y-F, Swinburne I, Yelon D. 2012. Multiple influences of blood flow on cardiomyocyte hypertrophy in the embryonic zebrafish heart. *Developmental Biology* 362:242-253.
- Lin YY. 2012. Muscle diseases in the zebrafish. *Neuromuscular Disorders* 22:673-684.
- Martinsen BJ. 2005. Reference guide to the stages of chick heart embryology. *Developmental Dynamics* 233:1217-1237.
- McCurlley AT, Callard GV. 2008. Characterization of housekeeping genes in zebrafish: male-female differences and effects of tissue type, developmental stage and chemical treatment. *Bmc Molecular Biology* 9.
- Meyer A, Schartl M. 1999. Gene and genome duplications in vertebrates: the one-to-four (-to-eight in fish) rule and the evolution of novel gene functions. *Current Opinion in Cell Biology* 11:699-704.
- Miyasaka KY, Kida YS, Banjo T, Ueki Y, Nagayama K, Matsumoto T, Sato M, Ogura T. 2011. Heartbeat regulates cardiogenesis by suppressing retinoic acid signaling via expression of miR-143. *Mechanisms of Development* 128:18-28.
- Nagai R, Friedman SL, Kasuga M, editors. *The Biology of Krüppel-like Factors*. Springer.
- Nagai R, Friedman SL, Kasuga M. 2009. *The Biology of Krüppel-like Factors*. Springer.
- Oates AC, Pratt SJ, Vail B, Yan YL, Ho RK, Johnson SL, Postlethwait JH, Zon LI. 2001. The zebrafish klf gene family. *Blood* 98:1792-1801.
- Parker T, Libourel P-A, Hetheridge MJ, Cumming RI, Sutcliffe TP, Goonesinghe AC, Ball JS, Owen SF, Chomis Y, Winter MJ. 2014. A multi-endpoint in vivo larval zebrafish (*Danio rerio*) model for the assessment of integrated cardiovascular function. *Journal of Pharmacological and Toxicological Methods* 69:30-38.
- Parmar KM, Larman HB, Dai GH, Zhang YH, Wang ET, Moorthy SN, Kratz JR, Lin ZY, Jain MK, Gimbrone MA, Garcia-Cardena G. 2006. Integration of flow-dependent endothelial phenotypes by Kruppel-like factor 2. *Journal of Clinical Investigation* 116:49-58.
- Piekarski K, Munro M. 1977. TRANSPORT MECHANISM OPERATING BETWEEN BLOOD-SUPPLY AND OSTEOCYTES IN LONG BONES. *Nature* 269:80-82.
- Pierpont ME, Basson CT, Benson DW, Jr., Gelb BD, Giglia TM, Goldmuntz E, McGee G, Sable CA, Srivastava D, Webb CL. 2007. Genetic basis for congenital heart defects: Current knowledge - A scientific statement from the American heart association congenital cardiac defects committee, council on cardiovascular disease in the young. *Circulation* 115:3015-3038.

- Renz M, Otten C, Faurobert E, Rudolph F, Zhu Y, Boulday G, Duchene J, Mickoleit M, Dietrich AC, Rampscher C, Steed E, Manet-Dupe S, Benz A, Hassel D, Vermot J, Huisken J, Tournier-Lasserre E, Felbor U, Sure U, Albiges-Rizo C, Abdelilah-Seyfried S. 2015. Regulation of beta 1 Integrin-Klf2-Mediated Angiogenesis by CCM Proteins. *Developmental Cell* 32:181-190.
- Robu ME, Larson JD, Nasevicius A, Beiraghi S, Brenner C, Farber SA, Ekker SC. 2007. p53 activation by knockdown technologies. *Plos Genetics* 3:787-801.
- Rosa N, Simoes R, Magalhaes FD, Marques AT. 2015. From mechanical stimulus to bone formation: A review. *Medical Engineering & Physics* 37:719-728.
- Ruparelia AA, Zhao M, Currie PD, Bryson-Richardson RJ. 2012. Characterization and investigation of zebrafish models of filamin-related myofibrillar myopathy. *Human Molecular Genetics* 21:4073-4083.
- Santhanakrishnan A, Miller LA. 2011. Fluid Dynamics of Heart Development. *Cell Biochemistry and Biophysics* 61:1-22.
- Schneider CA, Rasband WS, Eliceiri KW. 2012. NIH Image to ImageJ: 25 years of image analysis. *Nature Methods* 9:671-675.
- Schwerte T. 2009. Cardio-respiratory control during early development in the model animal zebrafish. *Acta Histochemica* 111:230-243.
- Sidi S, Rosa FM. 2004. Mechanotransduction of hemodynamic forces regulates organogenesis. *M S-Medecine Sciences* 20:557-561.
- Stainier DYR, Weinstein BM, Detrich HW, Zon LI, Fishman MC. 1995. CLOCHE, AN EARLY ACTING ZEBRAFISH GENE, IS REQUIRED BY BOTH THE ENDOTHELIAL AND HEMATOPOIETIC LINEAGES. *Development* 121:3141-3150.
- Staudt D, Stainier D. 2012. Uncovering the Molecular and Cellular Mechanisms of Heart Development Using the Zebrafish. *Annual Review of Genetics*, Vol 46 46:397-418.
- Taber LA, Eggers DW. 1996. Theoretical study of stress-modulated growth in the aorta. *Journal of Theoretical Biology* 180:343-357.
- Taber LA, Ng S, Quesnel AM, Whatman J, Carmen CJ. 2001. Investigating Murray's law in the chick embryo. *Journal of Biomechanics* 34:121-124.
- Thisse B, Christine. 2004. Fast Release Clones: A High Throughput Expression Analysis. ZFIN Direct Data Submission. In.
- Thisse B, SophieFurthauer, MaximilianLoppin, BenjaminHeyer, VincentDegrave, AgnesWoehl, RoxaneLux, ASteffan, TaniaCharbonnier, X. Q.Thisse, Christine. 2001. Expression of the zebrafish genome during embryogenesis (NIH R01 RR15402). ZFIN Direct Data Submission. In.
- Thisse C, Thisse B. 2008. High-resolution in situ hybridization to whole-mount zebrafish embryos. *Nature Protocols* 3:59-69.
- Thompson TG, Chan YM, Hack AA, Brosius M, Rajala M, Lidov HGW, McNally EM, Watkins S, Kunkel LM. 2000. Filamin 2 (FLN2): A muscle-specific sarcoglycan interacting protein. *Journal of Cell Biology* 148:115-126.
- Tobita K, Garrison JB, Liu LJ, Tinney JP, Keller BB. 2005. Three-dimensional myofiber architecture of the embryonic left ventricle during normal development and altered mechanical loads. *Anatomical Record Part a-Discoveries in Molecular Cellular and Evolutionary Biology* 283A:193-201.

- Tu S, Chi NC. 2012. Zebrafish models in cardiac development and congenital heart birth defects. *Differentiation* 84.
- Untergasser A, Nijveen H, Rao X, Bisseling T, Geurts R, Leunissen JAM. 2007. Primer3Plus, an enhanced web interface to Primer3. *Nucleic Acids Research* 35:W71-W74.
- Valdes-Mas R, Gutierrez-Fernandez A, Gomez J, Coto E, Astudillo A, Puente DA, Reguero JR, Alvarez V, Moris C, Leon D, Martin M, Puente XS, Lopez-Otin C. 2014. Mutations in filamin C cause a new form of familial hypertrophic cardiomyopathy. *Nature Communications* 5.
- Van der Velde ET, Vriend JWJ, Mannens M, Uiterwaal C, Brand R, Mulder BJM. 2005. CONCOR, an initiative towards a national registry and DNA-bank of patients with congenital heart disease in the Netherlands: Rationale, design, and first results. *European Journal of Epidemiology* 20:549-557.
- Verbruggen SW, Vaughan TJ, McNamara LM. 2014. Fluid flow in the osteocyte mechanical environment: a fluid-structure interaction approach. *Biomechanics and Modeling in Mechanobiology* 13:85-97.
- Vermot J, Forouhar AS, Liebling M, Wu D, Plummer D, Gharib M, Fraser SE. 2009. Reversing Blood Flows Act through klf2a to Ensure Normal Valvulogenesis in the Developing Heart. *Plos Biology* 7.
- Wang L, Zhang P, Wei Y, Gao Y, Patient R, Liu F. 2011. A blood flow-dependent klf2a-NO signaling cascade is required for stabilization of hematopoietic stem cell programming in zebrafish embryos. *Blood* 118:4102-4110.
- Yelon D. 2001. Cardiac patterning and morphogenesis in zebrafish. *Developmental Dynamics* 222:552-563.
- Yelon D, Ticho B, Halpern ME, Ruvinsky I, Ho RK, Silver LM, Stainier DYR. 2000. The bHLH transcription factor Hand2 plays parallel roles in zebrafish heart and pectoral fin development. *Development* 127:2573-2582.
- Yokoi H, Yan Y-L, Miller MR, BreMiller RA, Catchen JM, Johnson EA, Postlethwait JH. 2009. Expression profiling of zebrafish sox9 mutants reveals that Sox9 is required for retinal differentiation. *Developmental Biology* 329:1-15.
- Zhou ZN, Rawnsley DR, Goddard LM, Pan W, Cao XJ, Jakus Z, Zheng H, Yang JS, Arthur JSC, Whitehead KJ, Li DA, Zhou B, Garcia BA, Zheng XJ, Kahn ML. 2015. The Cerebral Cavernous Malformation Pathway Controls Cardiac Development via Regulation of Endocardial MEK3 Signaling and KLF Expression. *Developmental Cell* 32:168-180.

APPENDIX

APPENDIX 1

Using the MATLAB KAT interface.

Registering and Normalizing Image Sequences

1. Check the “AS” checkbox (AS = Anti-shake).
2. Click “Open Sequence”.
3. Choose the first file in the sequence and click “Open”. This will load in the first image. There will be a blue rectangle around the whole image and a green rectangle in the middle.
4. Use the blue rectangle to specify the area of the image you want to keep
5. Place the green rectangle in a static part of the image (not somewhere that the heart will overlap at any point in the cycle). Make sure there are high-contrast features present within the green box (cells on the chest or pigmentation are usually a good option). The green box is the template box used to align all images in the sequence. The green box does not have to be within the blue box.
6. Click “Open Sequence”. The computer will attempt to remove all camera shake present (i.e. register the image) and will crop the image as specified.
7. Click “New RL”. Draw a reference line in a gray part of the image which does not overlap the heart. Avoid very dark or very light parts of the image. This will be used to normalize the lighting, which will remove electricity-based lighting fluctuations.

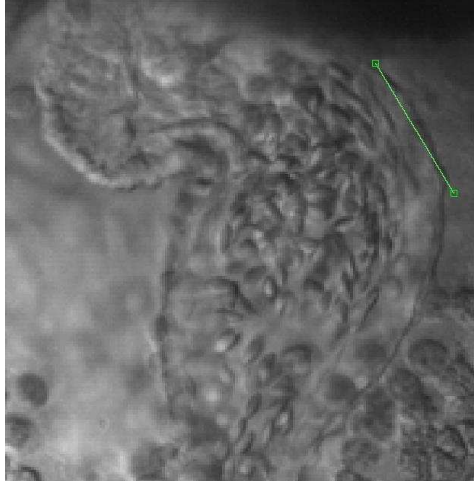
8. Click "ST Plot". If there are lighting fluctuations, there will be vertical banding in the ST plot.
9. Click "Normalize Light". This will fix the fluctuations.
10. Click "Export Frames" and choose an appropriate folder and base file name. This will save the entire normalized image sequence.

Analyzing Heart Function

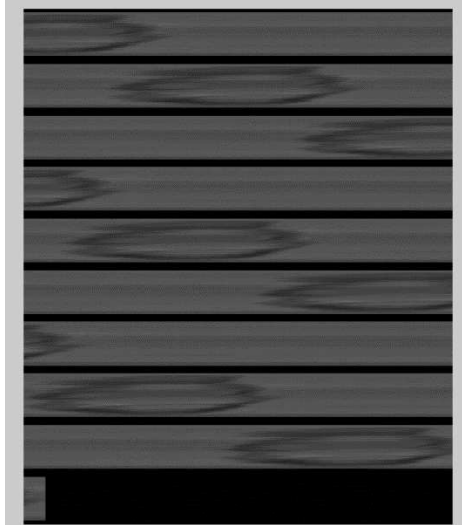
1. Leave the "AS" checkbox unchecked.
2. Click "Open Sequence".
3. Choose the first file in your NORMALIZED sequence and click "Open". This will load in the first image. You have the option of cropping the image, but if everything is registered/normalized, then don't crop it.
4. Click "Open Sequence" again. This will load in the rest of the images.

HEART RATE

5. Click "New RL"
6. Draw a new reference line on the image. Position it so that the edge of the heart overlaps the line, but make sure that the line is not in an area of prominent blood flow. (Example is in image below.)



7. Click "ST Plot", resulting plot should resemble image below.



8. Click "Calc HR". Pattern should align and a line graph will pop up with a sharp negative peak.
 - a. If pattern is not aligning, you can go to Fr/Cyc and manipulate the number to align pattern yourself.



DIAMETER

9. Click "New RL".
10. Draw a new reference line which goes across the orifice of choice, perpendicular to the direction of blood flow. Once line is placed, click "Set KF" (key frame), so the reference line can move as the orifice moves. Click the arrow to move through frames, and at each frame throughout a cycle that the AVJ seems to either change in speed and/or direction, adjust the position of the reference line over the AVJ and click "Set KF." Repeat this until the end of the cycle. As the end of the cycle approaches, the reference line should start to automatically position itself correctly.
11. Click "ST Plot".
12. Click "Save RL". Choose a folder to save it in. This folder will be also be holding other files related to the analysis of this image sequence. The beginning of the file name is set by default. I recommend adding a "D" to the end in order to specify that this is the Diameter reference line.
13. Click "Measure D". This opens a new form (KATD).
14. Choose the number of points to work with and click "Update". 20 is recommended.

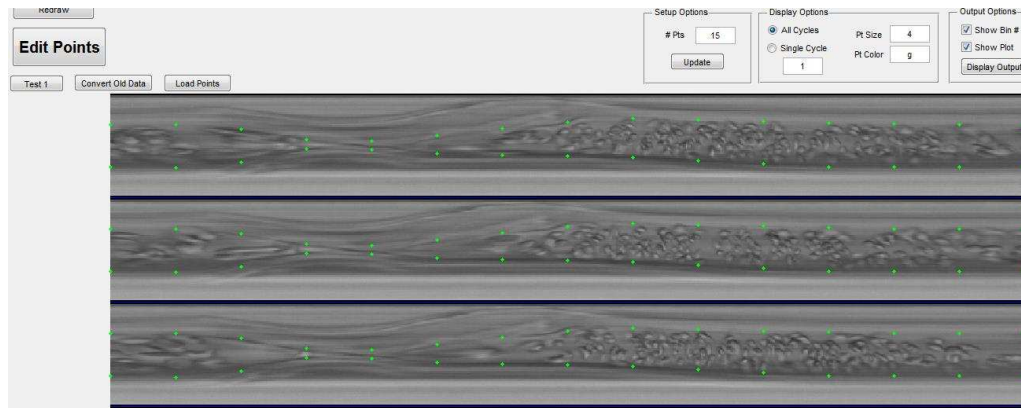
- a. At this point you can also choose “single cycle” to work with individual cycles.

This can sometimes make it easier to plot points.

15. Click “Edit Points”. Position the points so that they follow the edges of the flow boundary. To set a point in a new location, click near it. The point will turn red. Click in a new location to set it somewhere else. Repeat for all points. Press Ctrl+c to exit the point-editing mode.

- a. NOTE: If steps are not followed closely in this, errors will occur and the entire process must be started over (starting with uploading and heart rate).

Simply clicking outside of the ST plot when picking points can cause errors.



16. When you are satisfied with their position, increase the number of points and click “Update”. This will add points which are linearly interpolated between the other points you have set. You can verify that the points look to be in an accurate pattern.

17. Refine the position of the points along the flow boundary, if needed. When everything is set, close the form. Points are saved automatically.

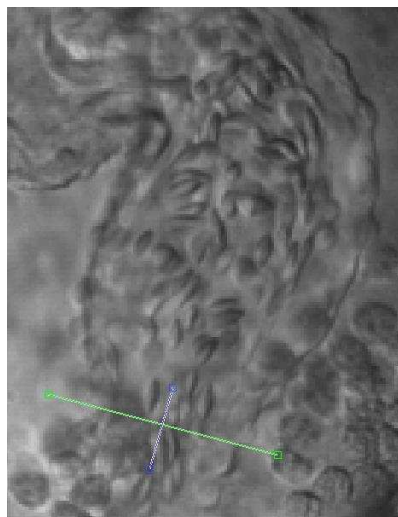
18. Checking the “Show D Pts” checkbox will display dots on the reference line corresponding to where the flow width was measured. You can then play back through the sequence to ensure that the point placement is accurate.

- a. NOTE: The D pts will not show up on the reference line if it moves around using key frames. There is an error in the display that causes it to position along some invisible static line. You will just have to pause the video at random points to make sure that the dots look the same distance apart as the AVJ diameter.

VELOCITY

19. Click “New RL”.

20. Draw a reference line which runs parallel to the direction of blood flow, and which is centered over the diameter reference line. Once placed, the diameter reference line will disappear, so pay attention to how you’re setting this new line.



21. Go forward and backward in the sequence as needed to determine exactly which angle the reference line should be positioned on the first frame. Once satisfied that it is parallel to the blood flow on the first frame, click "Set KF".
 - a. NOTE: Make sure a key frame is set on the first frame! Otherwise it will not interpolate the position of the reference line between the last key frame to the position on the next cycle.
22. Click ahead into the image sequence. The direction of flow will likely change. At some point, the reference line will not be aligned with the flow. You will be resetting its location at various key frames throughout the sequence. Its position will then be linearly interpolated between each key frame. If you understand this point, it should be easy to intelligently choose where to place key frames such that the reference line stays accurate. You should be able to pull this off with about 5 key frames. There isn't a lot of velocity error associated with minor variations in reference line angle vs. blood flow direction.
23. Once all key frames have been set, click "Save RL". Choose a folder to save it in. The beginning of the file name is set by default. I recommend adding a "V" to the end in order to specify that this is the Velocity reference line.
24. Click "Calc Vel.". The computer will go through its auto-calculation of velocity for each frame.
25. When the analysis is finished, click "Save All". Do not change the default name! It will save multiple files based on this name and you can goof everything up if you change it. Just click "Save" after you have you correct file location picked.

26. Click “Analyze Results”. This opens a new form (KATA). All of the raw results will be displayed.
27. You will almost certainly need to threshold the data to remove junk data points. Choose the “Threshold Data” option on the bottom left. Keep adjusting the “max/mean” number until the data looks as clean and accurate as possible. There should be few if any outliers.
- a. You can also click on “Cycle averaged” and adjust “max/mean” that way as well.
28. If you are copying the data into a spreadsheet, I recommend clicking the “Summary (Long)” option, then clicking “Copy Data Col”. This copies all of the results in the form of a single column of data. This is convenient for analysis and plotting in Excel.
29. Sample data column for a wildtype embryo below.

Dataset	NI1
Date	7-May-15
px/mm	1310
fr/s	1500
First Fr	3
Last Fr	3268
fr/bin	25
Bin incr	5
fr/cyc	514
# Cycles	6
Threshold	4.1
HR (bpm)	175.1
SV (nL)	0.05
CO (nL/min)	8.8
RF	0
Vmax (mm/s)	13.62
Vmean (mm/s)	4.9
Vel (mm/s)	
Time(N)	NI1
0	0
0.0101	0
0.0202	0
0.0303	0
0.0404	0

0.0505	0
0.0606	0
0.0707	0
0.0808	0
0.0909	0
0.101	0
0.1111	0
0.1212	0
0.1313	0
0.1414	0
0.1515	0
0.1616	0
0.1717	0
0.1818	0
0.1919	0
0.202	0
0.2121	0
0.2222	0
0.2323	0
0.2424	0
0.2525	0
0.2626	0
0.2727	0
0.2828	0
0.2929	0
0.303	0
0.3131	0
0.3232	0
0.3333	0
0.3434	0
0.3535	0
0.3636	0
0.3737	0
0.3838	0
0.3939	0
0.404	0
0.4141	0
0.4242	0
0.4343	0
0.4444	0
0.4545	0
0.4646	0
0.4747	0
0.4848	0
0.4949	0
0.505	0
0.5151	0
0.5252	0
0.5353	0
0.5454	0
0.5555	0
0.5656	0
0.5757	0
0.5858	0
0.5959	0
0.606	0
0.6161	0
0.6262	0
0.6363	0
0.6464	0
0.6565	0
0.6666	0
0.6767	0

0.6868	0
0.6969	0
0.707	0
0.7171	0
0.7272	0
0.7373	0
0.7474	0
0.7575	0
0.7676	0
0.7777	0
0.7878	0
0.7979	0
0.808	0
0.8181	0
0.8282	0
0.8383	0
0.8484	0
0.8585	0
0.8686	0.498
0.8787	1.554
0.8888	2.26
0.8989	2.452
0.909	3.296
0.9191	5.131
0.9292	4.828
0.9393	3.316
0.9494	3.154
0.9595	4.056
0.9696	5.136
0.9797	5.451
0.9898	7.078
0.9999	8.461
Dia (um)	
Time (N)	N11
0	12.802
0.0101	9.798
0.0202	7.065
0.0303	4.952
0.0404	3.189
0.0505	2.14
0.0606	1.91
0.0707	1.804
0.0808	1.76
0.0909	1.76
0.101	1.747
0.1111	1.714
0.1212	1.676
0.1313	1.636
0.1414	1.594
0.1515	1.596
0.1616	1.668
0.1717	1.768
0.1818	1.88
0.1919	2.006
0.202	2.107
0.2121	2.159
0.2222	2.185
0.2323	2.2
0.2424	2.201
0.2525	2.19
0.2626	2.148
0.2727	2.086

0.2828	2.016
0.2929	1.934
0.303	1.864
0.3131	1.851
0.3232	1.882
0.3333	1.93
0.3434	2.005
0.3535	2.087
0.3636	2.156
0.3737	2.213
0.3838	2.266
0.3939	2.312
0.404	2.354
0.4141	2.372
0.4242	2.366
0.4343	2.352
0.4444	2.321
0.4545	2.279
0.4646	2.209
0.4747	2.106
0.4848	1.99
0.4949	1.844
0.505	1.677
0.5151	1.545
0.5252	1.463
0.5353	1.403
0.5454	1.398
0.5555	1.44
0.5656	1.461
0.5757	1.447
0.5858	1.417
0.5959	1.339
0.606	1.214
0.6161	1.095
0.6262	0.992
0.6363	0.898
0.6464	0.827
0.6565	0.782
0.6666	0.758
0.6767	0.787
0.6868	0.851
0.6969	1.002
0.707	1.269
0.7171	1.556
0.7272	1.815
0.7373	2.053
0.7474	2.241
0.7575	2.352
0.7676	2.441
0.7777	2.596
0.7878	2.812
0.7979	3.154
0.808	3.744
0.8181	4.455
0.8282	4.95
0.8383	5.217
0.8484	6.001
0.8585	8.161
0.8686	11.167
0.8787	13.82
0.8888	16.042
0.8989	18.02
0.909	19.343

0.9191	20.179
0.9292	20.971
0.9393	21.697
0.9494	22.254
0.9595	21.642
0.9696	20.011
0.9797	18.38
0.9898	16.75
0.9999	15.119
Q (nL/min)	
Time (N)	NI1
0	0
0.0101	0
0.0202	0
0.0303	0
0.0404	0
0.0505	0
0.0606	0
0.0707	0
0.0808	0
0.0909	0
0.101	0
0.1111	0
0.1212	0
0.1313	0
0.1414	0
0.1515	0
0.1616	0
0.1717	0
0.1818	0
0.1919	0
0.202	0
0.2121	0
0.2222	0
0.2323	0
0.2424	0
0.2525	0
0.2626	0
0.2727	0
0.2828	0
0.2929	0
0.303	0
0.3131	0
0.3232	0
0.3333	0
0.3434	0
0.3535	0
0.3636	0
0.3737	0
0.3838	0
0.3939	0
0.404	0
0.4141	0
0.4242	0
0.4343	0
0.4444	0
0.4545	0
0.4646	0
0.4747	0
0.4848	0
0.4949	0
0.505	0

0.5151	0
0.5252	0
0.5353	0
0.5454	0
0.5555	0
0.5656	0
0.5757	0
0.5858	0
0.5959	0
0.606	0
0.6161	0
0.6262	0
0.6363	0
0.6464	0
0.6565	0
0.6666	0
0.6767	0
0.6868	0
0.6969	0
0.707	0
0.7171	0
0.7272	0
0.7373	0
0.7474	0
0.7575	0
0.7676	0
0.7777	0
0.7878	0
0.7979	0
0.808	0
0.8181	0
0.8282	0
0.8383	0
0.8484	0
0.8585	0
0.8686	2.925
0.8787	13.99
0.8888	27.411
0.8989	37.522
0.909	58.116
0.9191	98.457
0.9292	100.047
0.9393	73.553
0.9494	73.612
0.9595	89.523
0.9696	96.927
0.9797	86.783
0.9898	93.575
0.9999	91.144
AccVol (nL)	
Time (N)	NI1
0	0
0.0101	0
0.0202	0
0.0303	0
0.0404	0
0.0505	0
0.0606	0
0.0707	0
0.0808	0
0.0909	0
0.101	0

0.1111	0
0.1212	0
0.1313	0
0.1414	0
0.1515	0
0.1616	0
0.1717	0
0.1818	0
0.1919	0
0.202	0
0.2121	0
0.2222	0
0.2323	0
0.2424	0
0.2525	0
0.2626	0
0.2727	0
0.2828	0
0.2929	0
0.303	0
0.3131	0
0.3232	0
0.3333	0
0.3434	0
0.3535	0
0.3636	0
0.3737	0
0.3838	0
0.3939	0
0.404	0
0.4141	0
0.4242	0
0.4343	0
0.4444	0
0.4545	0
0.4646	0
0.4747	0
0.4848	0
0.4949	0
0.505	0
0.5151	0
0.5252	0
0.5353	0
0.5454	0
0.5555	0
0.5656	0
0.5757	0
0.5858	0
0.5959	0
0.606	0
0.6161	0
0.6262	0
0.6363	0
0.6464	0
0.6565	0
0.6666	0
0.6767	0
0.6868	0
0.6969	0
0.707	0
0.7171	0
0.7272	0
0.7373	0

0.7474	0
0.7575	0
0.7676	0
0.7777	0
0.7878	0
0.7979	0
0.808	0
0.8181	0
0.8282	0
0.8383	0
0.8484	0
0.8585	0
0.8686	0
0.8787	0.001
0.8888	0.003
0.8989	0.005
0.909	0.008
0.9191	0.014
0.9292	0.019
0.9393	0.024
0.9494	0.028
0.9595	0.033
0.9696	0.038
0.9797	0.043
0.9898	0.049
0.9999	0.054

NORMALIZING AND ORGANIZING DATA

When data is ready for more than one embryo, you will need to align data so the cycles align. An example Excel sheet has been placed on the lab computer.

DIAMETER

30. Find max value in all datasets for diameter. (Using the '=max' function.)
31. Grab max values and all data underneath and move to new column. (For each dataset individually)
32. Then grab the rest of the data and place it underneath its respective new column.
Now all diameters should be arranged with max at top.
33. Now you want to make the max be in the middle of the dataset, grab the lower half of the data square you currently have and place it at the top of new columns.

34. Then grab the top of the data set (max should be at top) and move it underneath.

Max should now be in the middle. (placed at time 0.5050)

35. To normalize data, divide each value in a column by its respective max value. This is your normalized diameter.

VELOCITY

36. Repeat max value organizing steps as described under diameter.

37. Now divide each value in a column by the max diameter in mm. (NOTE that your current diameter is in μm .)

38. Then divide this new value by the heart rate in seconds. (Current heart rate is in beats per minute, you will need to convert to beats per second.) This is your normalized velocity.

Q - Flow

39. Repeat max value organizing steps as described under diameter.

40. First you need to convert to m^3/min . This is done by multiplying each value by 10^{12} .

41. Then you need to convert to m^3/s . This is done by dividing each value by 60.

42. Next, normalize to give units $1/\text{s}$. You will divide each value by max diameter in mm^3 .

(You will need to convert this from your max diameter values.)

43. Last step is to normalize time to make dimensionless. Divide each value by heart rate in seconds. This is your normalized flow rate.